DESIGN METHODS IN ACTIVE VALVE

PULSE TUBE REFRIGERATOR

By

Jong Hoon Baik

A DISSERTATION SUBMITTED IN PARTIAL FULFILLMENT OF
THE REQUIREMENTS FOR THE DEGREE OF

DOCTOR OF PHILOSOPHY

(Mechanical Engineering)

at the

UNIVERSITY OF WISCONSIN – MADISON

2003

Dedicated to

Sun Young, In Young, Mom, Dad,

And

The Heavenly Father.

Acknowledgements

First of all, I would like to give thanks to The Heavenly Father for allowing me to do this project. I have come to realize the fact that it was He who called me when I was in the dark, healed me when I was sick, and trained me when I was out of his lap. Heavenly Father, thank you for your love and forgiveness.

I am deeply indebted to my academic advisor, professor John M. Pfotenhauer. His endless support and encouragement both academically and spiritually made it possible for me to finish this project. I was very fortunate to have a teacher who prayed for me and taught me to partner with God in this world especially in doing research. Thank you so much for your precious efforts and invaluable experiences.

The dissertation committee including professor Sanford A. Klein, Christopher J. Rutland, Michael L. Corradini and Gregory F. Nellis are much appreciated for their helpful discussions and critical evaluations.

The financial support provided by The Department of Energy through Lockheed Marten and Atlas Scientific was greatly appreciated.

I would like to acknowledge all the members in the Cryogenic Engineering Lab at UW- Madison. Dr. James Maddocks inspired me in the proper attitude I should have as an engineer. Mr. Orrin Lokken was a fine teacher in mechanical design, a wonderful expert in apparatus fabrication, a generous 'father-in-Madison', as well as a 'personal

911' to me. Mr. Edward Dreier kept me alive with his humorous jokes and helpful advice about the lab activities. Also, I will never forget the times spent with Tim Martens, my officemate, doing research and our Bible studies.

Special thanks go to professor Ho-Myung Chang who has been a faithful teacher since 1990. His immeasurable support and encouragement helped me to reach my goal. Thank you so much, professor Chang.

My deepest thanks go to my parents whose endless sacrifices bring tears to my eyes. May they always share in the joy of accomplishment I feel today. Thanks Mother and Father, I love you and am very proud to be your son.

Also, other family members, Jennie Baik, The Lees and Ohs in Los Angeles, and the Moons in Korea are really appreciated in my heart for their unimaginable support and encouragement. Frederick McGibbon and Sarah Kim are also appreciated for their kindness and friendship in Madison.

Finally, and most of all, my heartfelt love and appreciation go to my wife, Sun Y. Moon. From the beginning to the end of this project, she has been a constant support. Her ceaseless devotion and prayers kept me going and inspired me to find the right ways. I will always remember those lonely nights she spent with me in the corner of the lab. Thank you Sun, for everything.

Abstract

The goal of this research is to develop a reliable and scalable design tool for active valve G-M (Gifford-McMahon) type pulse tube refrigerators. The design tool builds upon a thermodynamic code developed at UW-Madison, is based on given compressor power, and requires a deep understanding of key loss mechanisms. A test of the model has resulted in the fabrication of a single stage G-M type 5-valve pulse tube refrigerator designed to operate at 30 K and provide a nominal cooling power in excess of 30 watts.

The design tool begins by focusing on the limitations imposed by the reciprocating-type compressor commonly used for G-M type pulse tube refrigerators and maximizes the ideal pulse tube cooling power that can be produced from a compressor of fixed capacity. The method provides a physical understanding of the various important factors. The process is illustrated using the specifications for a commercial compressor that draws a maximum electrical power of 5.5kW. The design defines the mass flow and compressor power as a function of the discharge and suction pressures, thereby producing a compressor performance map. The compressor map in turn provides a framework from which the pulse tube system geometry can be optimized for maximum cooling power. Various real constraints, such as acceptable pressure drop through the valves and regenerator, a laminar boundary Stokes layer along the pulse tube walls, and acceptable

conduction losses are included in the design process and are shown to significantly impact the optimized result.

Accounting for the loss mechanisms in the design process is crucial in order to predict the performance of valved pulse tube refrigerators accurately and efficiently. In particular, it is essential to understand the DC flow and shuttle heat loss mechanisms which can be the main loss mechanisms in the G-M type pulse tube refrigerator. A complete analysis of DC flow and shuttle heat loss has been explored using both a fluid dynamic model that includes boundary layer analyses, as well as thermodynamic considerations. The analysis incorporates valve timing and considers the cold end temperature in the pulse tube. An example analysis investigates the boundary layer development and associated heat transfer through each of the various types of flow conditions realized during the 6-step cycle of a 5-valve pulse tube refrigerator. The combined effects of DC flow and the shuttle heat loss on the temperature dependent cooling power are predicted by a numerical model of the 5-valve cycle. The analysis provides an improved prediction of DC flow and shuttle heat loss and an enhanced ability to scale the design of G-M type pulse tube refrigerators. Further considerations including imperfect, that is, actual heat exchanger performance and pressure loss in the regenerator are investigated to enhance the ability to predict the performance of the experimental refrigerator using the numerical model. The modified numerical model is compared to a series of experimental results. Two parameters including the cooling load and the valve timing are investegated for three different geometries of pulse tubes and two

regenerators. The comparisons of the numerical mdoel with experimental results display

good agreements.

Approved :

_____

Date   Professor John M. Pfotenhauer
                                                      Department of Mechanical Engineering

Table of Contents

List of Figures

List of Tables

Nomenclature

A	Area
C	Clearance volume ratio ($= V_c / V_d$) of the compressor
C_d	Discharge coefficient
C_f	Friction coefficient
CHX	Cold heat exchanger
C_p	Specific heat at constant pressure
C_v	Specific heat at constant volume
D	Diameter
f	Frequency
H	Convective heat transfer coefficient, Length scale in eqn. (5.40)
h	Specific enthalpy, infinitecimal time increment in the numerical integration
HHX	Hot heat exchanger
ID	Inner diameter
k	Thermal conductivity
K_t, K_s	Coefficients defined in the reference [30]
L	Length, length scale
$m, \dot{m}$	Mass, mass flow rate
$\dot{m}_h$	Mass flow rate between the hot end of the pulse tube and the hot heat exchanger
$\dot{m}_o, \dot{m}_{o_{1\sim5}}$	Mass flow rate at the orifice valves
n	Polytropic exponent
np	Number of discrete volumes in the pulse tube
nr	Number of discrete volumes in the regenerator
Nu	Nusselt number
OD	Outer diameter
P	Pressure
P_{ch}	Charging pressure
P_H	High pressure
P_{in}	Inlet pressure of a compressor
P_L	Low pressure
P_{M1}, P_{M2}	Intermediate pressures
P_{out}	Outlet pressure of a compressor
PT	Pulse tube
$Q, \dot{Q}$	Heat transfer, heat transfer rate
q''	Heat flux
Q_A	Heat transfer at the aftercooler

Q_C	Heat transfer at the cold heat exchanger
Q_H	Heat transfer at the hot heat exchanger
$Q_{gas\text{-}wall}$	Heat transfer from gas to wall
$Q_{wall\text{-}gas}$	Heat transfer from wall to gas
R	Ideal gas constant
Re	Reynolds number
Pr	Prandtl number
S	Compressor speed
St	Stanton number $= Re/(Nu \cdot Pr)$
T	Temperature
t	time
T_{in}	Temerature at the inlet of a compressor
T_{pt}	Gas temperature in the pulse tube
T_{reg}	Gas temperature in the regenerator, load mean temperature
u	Internal energy
V	Volume
$V_1 {\sim} V_5$	Solenoid valves
V_b	Volume of reservoir
V_c	Clearance volume
V_{chx}	Volume of cold heat exchanger
V_d	Dispaced volume
V_{hhx}	Volume of hot heat exchanger
V_o	Orifice valves
$V_{o\text{-}H}$, $V_{o\text{-}L}$, $V_{o\text{-}R}$	Orifice valves at high,low and reservoir pressures
V_{reg}	Volume of regenerator
$VT_1 {\sim} VT_3$	Valve timings
W_E	Electrical power

Superscripts

$',''$	Modified values by heat transfer with the pulse tube wall
$\underline{}$	Time-averaged value

Subscripts

1,2,..n	The position of the discrete volume in the pulse tube
a	Amplitude
actual	Actual case considering losses
amb	Ambient
ave	Average value
b	Buffer(= reservoir)
C,c	Cold temperature, cold heat exchanger, clearance volume, compressor
chx	Cold heat exchanger
cold volume	Imaginary volume of cold gas in the pulse tube
Cond	Conduction
Conv	Convection
D	Displaced volume, diameter of pulse tube
E,e	Electrical
exp	Experiment
H, h	High pressure, hot temperature, hot heat exchanger
hhx	Hot heat exchanger
i	Position
ideal	Ideal case without losses
in	Toward into control volume
in,mim	Minimum inlet
L	Low pressure
min	Minimum
n-1, n, n+1..	Position in the pulse tube system
net	Net amount
np	Number of discrete volumes in the pulse tube
nr	Number of discrete volumes in the regenerator
out	Toward out of control volume
out,max	Maximum outlet
pt	Pulse tube
R, r	Reservoir
REG, reg	Regenerator
w, wall	wall

Greeks

Δp	Pressure drop
Δt	Infinitesimal change of time
δ	Stokes boundary layer thickness, infinitesimal change
Γ	Ratio of the pulse tube volume to the dead volume in regenerator
γ	Specific heat ratio ($= C_p/C_v$)
η_{comb}	Combined efficiency of compressor
η_{vol}	Volumetric efficiency of compressor
λ	Thermal boundary layer thickness
μ	Viscosity
μ_w	Viscosity of the gas at the wall temperature
ν	Kinematic viscosity
ρ	Density
ρ_{in}	Density at the inlet of a compressor
τ	Period of one cycle
ω	Angular velocity

Chapter 1 Introduction

1.1 Motivation

Since the first observation of a cooling effect at one end of a hollow tube in which a pressure pulsation existed in early 1960's [1], the so-called 'pulse tube refrigerator' has become one of the most promising cryogenic refrigerators. Due to the lack of moving parts in the cold temperature region, and the associated advantages of reliability and simplicity, the pulse tube system has become one of the most fascinating research topics in the area of cryogenic refrigeration research. The pulse tube refrigerator has been mainly investigated for cooling various types of sensitive sensors such as infrared detectors for missiles, military aircraft, tanks, night visions and SQUID (superconducting quantum interference device). Recently, as the achievable temperature of the pulse tube refrigerator becomes lower, their useful range of use is being extended to various types of superconducting magnet applications.

For the past several years, various approaches have been pursued at the Cryogenic Engineering Lab at the UW-Madison to develop an efficient pulse tube refrigerator system and understand the physical mechanisms that determine its performance. An

extensive investigation into the thermodynamics of the pulse tube system followed by several tests have led to a new type of configuration, called a '5-valve pulse tube refrigerator'. The thermodynamic analysis and experimental confirmation performed in a previous study demonstrated the possibility of higher thermodynamic efficiency for a 5-valve pulse tube refrigerator as compared to other two-valve configurations [2-3]. Other investigators have also explored the multi-valve pulse tube refrigerators. The investigation of a single stage, 4-valve and 4-active buffer pulse tube refrigerator has been recently performed in Germany using a 7kW scroll compressor with four solenoid valves. The no-load temperature of 24.6K was achieved in this configuration [4].

The general purpose of the present study is to develop a reliable design approach for G-M (Gifford-McMahon) type pulse tube refrigerator systems based on realistic design constraints. Two elements have resulted − 1) a design method based on the real constraints of available compressors, and 2) a model that describes the pressure, flow, and temperature throughout the pulse tube system and over a complete cycle. Because the model accounts for fluid dynamics and heat transfer mechanisms as well as the thermodynamic processes, it provides a description of various loss mechanisms that play a significant role in real systems.

In any engineering system design, reliable design techniques must be based on understanding the characteristics of each component in the system. Since any pulse tube refrigerator requires a compressor to produce pressure oscillations, the design procedure should be performed based on the compressor performance. For GM type pulse tube

refrigerators, the pressure oscillation is produced with valves connected between the pulse tube/regenerator and the high and low pressure sides of the compressor. This configuration permits the use of the relatively inexpensive compressors that are mass produced for the air-conditioner and refrigeration industry. In the process of designing a G-M type pulse tube refrigerator, one must select a compressor from a finite set of fixed compressor capacities - deliverable work is not available as a continuum. In view of this constraint, it is relevant for a designer to ask, "what pulse tube geometry will best utilize the available power from a specific compressor?" - that is, which geometry will produce the highest cooling power for the fixed limitations of the compressor? To answer these questions, the first part of this report provides a general design procedure for G-M type pulse tube refrigerators – a procedure that enhances the physical understanding of various constraints.

A prior thermodynamic model [2] for a single stage G-M type 5-valve pulse tube refrigerator provided a qualitative agreement with measured performance. However, as shown in Fig. 1.1, the discrepancy between the model and experiment displayed a clear dependence on temperature. It is significant that the previous model did not include several temperature dependent loss mechanisms that have been reported in the literature but not well analyzed. To fully explore the loss mechanisms in the 5-valve pulse tube system, the model has been enhanced to include a fluid dynamic module that includes shuttle heat transfer, DC flow as well as thermodynamic considerations. The results of

these improvements will be discussed in the last part of this thesis, including several suggestions for further investigation.
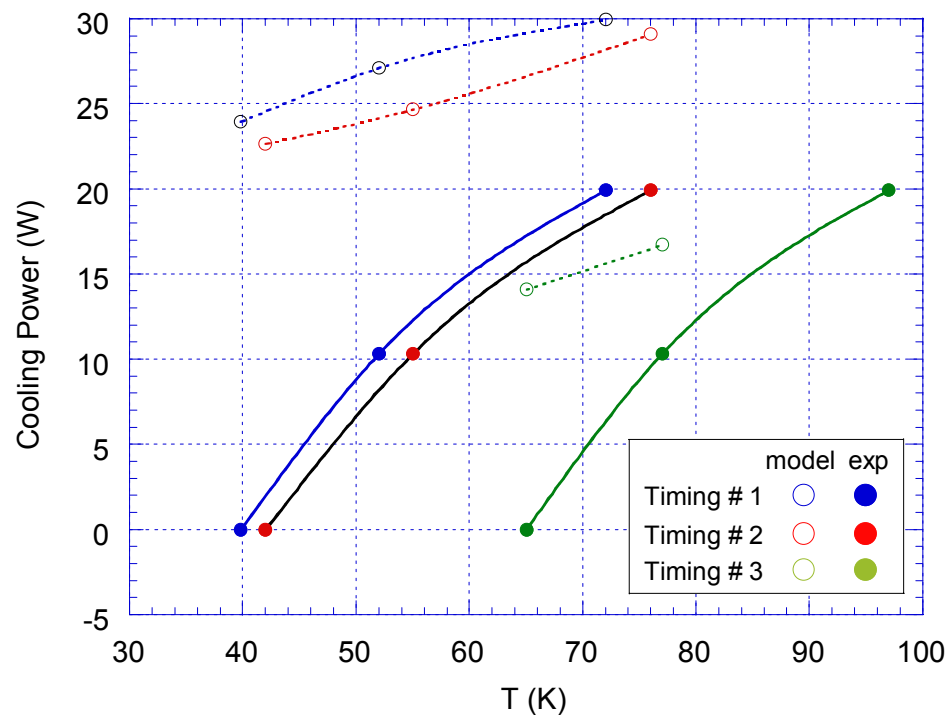
Figure 1.1 Comparion of performances between thermodynamic model and experiments as a function of temperature. (pulse tube/ regenerator volume : 360/123cc, compressor pressure : 2205/483kPa)

1.2 Scope

This report consists of seven chapters. *Chapter 2 Review of Literature* contains a general classification of pulse tube refrigerator systems, followed by a review of analyses by other researchers. Several types of pulse tube refrigerator configurations are schematically introduced. The theoretical cooling mechanisms of the pulse tube refrigerator are also explained for each configuration.

In *Chapter 3 Experimental Apparatus*, three different 5-valve pulse tube refrigerator systems built at the University of Wisconsin–Madison are introduced. The systems vary with respect to regenerator and pulse tube aspect ratio allowing an investigation into the influence of geometry on the cooling performance. The drawings and fabrication methods for these components are shown in detail. Also, the specifications for instrumentation, data acquisition, and control are included.

The main results of this report are addressed in *Chapter 4* and *Chapter 5*. In *Chapter 4 Compressor-Specific Design of a Single Stage Pulse Tube Refrigerator*, a compressor-specific design approach for single stage G-M type pulse tube refrigerators will be discussed. This chapter details the optimization procedure of a valved pulse tube refrigerator for given compressor specifications.

Chapter 5 Analysis of G-M type Pulse Tube Refrigerator describes a numerical analysis for a 5-valve pulse tube system including loss mechanisms. A detailed description of the numerical scheme is presented including the constituent equations,

assumptions, and computational algorithms. The comparison of the numerical results with experimental performance over the variety of geometries is quite good and supports the value of the enhanced design technique. The model also accurately reflects the performance of the system as the valve timing sequence is changed.

Chapter 6 is a conclusion of this report. In *Chapter 7 Proposed works*, several future activities are proposed to compliment the optimum design of a 5-valve pulse tube system based on compressor specifications.

Chapter 2   Review of Literature

2.1   Classification of Pulse Tube

The first report of pulse tube refrigeration by W. E. Gifford and R. C. Longsworth in 1963 [1] was enough to excite many researchers due to the potential of high reliability in spite of its simplicity. For several decades since then, many researchers have concentrated their efforts on improving the performance of pulse tube refrigerators in various ways. As a result, different configurations of pulse tube refrigerators have been introduced. Several representative configurations are detailed in this section including their cooling mechanisms and characteristics.

2.1.1 Basic Pulse Tube Refrigerator

Fig. 2.1 (a) shows a schematic diagram of a basic pulse tube refrigerator. A basic pulse tube refrigerator consists of a compressor, aftercooler, regenerator, cold heat exchanger, hot heat exchanger and pulse tube. The periodic pressurization and expansion produced by the compressor causes the gas to flow back and forth through the regenerator and the pulse tube. Fig. 2.1 (b) depicts the cooling mechanism of a basic pulse

refrigerator. During the compression process, pressurized gas moves towards the hot heat exchanger located at the closed end of the pulse tube. The gas element in the pulse tube experiences near adiabatic compression and an associated temperature rise. The gas at the boundary layer exchanges heat with the tube wall. Heat transfer, through the hot heat exchanger wall, cools the gas in the hot heat exchanger. During the subsequent expansion process, the depressurized gas moves towards the cold heat exchanger. The gas element experiences near adiabatic expansion and an associated temperature drop. The wall releases heat to the gas. The net heat transfer between the gas and the pulse tube wall thus shuttles heat from the cold end to the warm end. However the net amount of heat transferred is relatively small and disappears when the temperature gradient in the wall becomes sufficiently large to match the temperature excursions developed in the gas during the compression and expansion processes. This is the so-called 'surface heat pumping theory' that explains the cooling mechanism of the basic pulse tube [5]. Minimum temperatures of 79~165K have been achieved in various tests of the basic pulse tubes [3].

However, there is a severe limitation in the basic pulse tube refrigerator that is related to the mass flow and pressure wave. The phase difference between the pressure and the mass flow rate in a basic pulse tube refrigerator is 90°. In other words, when the pressure becomes the maximum, the mass flow rate becomes zero at the warm end of the pulse tube. Fig. 2.2 explains this problem more clearly.
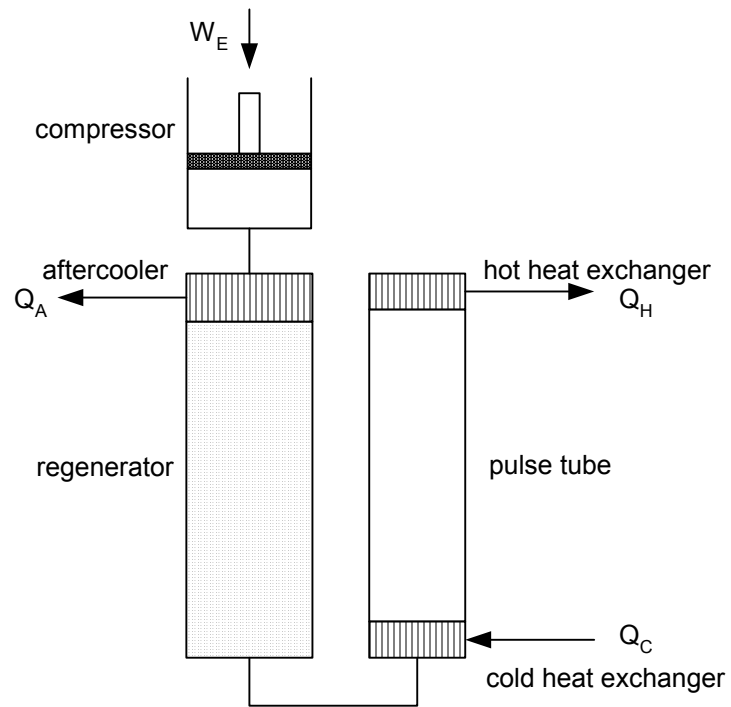
(a) basic pulse tube refrigerator
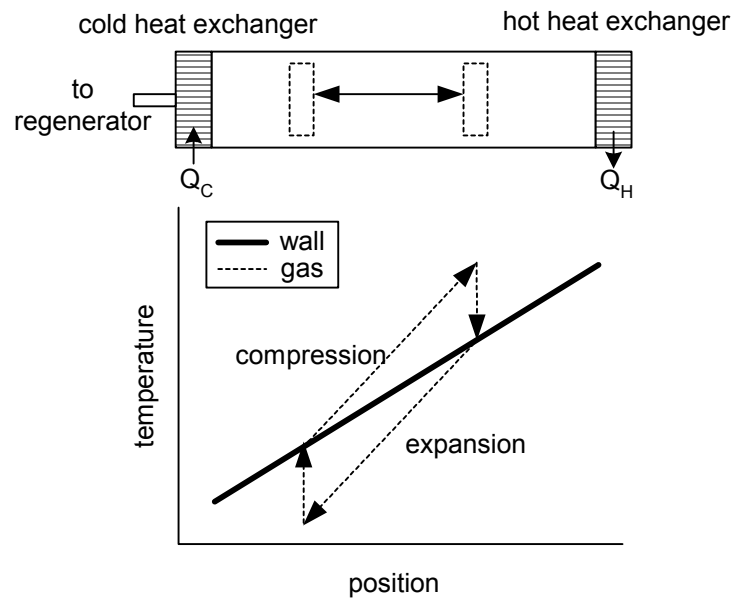
(b) surface heat pumping

Figure 2.1 Schematic diagram of a basic pulse tube refrigerator and its cooling mechanism.

Fig. 2.2 schematically shows the energy flow in a basic pulse tube refrigerator. For the control volume around the cold heat exchanger, the cooling power at any time ($\dot{Q}_c$) is the net enthalpy flow into the cold heat exchanger plus the rate of change of internal energy.

$$\dot{Q}_c = \dot{H}_{out} - \dot{H}_{in} + \left(\frac{dU}{dt}\right)_{chx} \tag{2.1}$$

If we assume there is neither heat transfer nor mechanical work at the gas boundary in the pulse tube, then the enthalpy flow coming from the cold heat exchanger, $\dot{H}_{out}$ is the same as that entering the hot heat exchanger. For the hot heat exchanger, energy conservation gives,

$$\dot{Q}_H = \dot{H}_{out} - \left(\frac{dU}{dt}\right)_{hhx} \tag{2.2}$$

Here, $\dot{Q}_H$ is the rate of heat transferred from the gas to the wall of the hot heat exchanger.
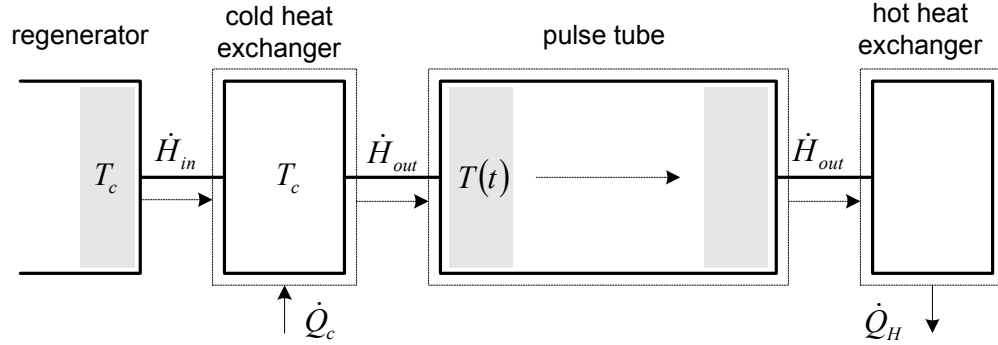
Figure 2.2 Schematic diagram of enthalpy flow in a basic pulse tube refrigerator.

With assumptions of ideal regenerator performance and ideal gas behavior of the working fluid, the cold end of the regenerator should be maintained at the same temperature as the cold heat exchanger (T_c) during a cycle. In this limit, the cyclic integration of $\dot{H}_{in}$ and $\dfrac{dU}{dt}$ over a steady state cycle gives zero for constant T_c, thus we get

$$\left\langle \dot{Q}_c \right\rangle = \left\langle \dot{H}_{out} \right\rangle - \left\langle \dot{H}_{in} \right\rangle + \left\langle \frac{dU}{dt} \right\rangle_{chx} = \left\langle \dot{H}_{out} \right\rangle - 0 + 0 = \left\langle \dot{Q}_H \right\rangle \qquad (2.3)$$

where, $\left\langle \; \right\rangle$ denotes $\dfrac{1}{\tau} \displaystyle\int_{t}^{t+\tau} (\;) \, dt$ and τ is the period of the cycle.

In eqn. (2.3), the net cooling power over a cycle, $\langle \dot{Q}_c \rangle$ is equal to the net enthalpy flow to the hot exchanger, $\langle \dot{H}_{out} \rangle$. Using an ideal gas assumption, the net enthalpy flow can be expressed as

$$\langle \dot{H}_{out} \rangle = \langle \dot{m} h \{ T(t) \} \rangle = \langle \dot{m} C_p T(t) \rangle \tag{2.4}$$

Here, T represents the temperature at the cold end of the pulse tube. Note that for adiabatic compression and expansion, temperature and pressure waves will always be in phase. For a sinusoidal pressure wave, the temperature and the mass flow rate can be written as,

$$T(t) = T_{ave} + T_a \cos(\omega t)$$

$$\tag{2.5}$$

$$\dot{m}(t) = \dot{m}_a \cos(\omega t + 90^o)$$

Here the subscripts *ave, a, and ω* represent respectively the average value, amplitude, and angular velocity. Since the phase difference between the pressure or temperature and mass flow rate is 90°, as shown in Fig. 2.3, the net enthalpy flow into the hot heat exchanger, $\langle \dot{H}_{out} \rangle$ must be zero and therefore the cooling power for the basic pulse tube refrigerator is also zero.
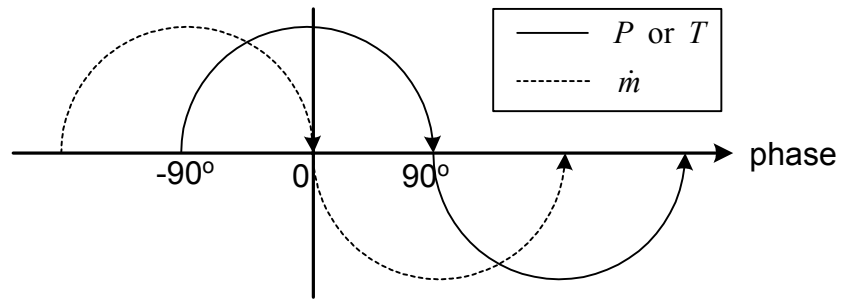
Figure 2.3 Phase difference of P, T and $\dot{m}$ for a sinusoidal pressure wave in pulse tube.

$$\left\langle \dot{H}_{out} \right\rangle = C_p \left\langle \dot{m}_a \cos\left(\omega t + 90^o\right)\left\{T_{ave} + T_a \cos\left(\omega t\right)\right\} \right\rangle = 0 \qquad (2.6)$$

From this simple derivation, we notice that the cooling mechanism for a basic pulse tube is only related to the heat transfer between the gas and the pulse tube wall, which is called the surface heat pumping mechanism. We also notice that additional cooling power can be achieved by changing the phase between the pressure and mass flow rates. By placing an orifice valve and a reservoir after the hot heat exchange, it is possible to reduce the phase difference between the pressure and the mass flow rate to a value less than 90°. This important advance in the pulse tube configuration was achieved by Mikulin et. al. in 1984 and is referred to as an orifice pulse tube refrigerator [6].

2.1.2 Orifice Pulse Tube Refrigerator

In Fig. 2.4, an orifice valve and a reservoir have been added at the end of the hot heat exchanger. The reservoir is large enough to be maintained at a nearly constant intermediate pressure during operation. The valve and the reservoir cause the gas to flow through the orifice valve at the points of maximum and minimum pressures. Therefore the reservoir improves the phase relationship between pressure and gas motion. The orifice pulse tube creates refrigeration through PV-work as well as surface heat pumping. The gas column in the pulse tube acts like the displacer in a Stirling cycle refrigerator. This PV-work is transferred from the compressor to the cold heat exchanger through the regenerator. It is continuously delivered from the cold end to the hot end of the pulse tube by changing the volume of the gas column in the pulse tube with associated pressure changes. Then, this PV-work is dissipated in the valve and transferred as heat in the hot heat exchanger. The surface heat pumping is also involved in this process as an additional factor that alters the temperature of the gas column. As a result, both the PV-work transferred by the gas column and the surface heat pumping near the pulse tube wall affect the cooling performance.

The range of the minimum achievable temperature that can be achieved with a single stage, orifice pulse tube is about 28K [7]. Lower temperature can be achieved by various modifications such as a multi-stage orifice pulse tube or multi-by pass orifice version [8-10]. The performance is strongly dependent on the resistance of the orifice valve. The disadvantage of the orifice pulse tube is the fact that a large amount of
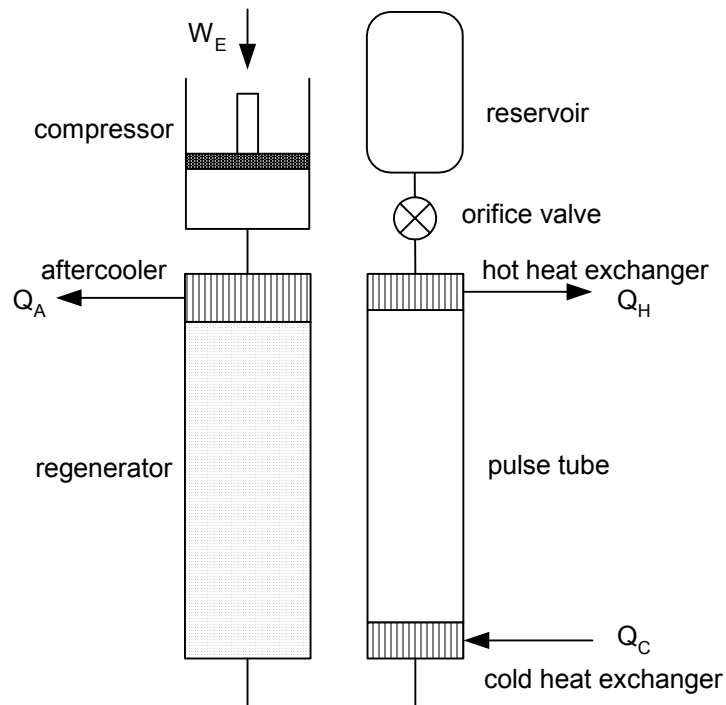
Figure 2.4 Schematic diagram of an orifice pulse tube refrigerator.

compressed gas that produces no actual refrigeration, must flow though the regenerator. This decreases the refrigeration power per unit of compressed mass and therefore increases the regenerator loss. The larger the mass flow rate in the regenerator is, the smaller the effectiveness of regenerator will be, and the larger the pressure loss will be. Both of these effects cause a reduced performance.

2.1.3 Double-inlet Orifice Pulse Tube Refrigerator

Matsubara and Gao [8] attempted a modification to overcome this disadvantage of the orifice pulse tube by adding a second orifice valve between the compressor and the

hot heat exchanger. The second orifice valve, or by-pass valve, helps pressurize the pulse tube without bringing all of the required gas through the regenerator. In their tests, a minimum temperature of 3.5K was achieved with a three-stage double-inlet pulse tube refrigerator.

Besides the basic, orifice, and double-inlet configurations described above, various other configurations have been suggested. For example, S. Zhu et. al. [9] suggest 'the active buffer pulse tube refrigerator system' that uses three reservoirs instead of a single reservoir. An impressive efficiency of 11% of Carnot efficiency was achieved at 80K. In 1995, C. Wang et. al. [10] performed experiments on a 'multi-bypass pulse tube refrigerator' with a middle bypass valve located between the middle of the regenerator and the middle of the pulse tube. A no-load temperature of 23.8K and a cooling load of 3.6W at 77K were obtained with a single stage multi-bypass pulse tube refrigerator.
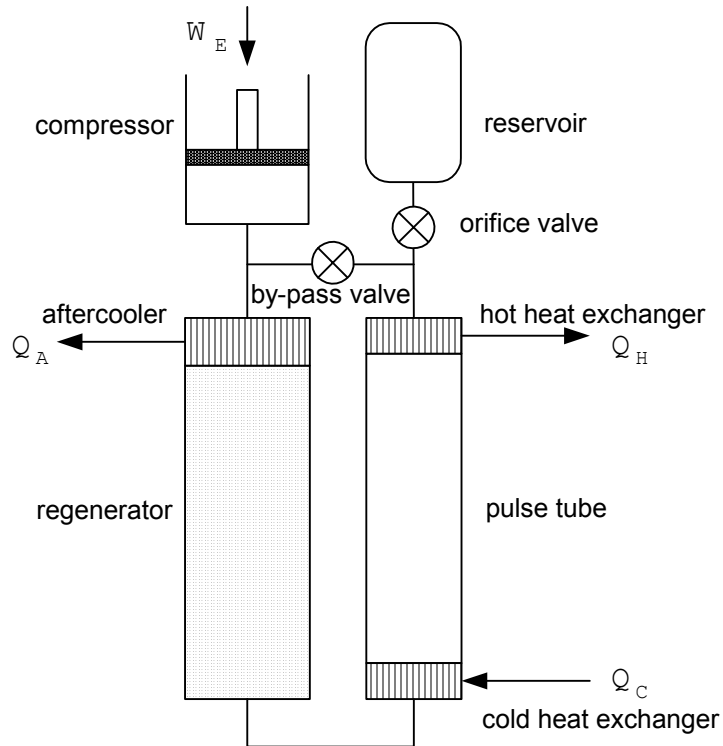
Figure 2.5 Schematic diagram of a double-inlet orifice pulse tube refrigerator.

2.1.4 Stirling Type and G-M Type Pulse Tube Refrigerators

Pulse tube systems can be classified as either a Stirling type or a G-M type according to the method of pressurization and expansion. For a Stirling type pulse tube shown in Fig. 2.6 (a), a piston-cylinder apparatus is connected to the system so that the pressure fluctuations are directly generated by the piston movement. The typical operating frequency is 10~100Hz, higher than that of a G-M type pulse tube. Because of

this high operating frequency and the absence of valve losses, Stirling type pulse tube systems generally produce higher cooling powers than G-M type pulse tubes [11]. However, the rapid heat exchange required in Stirling type pulse tube refrigerators limits their performance at low temperatures, such as at 10K and below. In this range, the longer time allowed for thermal diffusion by the slower frequency G-M type pulse tube refrigerator provides a higher efficiency option.

The G-M type pulse tube refrigerator distributes high/low-pressure gas into the pulse tube and other components by use of a valve system. The periodic opening/closing operation of the high/low pressure valves produces a pressure pulsation in the system. Because of the limitations associated with the valve operation, a typical G-M type pulse tube operates at frequencies of a few Hz. The valve system separating the compressor and pulse tube system provides the possibility of eliminating vibration problems caused by the compressor and permits remote location of the compressor from the cold head. Examples of G-M type pulse tube refrigerators are found in references [3], [8], and [12-14].
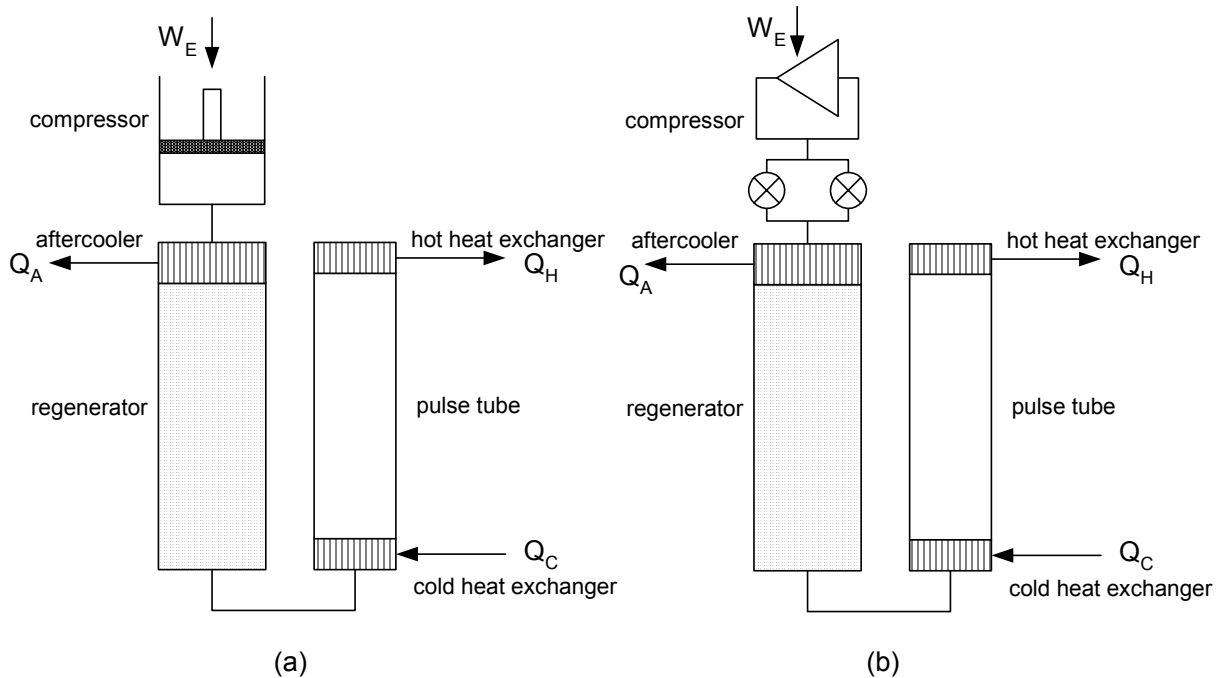
Figure 2.6 Stirling type and G-M type basic pulse tube refrigerators.

(a) Stirling type, (b) G-M type

2.2   A Single Stage, 5-valve Pulse Tube Refrigerator at UW-Madison

Fig. 2.7 depicts the single stage, G-M type 5-valve pulse tube refrigerator that has

been developed at the UW-Madison. This system is a variation of the G-M type, double-

inlet pulse tube refrigerator using the compressor as a pressure wave generator.   An

important characteristic of a G-M type pulse tube refrigerator is that the compressor

frequency is decoupled from the pulse tube frequency by the valve system. In the 5-valve

system, four solenoid valves connect the compressor to the pulse tube system and another

solenoid valve is located between the reservoir and the hot heat exchanger. By changing the order and duration of the opening/closing operation for the five solenoid valves, a virtually infinite number of pressure waves can be realized with this configuration. Fig. 2.8 shows a schematic of the typical valve opening sequences and resulting pressure variation in the 5-valve pulse tube refrigerator. In Fig. 2.8, P_H, P_L, P_{M1}, P_{M2} represent the high, low, intermediate-1 and intermediate-2 pressures during a cycle respectively.

The main advantage of the 5-valve pulse tube refrigerator system can be demonstrated by considering the concept of a Pressure-Volume diagram for the cold space in the pulse tube. Fig. 2.9 shows that the gas at the cold end of the pulse tube delivers P-V (pressure-volume) work that is transferred from compressor-regenerator-cold heat exchanger to the hot heat exchanger as it changes its volume. The integral of pressure against volume in the cold spaces equal to the area of the P-V diagram and represents the cooling power that is generated at the cold heat exchanger. The energy conservation for this cold gas volume gives,

$$\left(\frac{dU}{dt} \right)_{cold\ volume} = \dot{H}_{net} + \dot{Q}_{wall} - P \left(\frac{dV}{dt} \right)_{cold\ volume} \tag{2.7}$$

Here, $\dot{H}_{net}$ represents the net enthalpy flow from the cold heat exchanger to the pulse tube. Assuming that adiabatic compression and expansion eliminates the heat transfer term, $\dot{Q}_{wall}$ in eqn. (2.7), then the integration of both sides of eqn. (2.7) with respect to time through a steady state cycle gives,

$$\left\langle \dot{H} \right\rangle_{net} = \frac{1}{\tau} \int_0^\tau P \left(\frac{dV}{dt} \right)_{cold\ volume} dt = \frac{1}{\tau} \int_{V(0)}^{V(\tau)} PdV_{cold\ volume} = \dot{Q}_c \tag{2.8}$$

In eqn. (2.8) we see that the integration of the Pressure-Volume diagram of the cold space represents the cooling power of the system. A larger area of the P-V diagram will result in a larger cooling power.

Fig. 2.10 shows schematic comparisons of the P-V diagrams for various types of pulse tube refrigerators. For the basic pulse tube refrigerator, there is no cooling power related to P-V work and the area of the P-V diagram is zero. The surface heat pumping is the only cooling mechanism in this configuration. In reality, there may be a small amount of P-V work in the basic pulse tube related to the fact that gas moves a little further after the compression and expansion processes in order to compensate for the change of the gas volume caused by surface heat transfer. The orifice pulse tube has a small positive internal area in the P-V diagram. The double-inlet pulse tube refrigerator can produce even more cooling power than the orifice and basic pulse tube refrigerators. For the G-M type 5-valve pulse tube refrigerator, various combinations of valve openings can produce nearly constant pressure processes at high and low pressure in order to increase internal area of the P-V diagram. The G-M type 5-valve pulse tube configuration is being investigated because it is possible, through valve-timing control, to optimize the P-V work done per cycle by the cold gas volume in the pulse tube, and thereby optimize its cooling power.

Since the system performance is very sensitive to the effects of the solenoid valve timings and the resistances of the orifice valves, the precise controllability of these valves allows the system to operate at near optimal conditions for any given pulse tube geometry. For several years, various geometries of pulse tubes, regenerators and heat exchangers have been designed, built and tested at the UW-Madison. To date, the best no-load temperature achieved with these single stage pulse tubes is 24K using 5.5kW of compressor power. This is only slightly higher than the world record for a single stage pulse tube of 19.8K [15].

23
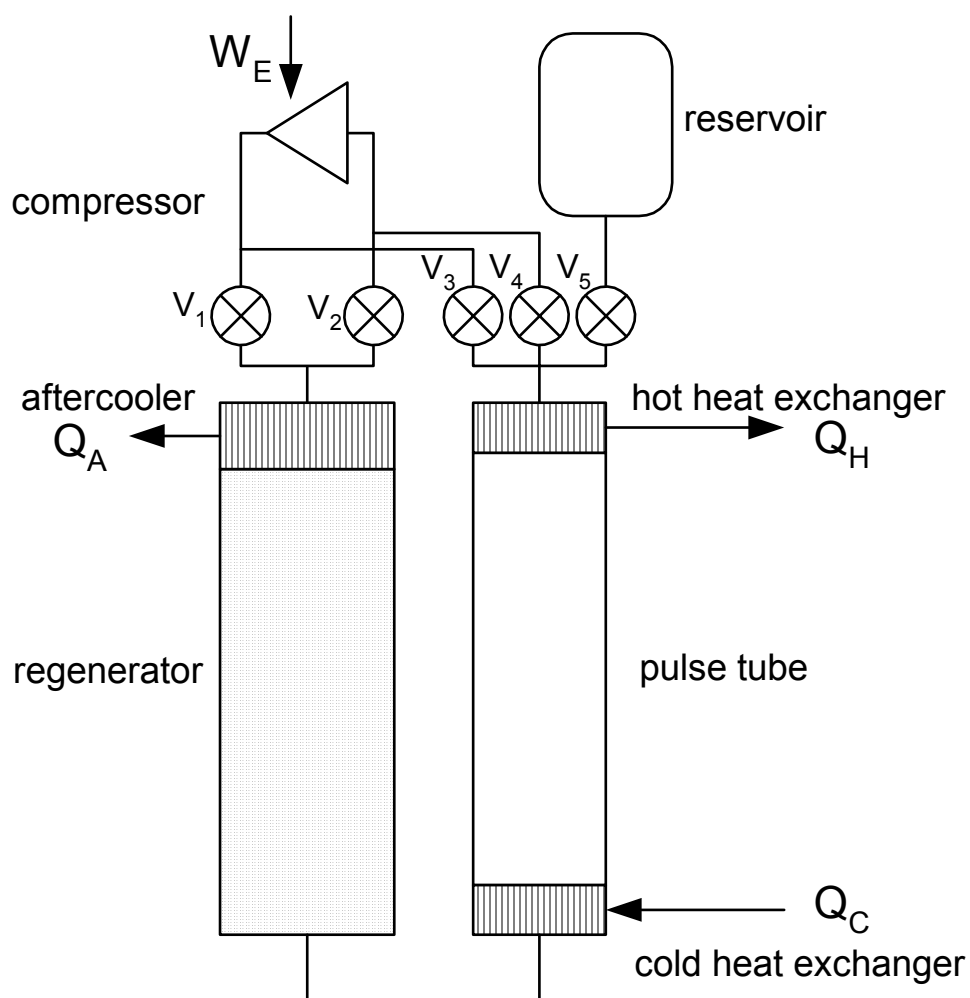
Figure 2.7 Schematic diagram of the single stage, 5-valve pulse tube refrigerator.
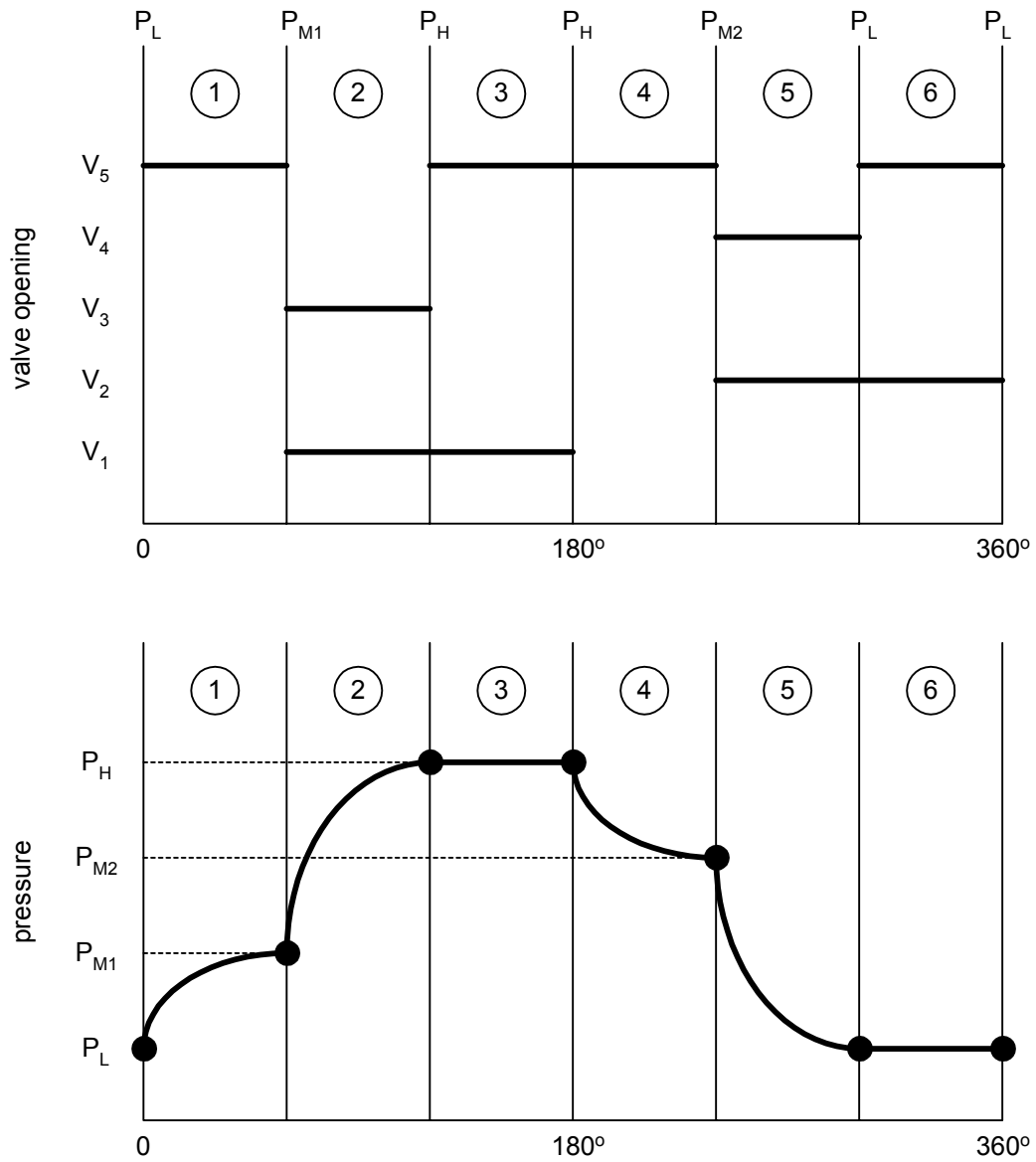
Figure 2.8 Typical valve opening sequences and corresponding pressure changes during a cycle.

(1: 1ˢᵗ compression, 2: 2ⁿᵈ compression, 3: P_H shuttle, 4: 1ˢᵗ expansion, 5: 2ⁿᵈ expansion, 6: P_L shuttle)
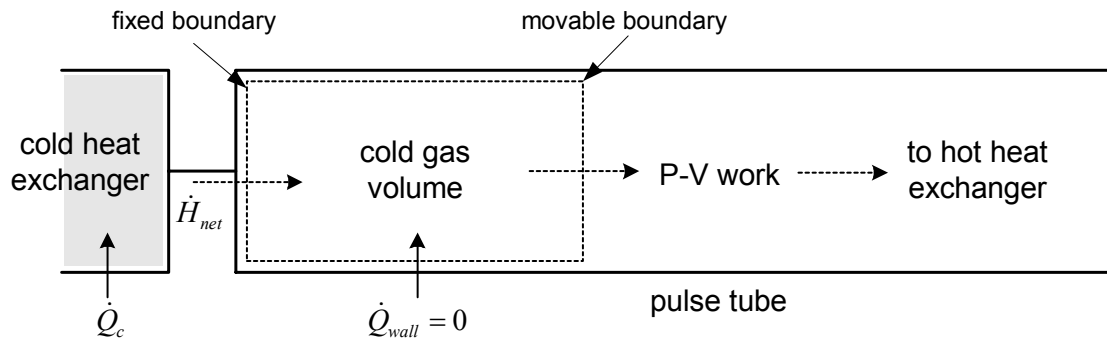
Figure 2.9 Imaginary cold gas volume in pulse tube delivering P-V work.
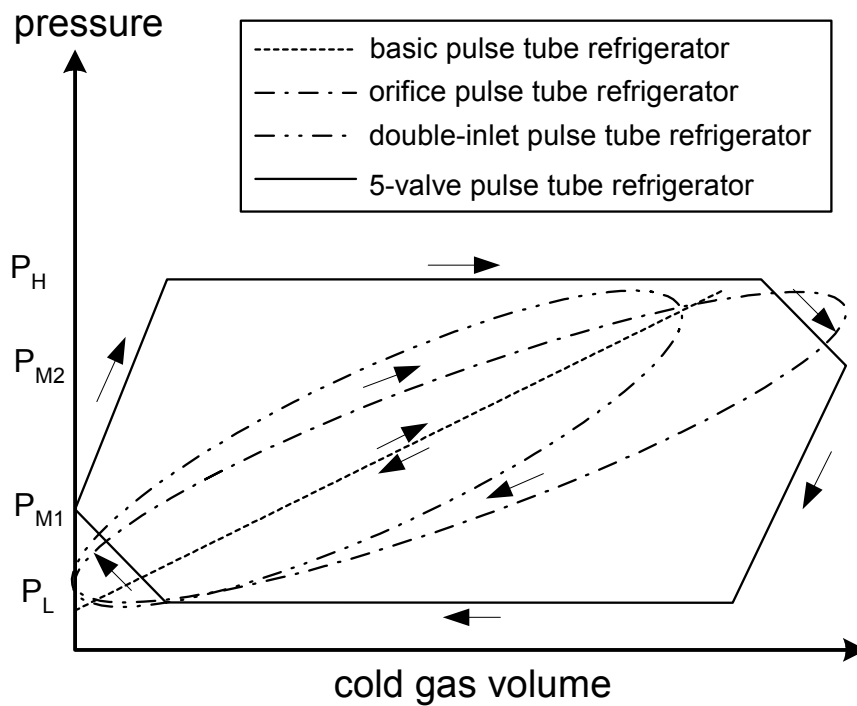
Figure 2.10 Schematic comparisons of P-V diagrams for various types of pulse tube refrigerators.

2.3   Pulse Tube Design

As mentioned in Chapter 1, the process of optimizing the geometric parameters to produce the highest cooling power for a fixed compressor capacity is an important issue. To date, this question has been answered largely through empirical means. For example, Fujimato et.al. [12] varied the length of their pulse tube, and found that cooling power increased with length, but that "the compressor power was too large for the pulse tubes used in [their] tests." Wang et. al. [13] found that the cooling capacity of their pulse tubes decreased as diameter (and volume) increased. An exception to the empirical approach is presented by Ravex et. al. [14] who confirmed the ability of their numerical model to optimize their pulse tube geometry for a specific compressor.

The possible loss mechanisms that have been identified for pulse tubes are DC flow, shuttle heat loss, pressure drop through the valve system and regenerator, conduction though the regenerator matrix, regenerator wall and pulse tube wall and radiation from the ambient. Several researchers have addressed these losses theoretically, experimentally and numerically. For example, L. W. Yang explored the shuttle heat transfer loss [16]. In his report, the surface heat pumping mechanisms between the gas and pulse tube wall for the basic, orifice and double-inlet orifice types of pulse tube were explained and compared. He also suggested a theoretical explanation defining certain limits in temperature at which the surface heat pumping mechanism turns into a shuttle heat loss. The amount of shuttle heat transfer was calculated by approximating the moving distances of the gas piston. Charles et. al. [17] demonstrated the effects of DC

flow (so-called permanent flow) in the double-inlet configuration by measuring temperature profiles along the regenerator and pulse tube wall. Their experiments indicated the direction of DC flow in a pulse tube system. A method for controlling DC flow was suggested.

In this report, three 5-valve pulse tube systems have been built to empirically investigate the effects of dimensions of pulse tube and regenerator. The iterative design method that optimizes the geometry of the 5-valve pulse tube system based on fixed compressor specification is detailed in Chapter 4. Also, in Chapter 5, the theoretical operating principle of the 5-valve pulse tube refrigerator is modeled numerically and other important loss mechanisms are analyzed in order to develop a realistic, predictive design tool.

Chapter 3 Experimental Apparatus

The 5-valve G-M type pulse tube refrigerator system consists of a compressor, regenerator, pulse tube, reservoir, heat exchangers and the valve system. This chapter includes detailed descriptions of the experimental apparatus that was used in the development of the 5-valve G-M type pulse tube refrigerator system. Three different pulse tube systems have been built to empirically investigate the effect of different dimensions of pulse tube and regenerator. One compressor was selected as the pressure generator and used to energize all three refrigeration systems.

3.1 Compressor

The main role of the compressor in a pulse tube refrigerator is to deliver high pressure working fluid to the regenerator and pulse tube. In this study, the Cryomech CP640 compressor has been selected. This compressor is a reciprocating, air-cooled, helium compressor that draws 5.5kW of electrical power. As shown in Fig. 3.1, two pressure gauges are located on the front panel and indicate the suction and discharge pressures. Two, flexible 5/8-inch AEROQUIP® hoses are used to connect the CP640

compressor to the valve system. The maximum and minimum operating pressure for the compressor are 325 psig and 45 psig, respectively. When the suction or discharging pressure reaches these limits, the compressor automatically shuts down. The helium gas used to charge the system should have a purity of 99.999% to remove any possibility of contaminating the compressor and the cold head of the pulse tube.
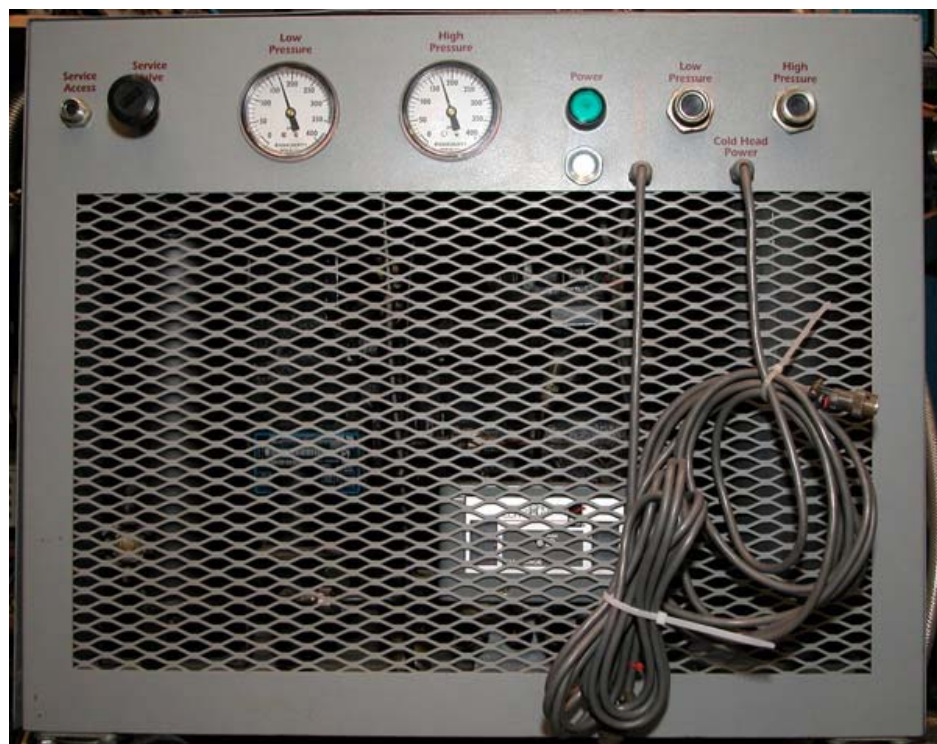
Figure 3.1 Cryomech CP640 helium compressor

3.2   Valve System

3.2.1 Orifice and solenoid valves

The valve system plays a very important role in the 5-valve pulse tube refrigerator. It controls the mass flow rate between the compressor and the pulse tube in order to generate an appropriate pressure wave. In the 5-valve pulse tube refrigerator, two different types of valves are required: orifice and solenoid valves.

The passive, orifice valves are manually opened and closed by turning a valve stem. Three passive orifice valves are installed in the system, as shown in Fig. 3.2 (V_{o-H}, V_{o-L} and V_{o-R}) and Fig. 3.3. All orifice valves are NUPRO$^{®}$ "L" series metering valves. The specifications and flow coefficient curve for the NUPRO$^{®}$ "L" series metering valves are shown in Table 3.1 and Fig. 3.4, respectively [18].

The active, solenoid valves are electronically operated by the valve timing controller, described in a later section. The CO-AX$^{®}$ solenoid valve (Model MK10) was selected based on the required response time and flow coefficient. The specifications are shown in Table 3.2 [19].
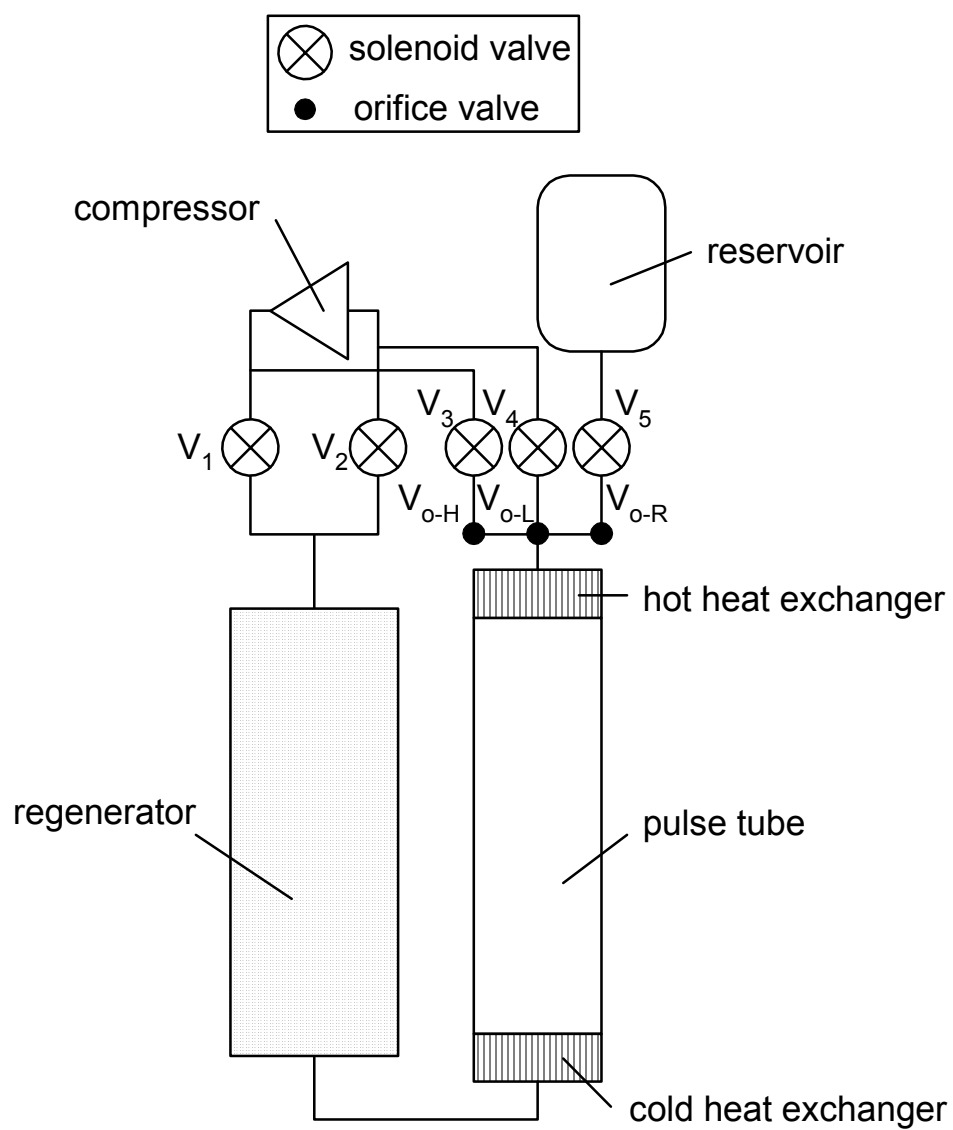
Figure 3.2 Location of orifice and solenoid valves in the 5-valve pulse tube refrigerator.
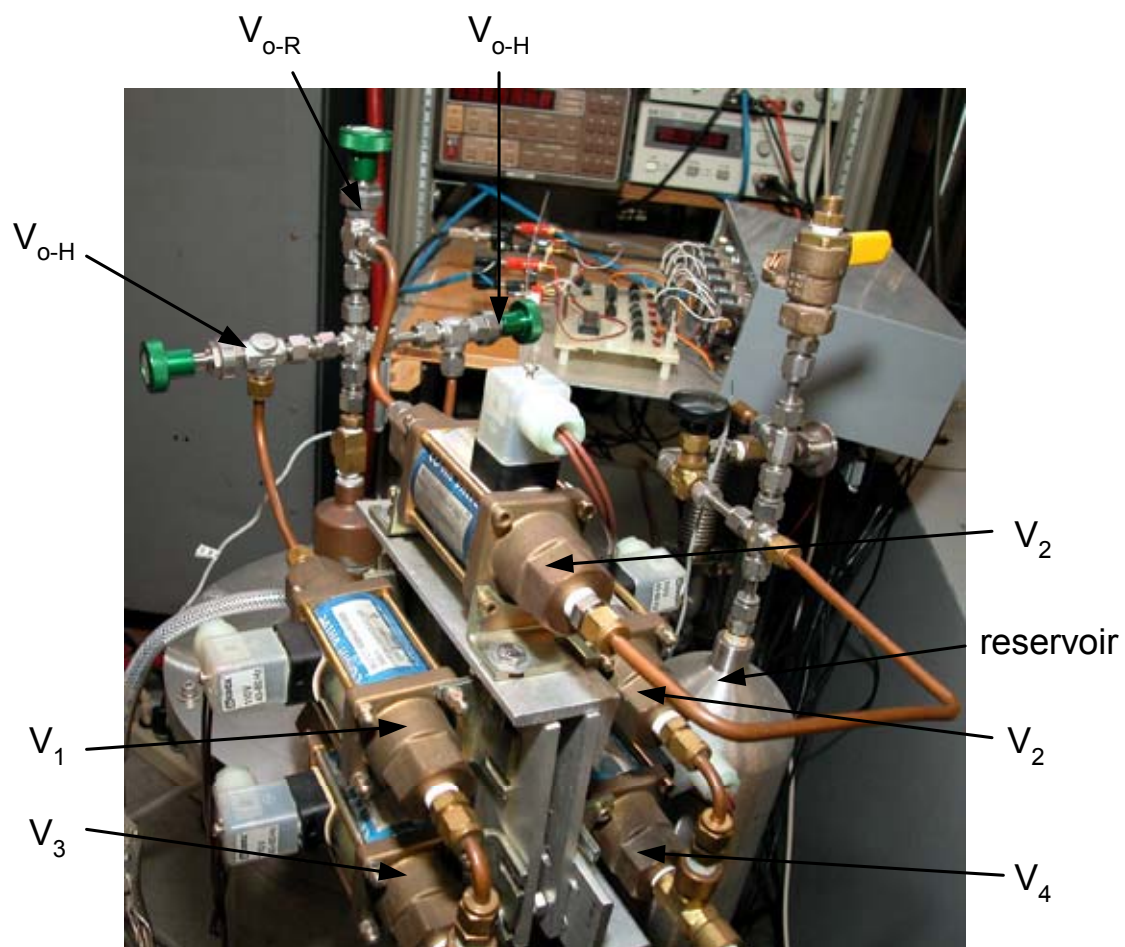
Figure 3.3 The valve system in the 5-valve pulse tube refrigerator.
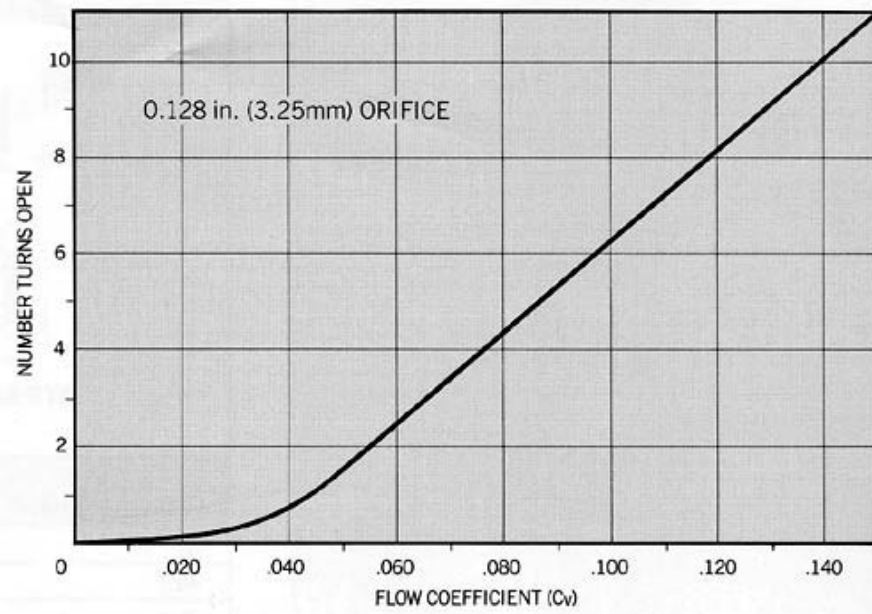
Figure 3.4 Flow coefficient for NUPRO® L-series fine metering valve[18].

Table 3.1 Specifications for NUPRO® L- series fine metering valve[18]

Orifice diameter	3.25 mm
Number of turns to open	0 ~ 11.75 turns
Maximum flow coefficient	C_v=0.15
Maximum working pressure	6.8 MPa

Table 3.2 Specifications for CO-AX® MK10 solenoid valve[19]

Orifice diameter	10 mm
Response time	25 msec
Maximum flow coefficient	C_v=3.5
Leak rate in vacuum	$<10^{-6}$ mbar/liter/s^{-1}

3.2.2 Valve timing controller

The valve timing controller has been designed and built in order to affect various pressure waves in the pulse tube during a previous study [3] at the UW-Madison. Here, the valve timing controller is adopted with no modification. The controller consists of two, three-state buffers (Model 74126), six triac drivers (Motorola, Model MOC3011), one synchronous pre-settable binary counter (Model SM74AS869) and one re-programmable EPROM (Model 2764A). Fig. 3.5 shows a circuit diagram of the valve timing controller and Fig. 3.6 shows the physical hardware. The valve timing controller controls the on/off states of five solenoid valves independently at any time in a cycle. The signal flow and valve control process are described in this section.

A binary square wave signal (0V or 5V) generated at the signal generator (Hewlett Packard, Model 3245A universal source) sends a clock signal to the synchronous, pre-settable binary counter. One cycle of valve operations is divided into 64 steps, enough to produce the pressure wave properly. The number of steps is adjustable and independent of the period of cycle. Thus the operating frequency of the refrigerator can be adjusted by varying the signal frequency produced by the signal generator. For example, when the signal generator sends a square wave to the valve controller at a frequency of 128Hz, the cycle frequency of the refrigerator system is 2Hz (=128/64). The re-programmable EPROM contains 64 pieces of binary information that represent which valve should be opened and closed during each step of a cycle. By changing this information using the EPROM programmer and eraser (Walling Co., Model Datarase II),

the valve timing controller can generate a virtually infinite number of valve opening/closing combinations. An excitation signal passed through the EPROM is sent to triac drivers, which open and close the five solenoid valves by providing 100V signals to each solenoid relay.
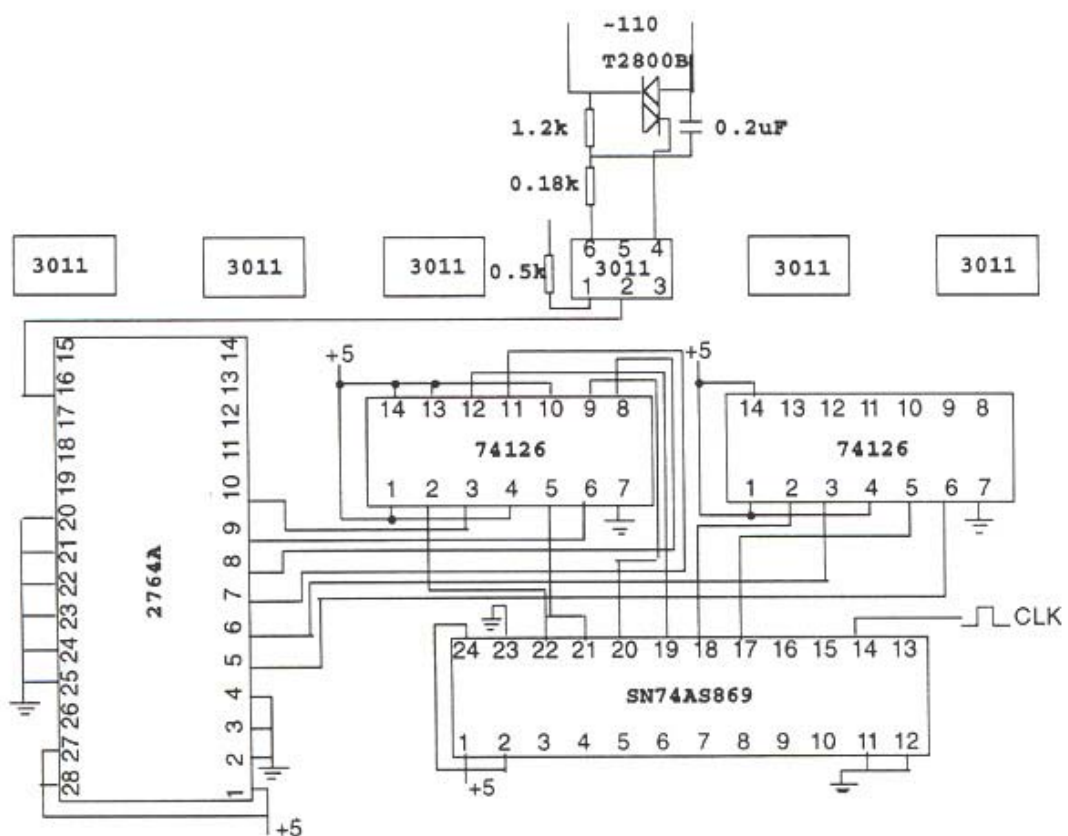
Figure 3.5 Circuit block diagram of valve timing controller[3].
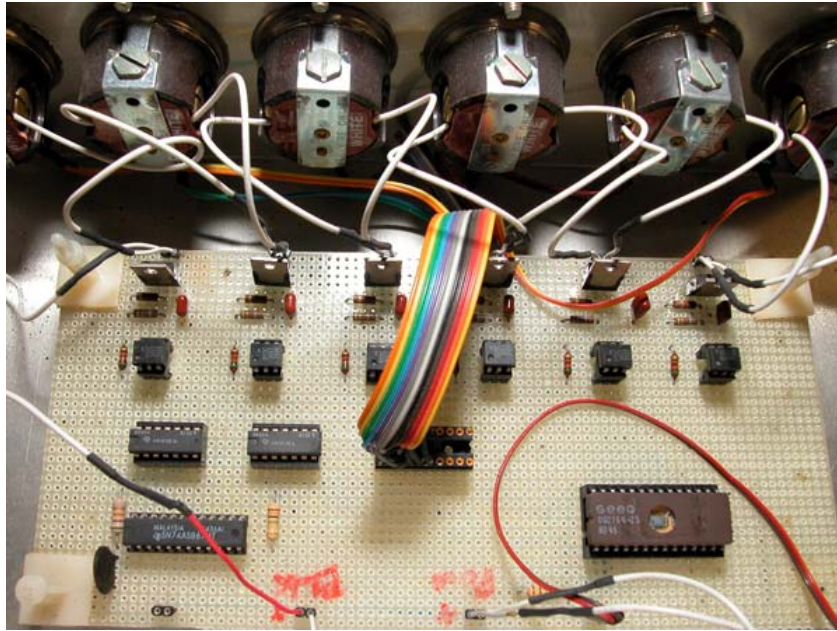
Figure 3.6 The valve timing controller

3.3 Refrigeration System

The refrigeration system exclusive of the compressor and the valve system consists of the regenerator, the pulse tube and the cold and hot heat exchangers. Three refrigeration systems with different dimensions of regenerator and pulse tube have been designed, built and tested. The aspect ratios of the regenerator and pulse tube were varied to investigate its effect on cooling power. All of the three systems use the same compressor and valve system, described in the previous sections. Tables 3.3 and 3.4 show the dimensions of the pulse tube and regenerator for systems I, II, and III.

Table 3.3 Pulse tube dimensions for various systems

Dimension	System I	System II	System III
Outer diameter	33.7 mm	38.2 mm	55.5 mm
Inner diameter	32.0 mm	37.4 mm	53.8 mm
Length	448 mm	332 mm	94.2 mm
Internal volume	360 cm^3	365 cm^3	214 cm^3
Aspect ratio*	14	8.9	1.75

(* Aspect ratio = Length / Inner diameter)

Table 3.4 Regenerator dimensions for various systems

Dimension	System I	System II	System III
Outer diameter	36.5 mm	36.5 mm	66.4 mm
Inner diameter	35.5 mm	35.5 mm	60.2 mm
Length	213 mm	213 mm	65 mm
Porosity (screens / lead shots)	0.685 / 0.38	0.685 / 0.38	0.685 / 0.38
Dead volume	123 cm^3	123 cm^3	108 cm^3
Aspect ratio*	6	6	1.1

(* Aspect ratio = Length / Inner diameter)

Both the regenerator and pulse tube are made of a thin stainless steel tube to decrease conduction loss from ambient to the cold end. Four, 0.5-inch thick CONFLAT flanges are welded to each end of the regenerator and pulse tube. The CONFLAT flanges facilitate changing regenerator and pulse tube.

The regenerator matrix is composed of 200x200 mesh stainless steel screens, 200x200 mesh copper screens and 250~500 micron diameter lead shots. These materials are stacked in order from the hot to the cold end. The volumes of the three materials are approximately equal.

The cold heat exchanger is designed to allow heat exchange between the gas and the load heater and also act as a flow straightener. It must also function as a copper gasket between the CONFLAT flanges on the regenerator and the pulse tube. The cold heat exchanger is made of a cylindrical oxygen free copper (OFCu) block. Several 200x200 mesh copper screens are soldered to the inner surface of the block to increase the heat transfer area between the gas and the heat exchanger wall. The machining drawing and a picture of the cold heat exchanger are shown in Figures 3.7 and 3.8. A 0.2-inch diameter of hole is drilled from the outer side of the copper block in order to mount a temperature sensor. Also, a Minco-brand tape is attached to the outer surface of the cold exchanger block in order to apply a heat load. The cold heat exchanger block has the correct dimension to fit in the standard CONFLAT knife-edge so that it can be directly located between the CONFLAT flanges on the pulse tube and the regenerator.
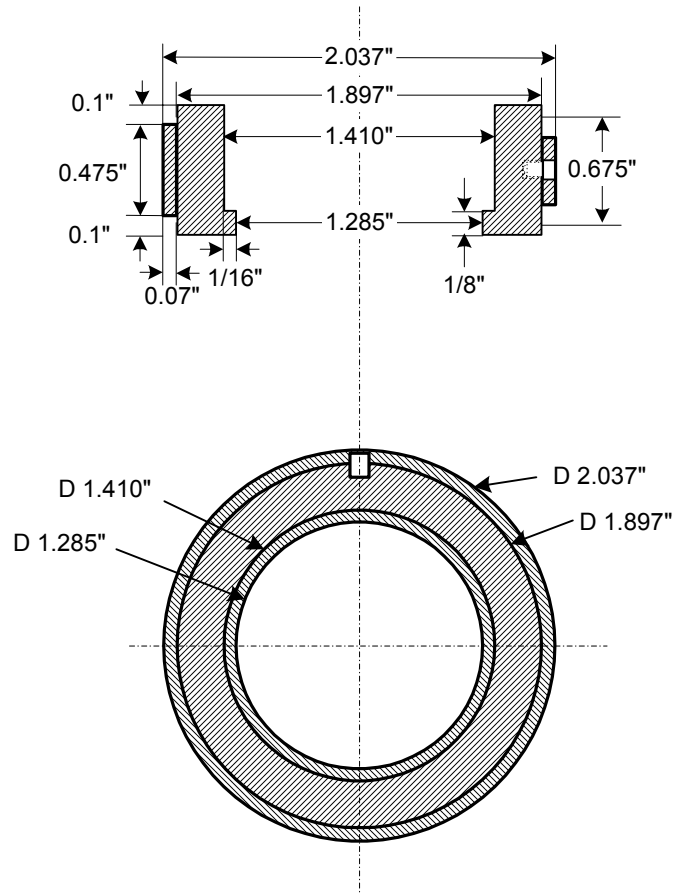
Figure 3.7 Machining drawing of cold heat exchanger for System I and II. (unit : inch)
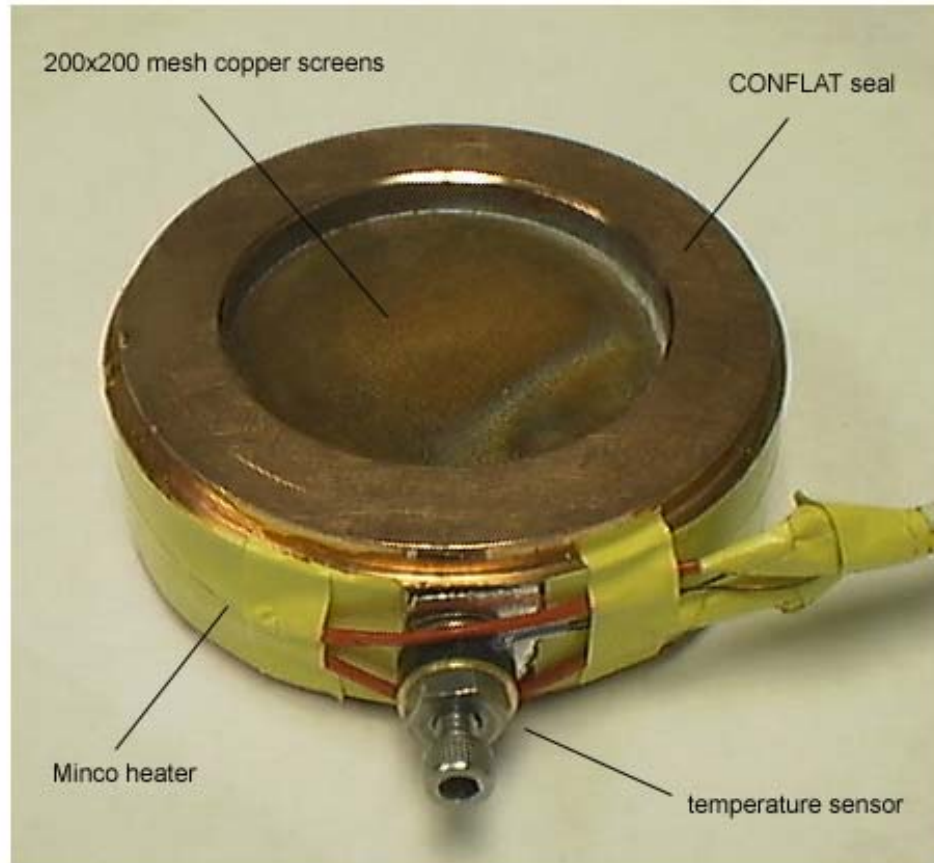
Figure 3.8 Cold heat exchanger with Minco® tape heater and Lakeshore® silicon diode temperature sensor.

A shell-and-tube type heat exchanger has been designed and built to extract heat out of the helium gas at the hot end of the pulse tube. Helium gas flow though a total of 19, 1/8-inch outer diameter stainless steel tubes that are cooled by a continuous flow of 15°C cold water. The outer shell of the heat exchanger is made of 1.5-inch outer diameter

copper tube and is silver-brazed to the flow straightener that separates the hot heat exchanger and pulse tube. The flow straightener has a flat surface that is compatible with the knife-edge welded on the top flange of the vacuum chamber. Fig. 3.9 shows a schematic assembly of the hot heat exchanger.

Figures 3.10, 3.11 and 3.12 show the three refrigeration systems. All of the components have been leak tested to 10^{-5} Torr and pressure tested to 2500kPa in order to qualify the welded joints and CONFLAT flanges prior to installation.

to reservoir

cooling
water

19, 1/8" OD
tubes

helium flow

cooling
water

bolted to
top flange

to CONFLAT flange
on the pulse tube
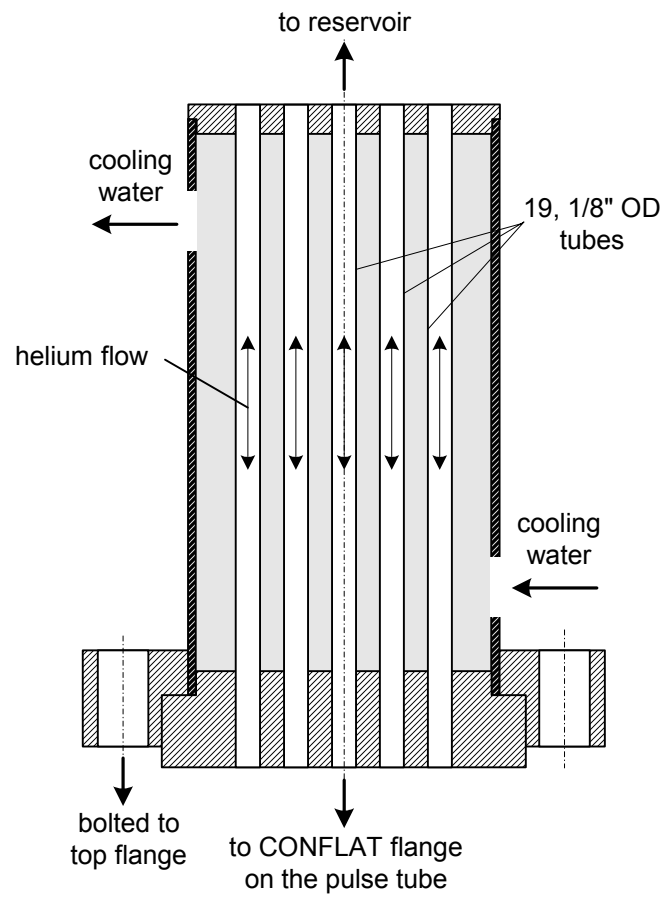
Figure 3.9 Hot heat exchanger assembly.
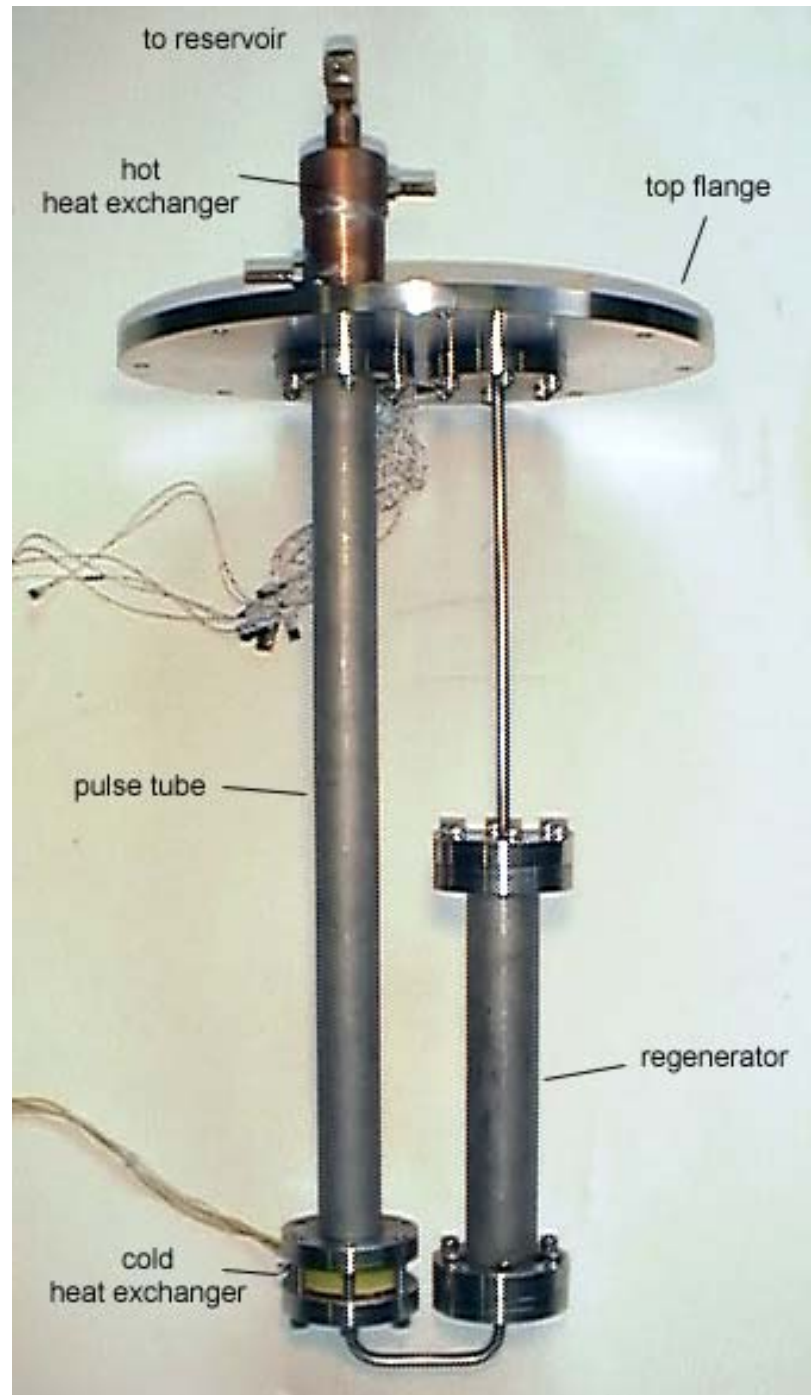
Figure 3.10 System I
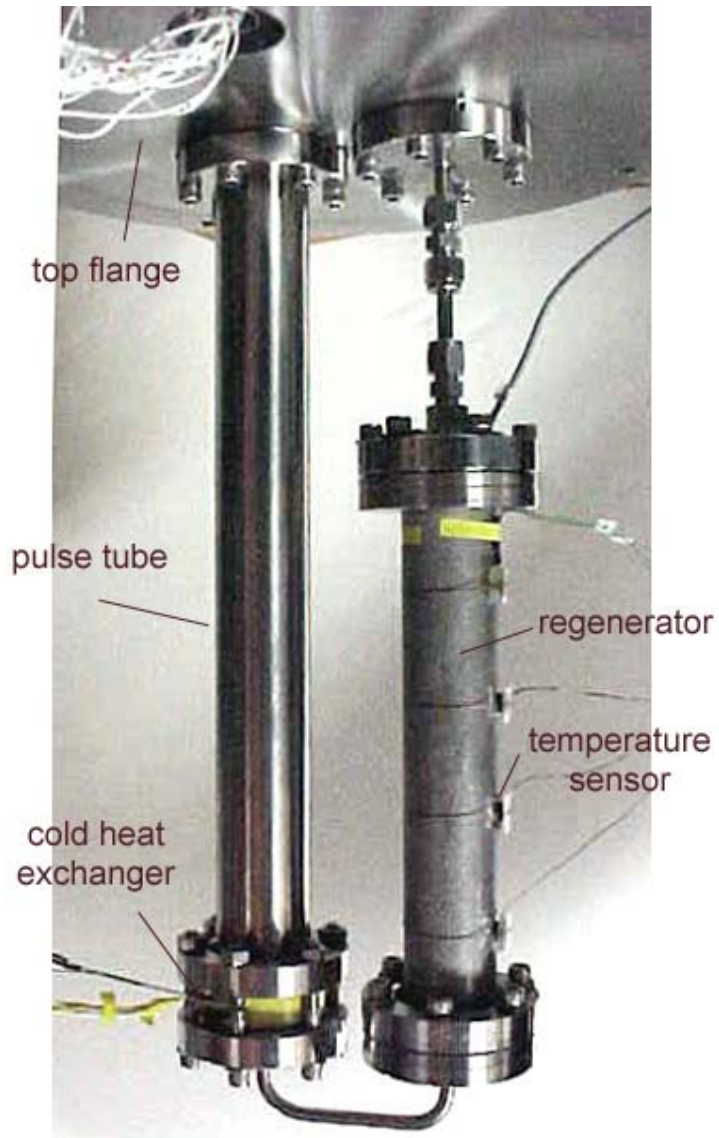
Figure 3.11 System II
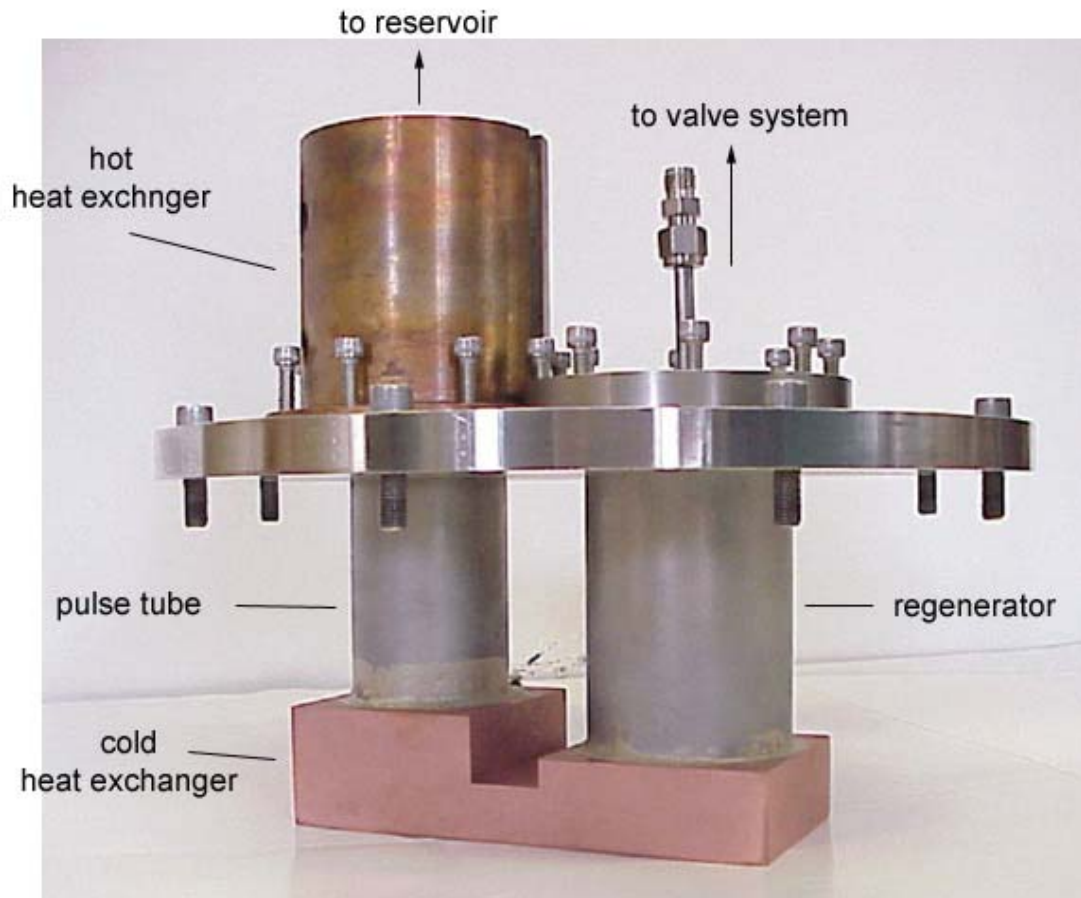
Figure 3.12 System III

3.4 Instrumentation

The measurements taken with the various types of refrigeration systems provide a description of the effect of regenerator and pulse tube geometry on the minimum cold end temperature and the temperature dependent cooling power. The information is provided in the form of of pressure and temperature measurements.

Experimentally, it is found that the cooling performance of the pulse tube refrigerator is strongly dependent on the temporal shape of the pressure wave in the pulse tube. Three piezoresistive pressure transducers (ENDEVCO, Model 8510B-500) have been installed at the hot end of the regenerator, the hot end of the pulse tube and at the reservoir to provide the pressure information. The pressure transducers show very good linearity. All of the pressure sensors are calibrated by a Bourden gauge up to 350psig. The main specifications and the calibration curves are shown in Table 3.5 and Fig. 3.13 [20].

Five temperature sensors have been installed in the regenerator, the pulse tube, and the cold heat exchanger in order to measure the temperature profiles along the pulse tube and regenerator wall. Their mounting locations are shown in Fig. 14. Three silicon diode temperature sensors (SD, Lakeshore, Model DT-470-SD) were selected to measure the lower temperature region of the pulse tube wall and the cold heat exchanger. Two platinum resistance thermometers (PRT, Lakeshore, Model PT-103) were mounted on the middle section of the regenerator and the hot region of pulse tube wall. The specifications

of the temperature sensors are summarized in Table 3.6 [21]. The specifications of other instruments including the DC power supply, current source, oscilloscope etc. are shown in Table. 3.7.

A turbo-molecular vacuum pump system combined with mechanical vacuum pump (Leybold, Model TOPS) was used to provide less than 10^{-5} Torr of vacuum pressure in the vacuum chamber. The pirani gauge (Leybold, Model TR901) and the ion gauge (LDS, Model G-75) measure the pressure in the vacuum chamber.

The cleaning process during assembly and prior to the gas purging process is required to avoid the possibility of contamination in the system. The pulse tube and the regenerator were cleaned with Acetone to remove any oil residue and then completely dried. All of the tubings that connect the components and the vacuum chamber were cleaned, too. The refrigeration system was purged several times after the assembly by sequentially charging the system to 2000kPa with 99.999% pure helium gas and then evacuating it to less than 10^{-5} Torr.

Fig. 3.15 shows a photograph of the 5-valve G-M type pulse tube refrigerator integrated with the Cryomech CP640 compressor.

Table 3.5 Specifications for the ENDEVCO® 8510B-500 pressure transducers[20]

Operating pressure	0-500 psig
Operating temperature	255 K – 366 K
Resonance frequency	500 kHz
Sensitivity	0.6 ± 0.2 mV/psi
Excitation	DC 10 V
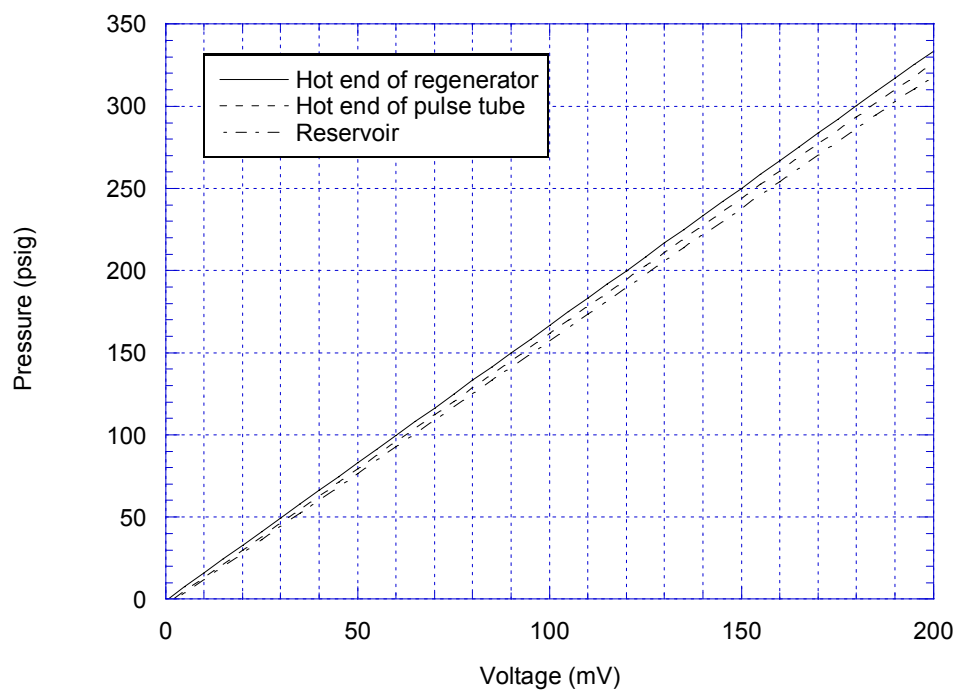
Figure 3.13 Calibration curves for the three pressure transducers.
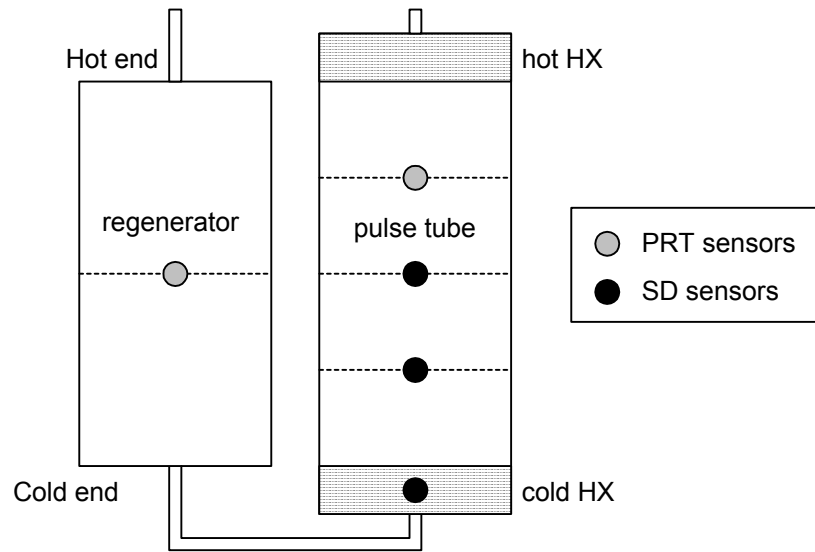
Figure 3.14 Installation locations of the Lakeshore® temperature sensors.

Table 3.6 The specifications of the Lakeshore® temperature sensors[21]

Model	SD-470	PT-103
Operating temperature range	1.4K - 475 K	14 K - 873 K
Accuracy	± 20 mK at <10K ± 50mK at 10 K to 330 K	$\pm$ 20 mK at 100K $\pm$ 35 mK at 300K
Thermal response time	Typical < 10 ms at 4.2 K 100 ms at 77 K 200 ms at 305 K	1.75 S at 77K 12.5 S at 273 K
Excitation current	10 µA ± 0.05%	1 mA
Dimensions	1 mm (H) x 1.9 mm (W) x 3.2 mm (L)	1.6 mm (D) x 12.1 mm (L)

Table 3.7 The specifications of other instruments used in the experiment

Product	Manufacturer & Model	Functions
Oscilloscope	Hewlett Packard 54540A	Acquirement of pressure wave from pressure transducer
Multimeter	Hewlett Packard 3458A	Acquirement of voltages from SD and PTR sensors
Triple output power supply	Hewlett Packard 6236B	Excitation of pressure transducers
DC power supply	Hewlett Packard 3611A	Excitation of tape heater at cold heat exchanger
Current source I	Lakeshore 120	Excitation of SD sensors
Current source II	Keithley 222 programmable	Excitation of PTR sensors
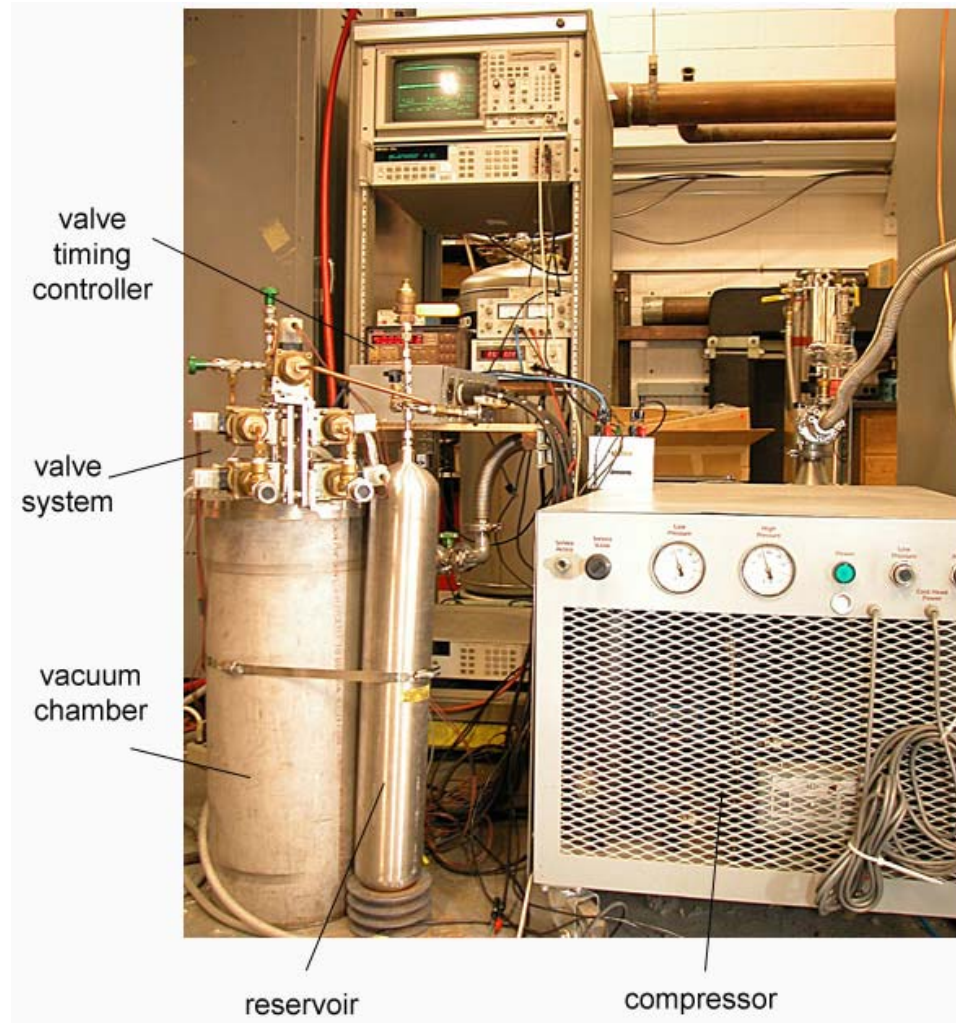
Figure 3.15 The G-M type 5-valve pulse tube refrigerator.

3.5 Operation

After the purging process, the pulse tube system is ready to operate. The detailed operation procedures are as the followings.

1. All of the instrumentations are turned on to monitor the pressure and the temperatures of the system.

2. The turbo-molecular vacuum pump is connected to the vacuum chamber. The vacuum chamber is evacuated to less than 5×10^{-5} Torr and maintained during the operation.

3. The EPROM programmed with the desired valve opening timing is installed in the valve timing controller.

4. The five solenoid valves start to operate with three orifice valves completely opened.

5. The cold water is supplied to the hot heat exchanger.

6. The initial pressurization is started by opening the regulating valve of the high pressure helium gas cylinder. The refrigeration system and the compressor is charged with helium gas to 190~200psig. After the pressurization, the regulator valve is closed and the solenoid valves are still opened until the pressure in the system is stabilized. It usually takes less than a minute.

7. Three orifice valves are adjusted to proper openings.

8. The compressor starts to operate and the pressure and the temperatures are monitored as a function of time and position until the steady state conditions are obtained.

9. The three orifice valves can be adjusted during the operation, if needed.

10. The no-load temperature is measured and the corresponding pressure waves are recorded at the oscilloscope.

11. The heat load is applied to measure temperature dependent cooling power.

In this study, approximately forty valve opening timings have been recorded in the re-programmable EPROMs, and all of them have been tested for three different refrigeration systems to determine the optimal operating conditions. For each valve opening timing and the refrigeration system, at least two operations were performed to verify the repeatability of the performance. The system usually reached the steady state condition within 2-3 hours. The ranges of the no-load temperatures were varied from 24.6K to 130K with three refrigeration systems. The heat loads applied from 3W to 20W, which were dependent on the system performance. All of three refrigeration systems reached 50K. The lowest temperature of 24.6K was achieved with the system-I. Overall, the system-I showed better performances than other systems for various valve opening timings.

Chapter 4 Compressor-specific Design of a Single Stage Pulse Tube Refrigerator

This chapter outlines a procedure for designing a G-M type pulse tube refrigerator that will provide the maximum possible cooling capacity for a fixed compressor. The procedure identifies the constraints imposed by the compressor, as well as those associated with the pulse tube and regenerator geometries. The process begins by defining a compressor map in terms of mass flow, compressor work, and the inlet and outlet pressures. Practical considerations regarding the pulse tube volume and valve system determine the attainable region of the compressor map, and an iterative method is presented to optimize the geometry of the pulse tube refrigerator. The specific characteristics of a Cryomech CP640 compressor are used to illustrate the compressor constraints. In the iterative process, the thermodynamic model developed by Yuan & Pfotenhauer [2] is used to calculate the geometry dependent cooling capacity of a 5-valve pulse tube refrigerator. However, the same process can be used to optimize other pulse tube configurations with alternate methods for calculating the cooling power.

4.1 Compressor Characteristics

The mass flow delivered by a reciprocating compressor can be expressed (see for example references [22-24]) in terms of the displaced volume V_d, the clearance volume V_c, clearance volume ratio $C = V_c / V_d$, compressor speed S, the inlet and discharge pressures P_{in}, P_{out}, and the polytropic compression exponent n, according to the eqn.:

$$\dot{m} = \left[1 + C - C \left(\frac{P_{out}}{P_{in}} \right)^{1/n} \right] \rho_{in} V_d S \qquad (4.1)$$

Here the polytropic exponent, n is associated with the expression

$$PV^n = \text{Constant} \qquad (4.2)$$

that describes the relationship between pressure and volume during the compression and expansion processes. The possible values of n are bounded by $n = 1$ (minimum) for an isothermal compression process, and $n = C_p/C_v$ (maximum) for an adiabatic compression process. Here C_p and C_v are the specific heat at constant pressure and constant volume, respectively. The expression given in eqn. (4.1) results from considerations regarding the volumetric efficiency of a reciprocating compressor and has been extensively verified in a recent investigation [24] of commercial compressors used in the refrigeration industry. An expression for the electric power consumed by the compressors is also provided in the same study [24], and is given as:

$$\dot{W}_e = \dot{m}\frac{n}{n-1}RT_{in}\left[\left(\frac{P_{out}}{P_{in}}\right)^{\frac{n-1}{n}}-1\right]/\eta_{comb} \qquad (4.3)$$

Here η_{comb} is the combined efficiency associated with converting electrical power to mechanical power and mechanical power to *P-V* work. A typical value of this efficiency is $\eta_{comb} \approx 0.6$ for a wide variety of compressors. Although the values for the clearance volume and the polytropic exponent that are required in eqn.s (4.1) and (4.3) are not readily available from the commercial compressor vendors, these can be obtained from a few performance measurements for the specific compressor of interest. Thus it is possible to accurately define the mass flow rate that will be delivered by a compressor for a given set of inlet and outlet conditions.

The compressor map defined by eqn.s (4.1) and (4.3) for the Cryomech CP640 is shown in Fig. 4.1. Using measurements of mass flow rate for various inlet and outlet pressures at an inlet temperature of 315K, we determined values of the clearance ratio *C* = 0.07 and polytropic exponent *n* = 1.55. The sensitivity of the mass flow rate to P_{in}, and its insensitivity to P_{out} can be understood in terms of the expression

$$\dot{m} = \rho_{in}V_d S\eta_{vol} \qquad (4.4)$$

Except through the relatively weak dependence of the volumetric efficiency, η_{vol} on the outlet pressure, the mass flow is determined by the inlet conditions. The compressor

work, on the other hand is dependent on both P_{in} and P_{out}, and is larger at higher values of P_{out}.

Constraints imposed by the compressor define three limitations to mass flow that can be identified on the compressor map. A minimum inlet (suction) pressure and a maximum outlet (discharge) pressure define the first two of these. For the Cryomech CP640, these are respectively defined by $P_{in} = 446$kPa and $P_{out} = 2308$kPa. The third constraint is unlikely to be encountered for a pulse tube system, but is defined by the condition $P_{in} = P_{out}$.

4.2 Optimization Design Process

Within the constraints imposed by the compressor, Fig. 4.1 displays a wide range of mass flow rates that are available and many combinations of inlet and outlet pressure. The cooling power of a pulse tube refrigerator depends on all three of these parameters. It is therefore of interest to determine both the region of the compressor map that affords the largest pulse tube cooling capacities and which of those regions are accessible in real systems. The first of these questions is answered for the case of a 5-valve pulse tube refrigerator using an iterative process described by the flow diagram in Fig. 4.2.
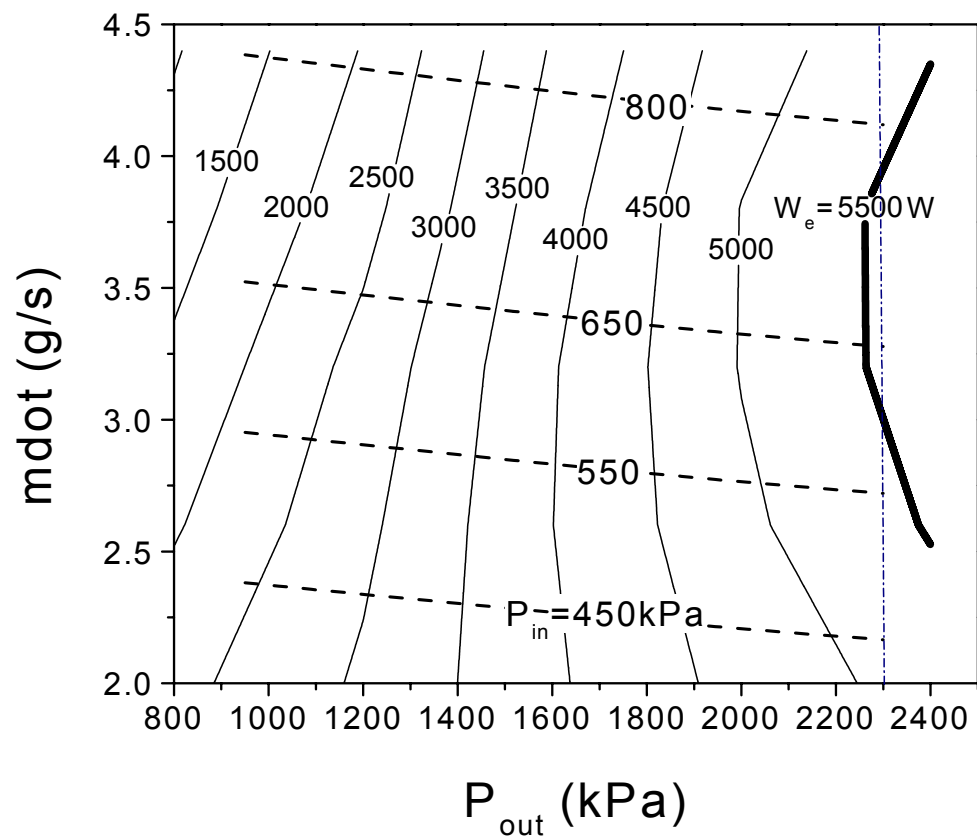
Figure 4.1 Compressor map for the Cryomech CP640 reciprocating compressor.
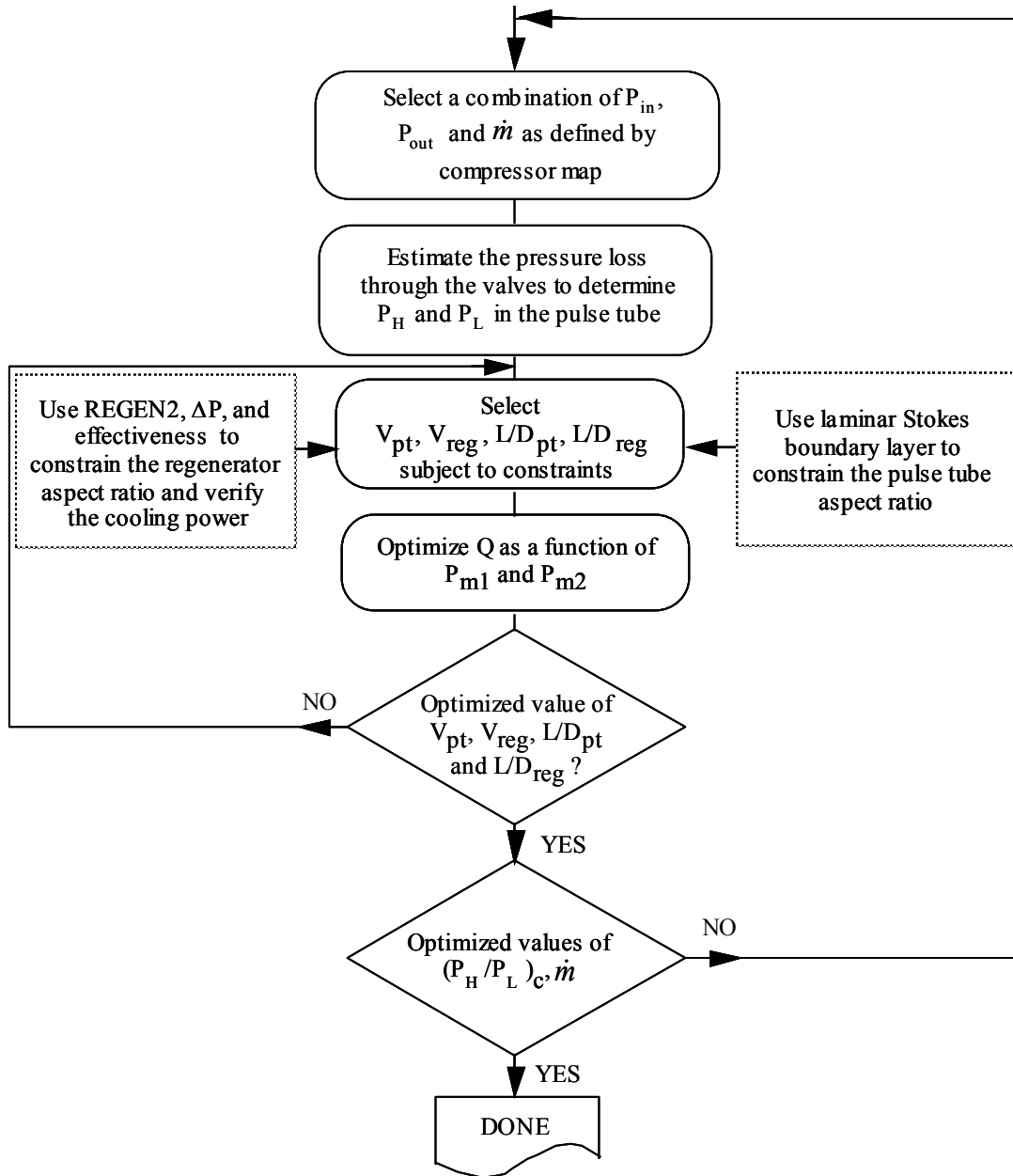
Figure 4.2 Flow diagram of iterative design process to optimize a pulse tube system geometry for

maximum cooling power given a specific values of P_H, P_L, and mass flow rate.

The iterative design process begins by considering pressure losses across the inlet and outlet valves connecting the pulse tube system to the compressor. In view of the energy losses that are directly associated with such a pressure drop, it is important to minimize the flow resistance associated with these valves. For all valved G-M type pulse tube systems, the pressure swings experienced in the pulse tube system will be less than those produced by the compressor. In Fig. 4.2, P_H and P_L represent the high and low pressures realized in the pulse tube system and not produced by the compressor.

The next step requires the selection of the pulse tube operating, or cold end, temperature. This selection is of course not arbitrary and must be based on reasonable limits for a single stage pulse tube cooler ($T_c \geq 20K$), appropriate selection of regenerator matrix material, and admittedly some previous experience. In the examples to follow, the value of T_c has been set at 30K. With the values of T_c, P_H, P_L, and mass flow rate through the pulse tube fixed, one might expect that the pulse tube volume would be fixed. In fact, an iterative process is required to determine the combination of pulse tube and regenerator gas volumes associated with the fixed conditions that maximize the resulting cooling power. The ratio of the pulse tube volume to the gas (or non-solid) volume in the regenerator (Γ) characterizes the competing effects of expansion volume and pressure loss: large values of Γ maximize the expansion volume in the pulse tube, but produce large pressure drops through the regenerator. While small values of Γ minimize the pressure loss through the regenerator but sacrifice expansion cooling in the pulse tube.

In addition to optimizing the cooling power as a function of Γ, the length-to-diameter aspect ratio of both the pulse tube and regenerator can be optimized for each value of Γ and mass flow rate. For the case of the pulse tube, the aspect ratio is chosen to be as large as possible in order to minimize conduction losses through the walls, but not so large that the boundary layer velocity becomes turbulent. The laminar to turbulent transition is defined by the condition that the Reynolds number be less than 280 [25]. The characteristic dimension in the Reynolds number is defined by the Stokes boundary layer thickness

$$\delta = \sqrt{\frac{2v}{\omega}} \qquad (4.5)$$

where v is the kinematic viscosity and ω is 2π times the operating frequency. The laminar condition constrains the cross sectional area of the pulse tube to be larger than a minimum value defined by

$$A_{min} \geq \frac{\dot{m}\delta}{Re\,\rho\,v} \qquad (4.6)$$

For the regenerator, the computer program REGEN2 is used to balance the conduction and regenerator ineffectiveness against the pressure drop through the regenerator [26]. In these designs, a maximum allowable pressure drop of 50kPa has been selected. Fig. 4.3 displays the cooling power, pulse tube volume, and regenerator

gas volume as a function of Γ for one set of P_H, P_L, and mass flow rate values. In this case, a decreasingly significant benefit is realized by increasing Γ beyond 8. In the interest of a compact design, this value of Γ is chosen for the optimized design.
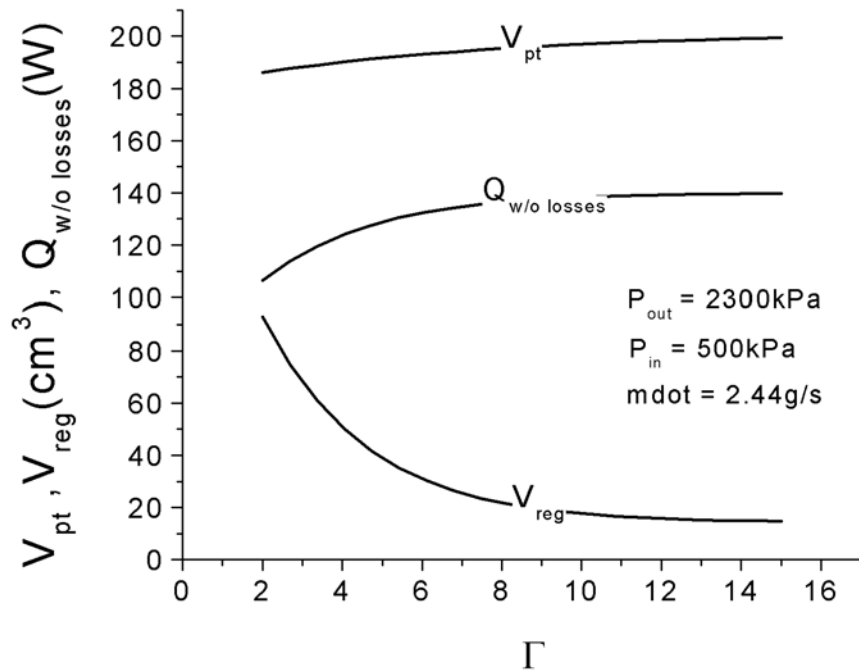
Figure 4.3 Geometry optimization of pulse tube and regenerator volumes for single set of P_H, P_L, and mass flow rate values.

During the optimization process for the regenerator and pulse tube geometries, two intermediate pressures, P_{M1}, P_{M2} are used as the optimizing parameters. As shown in Fig. 2.8 and Fig. 2.10, the intermediate pressures directly affect the net cooling power by changing the shape and internal area of the P-V diagram.

The same process described in the previous paragraph, carried out for a variety of inlet and outlet compressor pressures, results in the cooling powers shown in Fig. 4.4. At low values of the outlet pressure, a weak pressure wave is generated in the pulse tube and increasing the inlet pressure further reduces the pressure oscillations and therefore the cooling power. At high values of outlet pressure, the dependence of the cooling capacity Q on the inlet pressure is reversed. In this case, increased inlet pressures produce an increased density at the compressor inlet, a larger mass flow rate, and therefore more cooling power. It is of obvious interest to know which parts of this map are accessible for a real pulse tube system and what steps can be taken to reach the desirable region of combined high outlet and high inlet pressures.
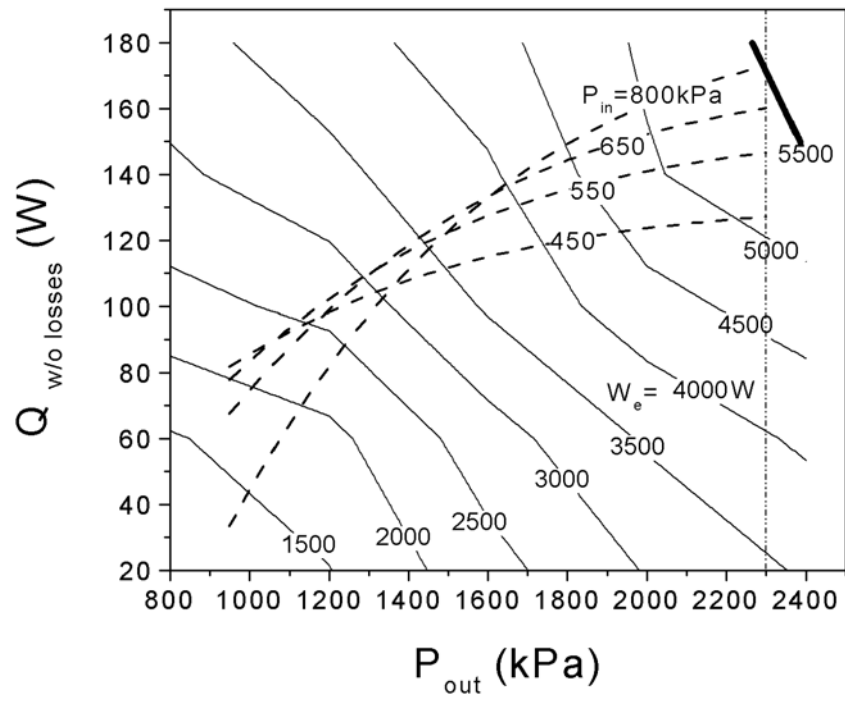
Figure 4.4 Pulse tube cooling capacities as a function of compressor characteristics.

4.3 Pulse Tube System Options

From the results displayed in Fig. 4.4, it is clear that the maximum outlet pressure permitted by the compressor corresponds closely with its rated power capacity. Operating at $P_{out,\max}$ is a necessary, but not sufficient condition for maximizing the cooling power of a pulse tube system attached to the compressor. It is also desirable to maximize P_{in} as well. How can this be achieved?

Beginning with the case of an ideal pulse tube system - that is, one with no losses - one can consider the influence of pulse tube size on the pressures in the pulse tube system. Fig. 4.5 depicts the high and low pressures that will result in a pulse tube system as a function of the charging pressure, for a small and large volume pulse tube system. The maximum and minimum charging pressures in the pulse tube system are constrained by the compressor's maximum discharge and minimum suction pressures respectively.

A small volume pulse tube system will experience large pressure oscillations, while the large volume will experience smaller pressure oscillations.   The arrows, represent the pressure swing that can be realized in each pulse tube system when it is charged to its maximum allowable pressure and reveal that although the pressure oscillations will decrease as the pulse tube volume is increased, for a constant P_{out}, the inlet pressure will increase with pulse tube volume.

This intuitive consideration is confirmed by the calculations displayed in Fig. 4.6. Here the same cooling powers as calculated in Fig. 4.4 are shown with their

corresponding optimized pulse tube volumes. For the highest values of P_{out}, Q clearly increases as the pulse tube volume is increased while at lower values of P_{out}, Q decreases with pulse tube volume.
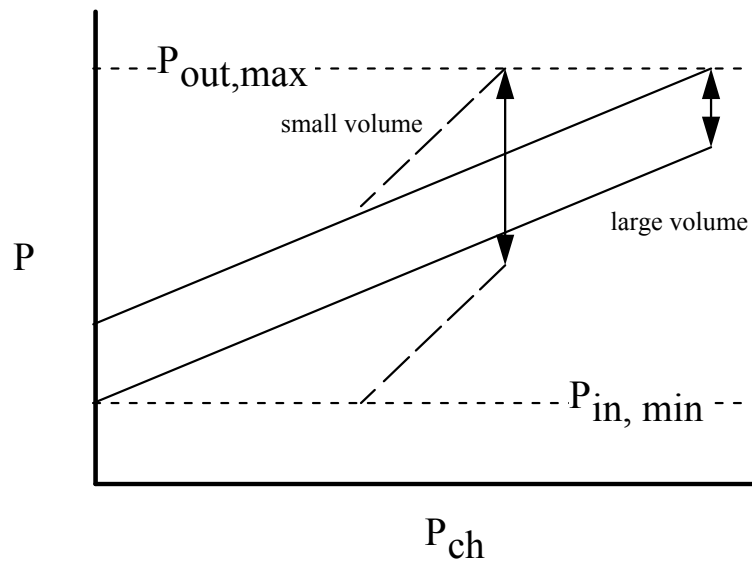
Figure 4.5 Depiction of pressures realized in pulse tubes as a function of the charging (average) pressure, P_{ch}, and as limited by the minimum and maximum pressures provided by the compressor.
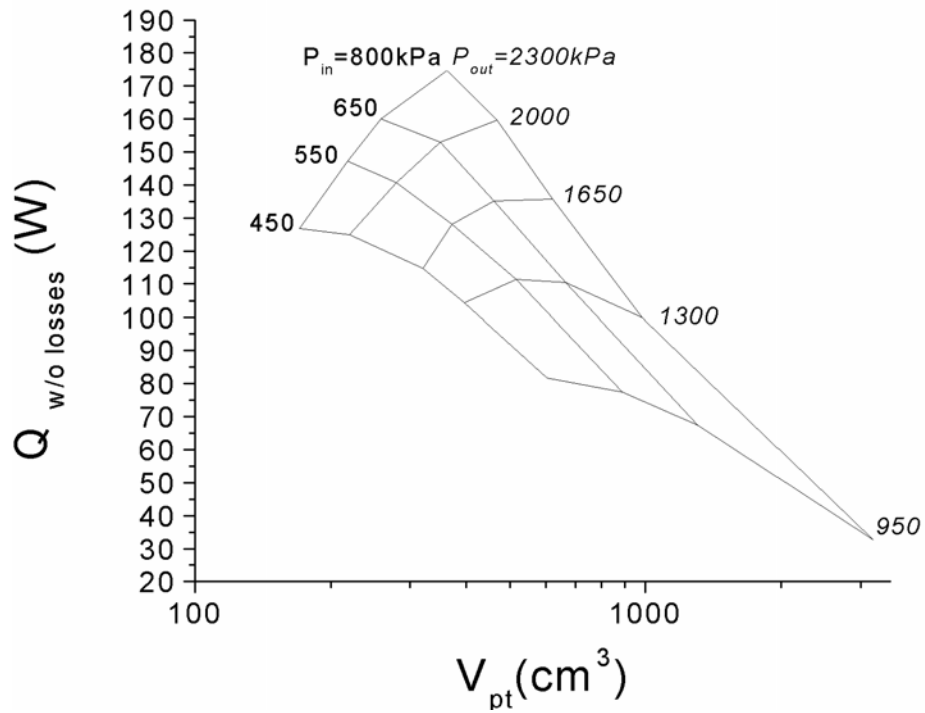
Figure 4.6 Ideal cooling power vs. the optimized pulse tube volume for the various combinations of high and low pressures produced by the Cryomech CP640 compressor.

4.4   Real System Constraints

Based on the calculations displayed in Fig. 4.6, one may wonder whether an upper limit to the pulse tube system volume exists. In a real pulse tube system, losses associated with the pressure drop through the valves and regenerator, and conduction losses (as the pulse tube volume increases, the optimized aspect ratio decreases) impose practical limits and define a different optimum pulse tube volume for maximum cooling power. Repeating the same procedure that resulted in Figs. 4.4 and 4.6, but including the losses realized in our valve system, the 50kPa pressure drop through the regenerator, and conduction losses through the pulse tube and regenerator structure, provides the results shown in Fig. 4.7. The optimum pulse tube volume falls to approximately 250cm^3, with associated values of $\Gamma \approx 12$, and a pulse tube aspect ratio of 8. For this design, a cooling power of 60W is expected at 30K. Two additional losses have yet to be included in our model; those associated with shuttle heat loss, and DC flows. We expect therefore that the actual cooling power will be significantly less than 60W at 30K. The significance of valve losses is clearly evident through this design process.

The results provided in Figs. 4.4, 4.6, and 4.7 also permit an estimate of efficiency for G-M type pulse tube refrigerators. For the ideal case (ignoring losses) depicted in Fig. 4.4, one finds that the COP - the ratio of cooling power to input power - associated with the maximum possible cooling power of a pulse tube operating at 30K and driven by

the CP640 compressor is 0.03, or 28% of Carnot. A more realistic value, including conduction losses and pressure drop through the regenerator is 0.015, or 14% of Carnot.

Applying the above procedure to the CTI 8500 compressor used by Ravex et.al. [14], we find that an optimum pulse tube volume for operation at 30K would be approximately three times larger than the geometry that they used (380cm^3 vs. 132cm^3), but that the aspect ratios of the pulse tube and regenerator would be similar. (L/D$_{pt}$ = 6 vs. 5, L/D$_{reg}$ = 3 vs. 2.8) Furthermore an optimum value of Γ = 9 and a cooling power of 82W is predicted for that case.
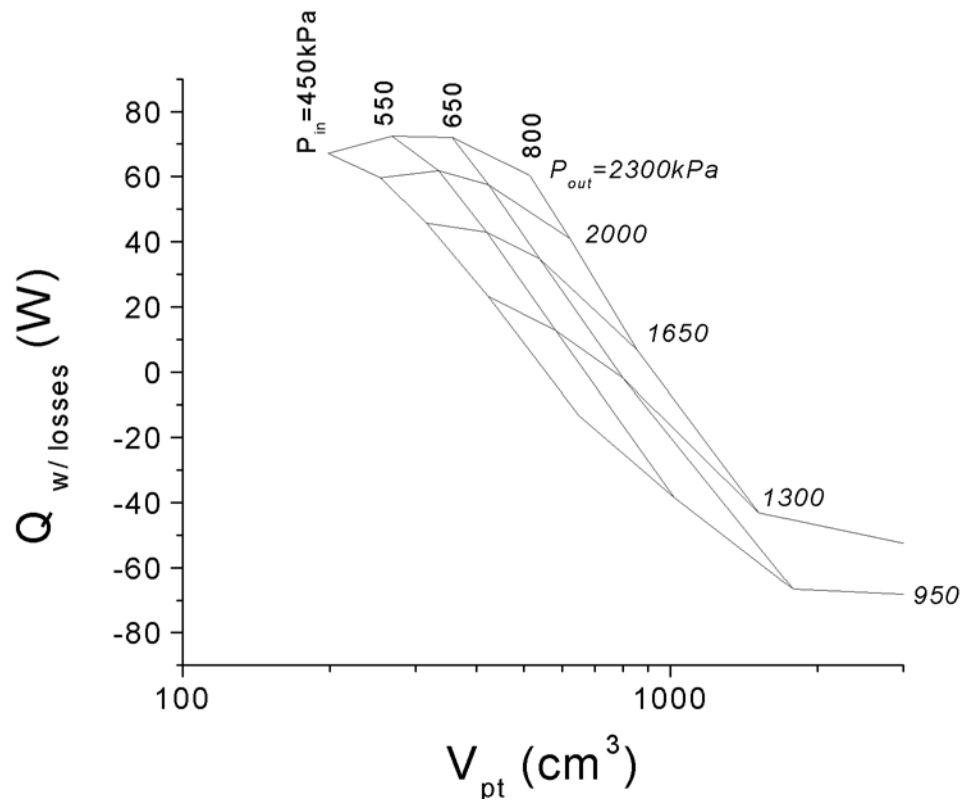
Figure 4.7 Cooling power vs. optimized pulse tube volume. The optimization process accounts for pressure losses through valves and regenerator, and conduction losses.

Chapter 5 Analysis   of   G-M   type   Pulse   Tube Refrigerator

The main goal of this report is developing a design tool for G-M type pulse tube refrigerators to optimize the design associated with a fixed compressor and to accurately predict its cooling performance. Achieving this goal requires analysis of the loss mechanisms in the pulse tube refrigerator system. In particular, it is important to account for the shuttle heat loss and the DC flow loss that are known as the most important loss mechanisms in the pulse tube refrigerator. These are related to the gas flow in the pulse tube and the heat transfer between the gas and the pulse tube wall. The numerical analysis must also reflect the unique features of the 5-valve pulse tube refrigerator such as the combination of the compressor and the valve timing controller. Finally, the choice of the heat transfer correlation associated with flow near the pulse tube wall is a critical factor that influences the analysis results.

In this chapter, an adiabatic, one-dimensional numerical analysis is described that includes both thermodynamic and fluid dynamic considerations for the flow acting within a valved pulse tube refrigerator. The assumptions employed to simplify the analysis are listed. The physical system and the one-cycle time period are discretized into small discrete volumes and short time steps. The governing equations to simulate the operation

of the 5-valve pulse tube system are derived for each discrete volume using mass conservation and energy balance relations. The computational algorithm including the solution approach, adjustable parameters, and convergence criteria for the numerical simulation is introduced in detail. Using an Eulerian approach, the pressure, temperature and mass flow rate are obtained as a function of time at every position in the system. The results of the cycle simulation for the selected operating condition are compared to the experiments to verify the reliability of the numerical analysis. Three reasonable heat transfer correlations are employed to calculate the amount of heat transfer and their adaptabilities are discussed. This data can also be viewed using a Lagrangian approach by determining the position and temperature variation for each gas packet in the pulse tube during a cycle. The temperature change along the trajectory of a gas packet clearly identifies both a DC flow and a shuttle heat transfer loss mechanism in the pulse tube. A 2nd order analysis has been performed to quantify the shuttle heat loss and the DC flow loss. Additional heat loss mechanisms associated with conduction, heat exchanger ineffectiveness, regenerator ineffectiveness and pressure drop are also considered in predicting the actual cooling performance. This approach provides good agreement with the experimental results.

5.1 Numerical Simulation

5.1.1 Physical Model

Fig. 5.1 shows a schematic diagram of the 5-valve pulse tube refrigerator and the typical valve opening sequence during a cycle. It consists of a compressor, regenerator, pulse tube, cold and hot heat exchangers, reservoir and five valves (V_1 through V_5) which connect the components to each other. The finite opening and closing times of the 5 valves produce an appropriate pressure wave through the system and define a complete cycle. As shown in Fig. 5.1, when V_1 and V_3 are opened, high-pressure gas flows from the compressor to the regenerator and the hot end of the pulse tube. When V_2 and V_4 are opened, the high-pressure gas expands, flowing from the regenerator and the hot end of the pulse tube to the suction side of the compressor. Between the compression and expansion processes, opening valves V_5 and V_1 or V_5 and V_2 for finite times allows a constant pressure gas shuttle process.

In the numerical simulation of these gas flows, several assumptions are employed to simplify the physical model.

    a. Helium, the working gas, behaves as a perfect gas (an ideal gas with constant specific heat).

    b. Flow in the system is one dimensional, so that there is no velocity component normal to the walls in each component.

c. The effectiveness of the regenerator is unity and the regenerator wall temperature distribution is constant.

d. The pressure drops in the regenerator and connection tubings are neglected. The pressure in the regenerator, pulse tube and heat exchangers are the same at any time.

e. In the cold and hot heat exchangers, the gas temperature is the same as that of the wall temperature of the heat exchanger, which is constant, i.e., heat transfer is perfect in the heat exchanger.

f. In the pulse tube, the flow is adiabatic

g. Flow through the orifice valves is adiabatic.

h. The temperature of the reservoir is isothermal.

Once a numerical simulation satisfies a cyclic steady state within the error tolerance, then an ideal cooling power can be obtained. Loss mechanisms including the ineffectiveness of the regenerator and heat exchangers, pressure drop through the regenerator, shuttle heat loss and DC flow loss are post calculated in the 2nd order analysis and applied to the ideal results in order to obtain a realistic prediction of the available cooling power.
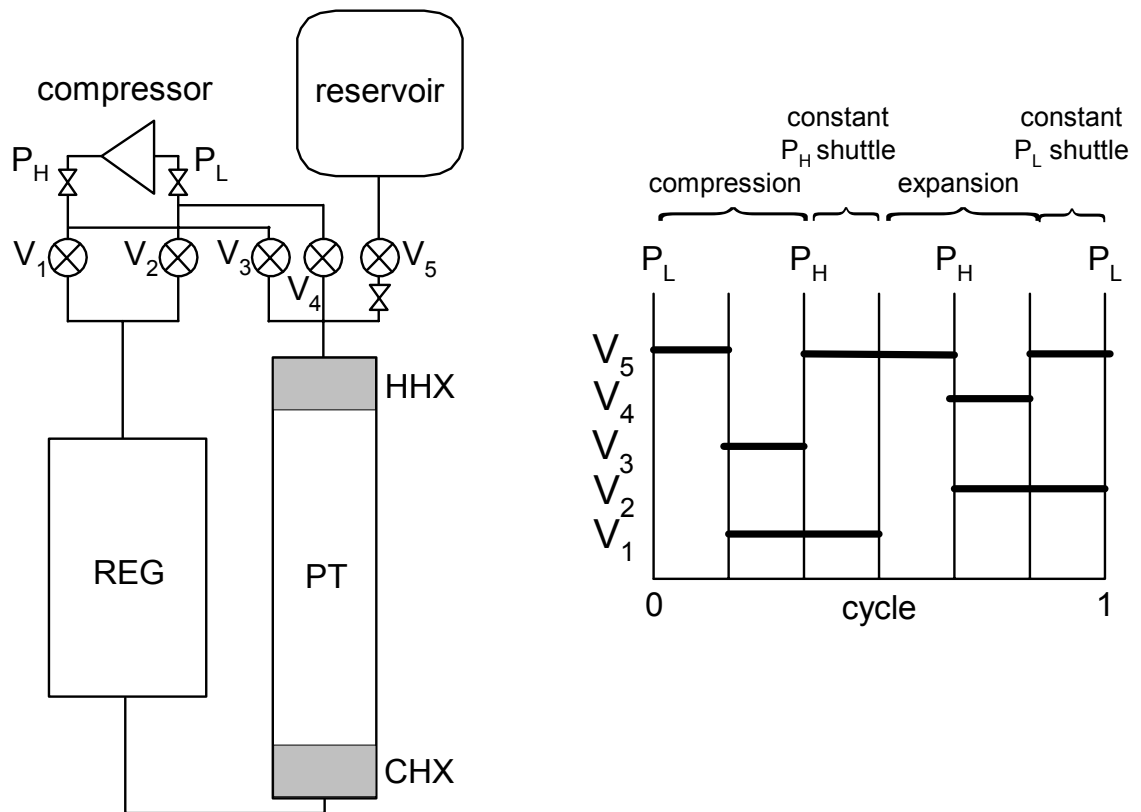
Figure 5.1 Schematic diagram of the 5-valve pulse tube refrigerator and typical valve opening sequence during a cycle. (REG : regenerator, HHX : hot heat exchanger, CHX : cold heat exchanger, PT : pulse tube)

5.1.2 Governing Equations

Fig. 5.2 shows a schematic diagram of the fixed discrete volume used in the numerical analysis. Applying a discrete volume method to any of the components in the system, the continuity equation and energy conservation equation for every component are as follows. For the arbitrary n^{th} discrete volume in the system, the continuity equation can be represented as,

$$\frac{dm_n}{dt} = \dot{m}_{n-1} - \dot{m}_n \tag{5.1}$$

while the energy conservation equation can be written as,

$$\frac{d(m_n u_n)}{dt} = \dot{m}_{n-1} h(T_{n-1}) - \dot{m}_n h(T_n) + \dot{Q}_n \tag{5.2}$$

where, m denotes the mass in a discrete volume, h the specific enthalpy, u the specific internal energy, T the temperature, and $\dot{Q}$ the heat transfer rate from the wall to the gas. The mass flow rate, $\dot{m}$, is defined as positive if gas flows towards the volumes of higher indices. The heat transfer, $\dot{Q}$, is defined as positive if heat flows into the gas.
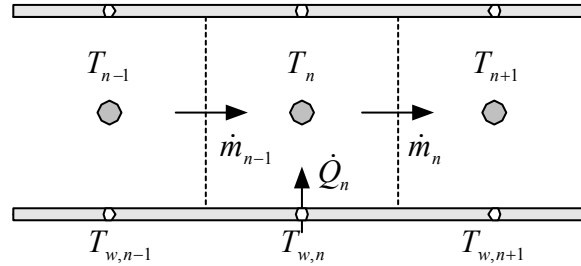
Figure 5.2 Schematic diagram of discrete volume analysis.

For a perfect gas, we can rewrite u and h as follows:

$$u \equiv C_v T , \quad h \equiv C_p T \tag{5.3}$$

where, C_p and C_v denote the specific heat at constant pressure and constant volume, respectively. In eqn. (5.3), the reference temperature for internal energy and enthalpy is absolute zero Kelvin (K).

For every discrete volume, the heat transfer, $\dot{Q}$, can be represented by

$$\dot{Q}_n = H_n A \left(T_{w,n} - T_n \right) \tag{5.4}$$

where H denotes the convective heat transfer coefficient, T_w the wall temperature, and A the heat transfer area. The gas within the pulse tube is considered to be adiabatic in that

there is no axial heat transfer between the gas in the pulse tube. Substitution of eqn. (5.3) and (5.4) into eqn. (5.2) gives,

$$\frac{d(m_n C_v T_n)}{dt} = \dot{m}_{n-1} C_p T_{n-1} - \dot{m}_n C_p T_n + H_n A_n \left(T_{w,n} - T_n \right) \tag{5.5}$$

Note that eqn. (5.5) represents general energy conservation for any discrete volume in the system. According to the assumption (f) above, the heat transfer term in eqn. (5.5) will be eliminated for the discrete volume in the pulse tube. The ideal gas law can be used to express the mass terms in eqn. (5.5) in terms of pressure (P), volume (V), temperature (T), and the ideal gas constant (R).

For the mass flow rate through the orifices ($\dot{m}_o$), an expression suitable for adiabatic orifice flow has been selected [27] as shown in eqn. (5.6).

$$\dot{m}_o = C_d A_o \left[\frac{2 \rho_{high} \left(P_{high} - P_{low} \right) \left(\frac{P_{low}}{P_{high}} \right)^{\frac{2}{\gamma}} \left(\frac{\gamma}{\gamma - 1} \right) \dfrac{1 - \left(\frac{P_{low}}{P_{high}} \right)^{\left(\frac{\gamma - 1}{\gamma} \right)}}{1 - \left(\frac{P_{low}}{P_{high}} \right)}}{1 - \left(\frac{A_o}{A_{up}} \right)^2 \left(\frac{P_{low}}{P_{high}} \right)^{\frac{2}{\gamma}}} \right]^{\frac{1}{2}} \tag{5.6}$$

Here, the subscript *high* denotes the high pressure, *low* the low pressure, *o* the orifice, and *up* the upstream. Further, γ is specific heat ratio of gas and C_d is discharge coefficient, which is a ratio of actual rate of flow to theoretical rate of flow. However, the apparent discharge coefficient that determines the amount of mass flow rate across the solenoid-orifice valve system in the 5-valve pulse tube refrigerator could be larger than unity, and also its value is dependent on the physical tubing dimensions, A_o and A_{up} of the 5-valve pulse tube system.

5.1.3 Discretization

In this analysis, we divide the regenerator into several (*nr*) evenly spaced discrete volumes, and the pulse tube into *np* discrete volumes. Twenty discrete volumes for the pulse tube and ten volumes for the regenerator were used in this analysis. The numbers of those discrete volumes were verified as being sufficient by comparing the temperature and the pressure profiles obtained from the sample calculation with larger number of discrete volumes. The hot and cold heat exchangers are each modeled as one discrete volume. Fig. 5.3 shows a schematic diagram of the discretized control volumes in the 5-valve pulse tube refrigerator including sign conventions and notations for mass flow rates, temperatures, pressures and other properties. In Fig. 5.3, the subscript *reg* and *r* denotes the regenerator, *chx* and *c* the cold heat exchanger, *hhx* and *h* the hot heat exchanger, *pt* the pulse tube, *b* the buffer (=reservoir), and *o* the orifice valve. The symbol $\dot{m}_h$ represents the mass flow rate between the 1st discrete volume of the pulse tube and the

hot heat exchanger. The symbols $\dot{Q}_h$ and $\dot{Q}_c$ represent the heat transfer rate at the hot

and the cold heat exchanger, respectively.
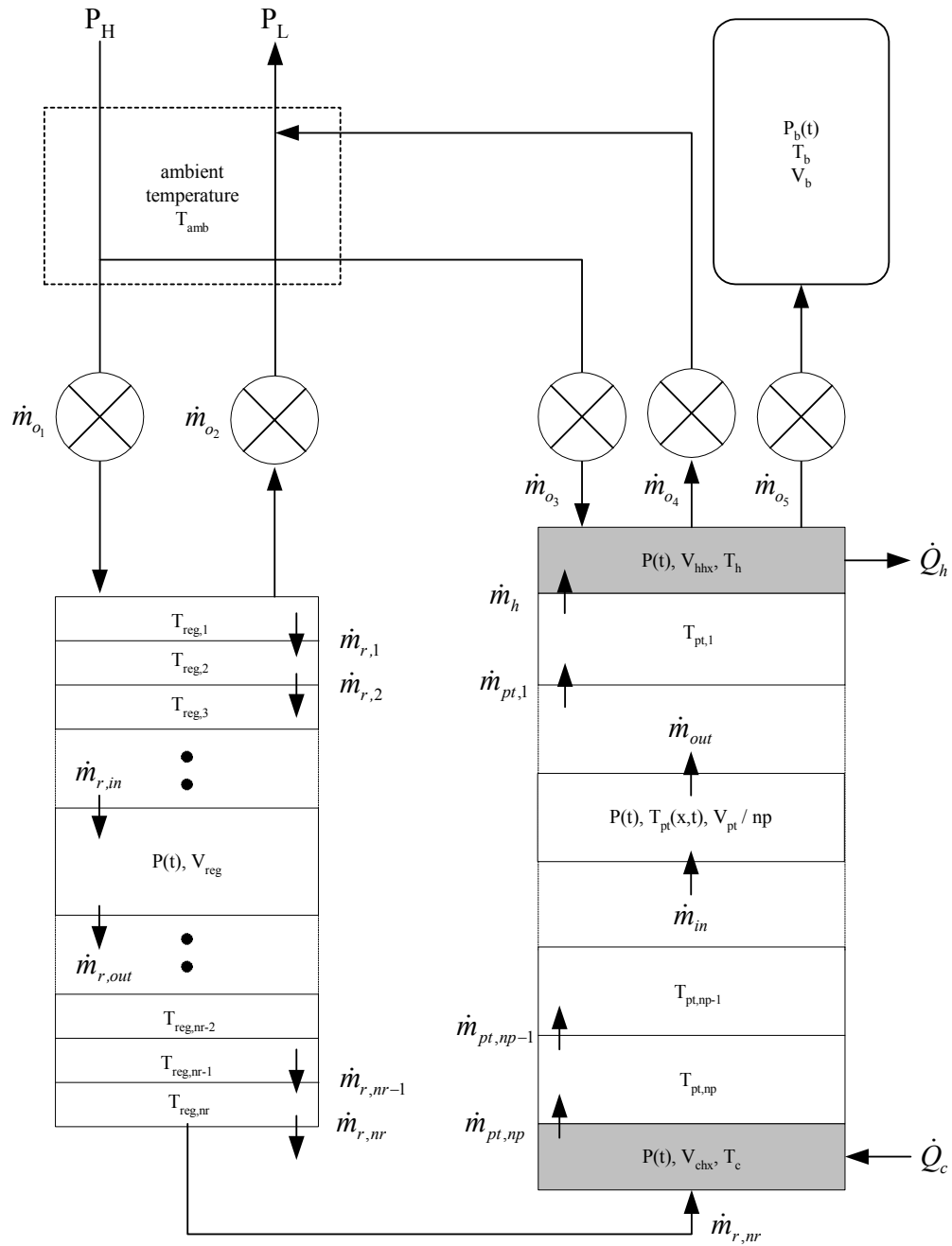
Figure 5.3 Schematic diagram of pulse tube system discretization.

5.1.4 Pressure Change Rate

In order to calculate pressure, temperature and mass flow rate as a function of time and position in the system, the governing equations are applied to all of the discrete volumes. These equations include the ideal gas law, the mass conservation equation and the energy conservation equations.

Substituting the ideal gas law into the mass conservation equations for the regenerator, cold heat exchanger and hot heat exchanger shown in Fig. 5.3 gives,

$$\left(\frac{dM}{dt}\right)_{reg} = \frac{d}{dt}\left(\frac{PV_{reg}}{RT_{reg}}\right) = \frac{V_{reg}}{RT_{reg}}\frac{dP}{dt} = \dot{m}_{o_1} - \dot{m}_{o_2} - \dot{m}_{r,nr} \tag{5.7}$$

$$\left(\frac{dM}{dt}\right)_{chx} = \frac{d}{dt}\left(\frac{PV_{chx}}{RT_c}\right) = \frac{V_{chx}}{RT_c}\frac{dP}{dt} = \dot{m}_{r,nr} - \dot{m}_{pt,np} \tag{5.8}$$

$$\left(\frac{dM}{dt}\right)_{hhx} = \frac{d}{dt}\left(\frac{PV_{hhx}}{RT_h}\right) = \frac{V_{hhx}}{RT_h}\frac{dP}{dt} = \dot{m}_{o_3} - \dot{m}_{o_4} - \dot{m}_{o_5} + \dot{m}_h \tag{5.9}$$

Note that T_{reg} is the log mean average temperature for the regenerator. If a linear temperature profile is assumed, T_{reg} is defined by

$$T_{reg} \equiv \frac{T_h - T_c}{\ln\left(\dfrac{T_h}{T_c}\right)} \tag{5.10}$$

For the pulse tube as shown in Fig. 5.3, we use the energy conservation equation instead of mass conservation. When flow is into the bottom and out of the top of the pulse tube (i.e., $\dot{m}_{pt,np}$ & $\dot{m}_h > 0$ in Fig. 5.4 (a)), the energy conservation equation for the pulse tube is,

$$\left(\frac{dU}{dt}\right)_{pt} = \dot{m}_{pt,np} h_c - \dot{m}_h h_{pt,1} \tag{5.11}$$

Substituting the ideal gas law into eqn. (5.11) gives,

$$\frac{C_v V_{pt}}{R}\frac{dP}{dt} = C_p \left(\dot{m}_{pt,np} T_c - \dot{m}_h T_{pt,1} \right)$$

or,

$$\frac{V_{pt}}{\gamma R T_c}\frac{dP}{dt} = \dot{m}_{pt,np} - \dot{m}_h \frac{T_{pt,1}}{T_c} \tag{5.12}$$

Summation of all the $\dfrac{dP}{dt}$ terms for the regenerator, hot/cold heat exchanger and pulse tube (eqn. (5.7), (5.8), (5.9), (5.12)) gives,

$$\frac{1}{R}\left(\frac{V_{reg}}{T_{reg}} + \frac{V_{chx}}{T_c} + \frac{V_{hhx}}{T_h} + \frac{V_{pt}}{\gamma T_c}\right)\frac{dP}{dt} = \dot{m}_{o_1} - \dot{m}_{o_2} + \dot{m}_{o_3} - \dot{m}_{o_4} - \dot{m}_{o_5} + \dot{m}_h\left(1 - \frac{T_{pt,1}}{T_c}\right)$$

or,

$$\frac{dP}{dt} = \frac{R\left[\dot{m}_{o_1} - \dot{m}_{o_2} + \dot{m}_{o_3} - \dot{m}_{o_4} - \dot{m}_{o_5} + \dot{m}_h\left(1 - \frac{T_{pt,1}}{T_c}\right)\right]}{\frac{V_{reg}}{T_{reg}} + \frac{V_{chx}}{T_c} + \frac{V_{hhx}}{T_h} + \frac{V_{pt}}{\gamma T_c}} \qquad (5.13)$$

Here, T_c denotes the temperature of the cold heat exchanger and $T_{pt,1}$ is the temperature of the 1st discrete volume, i.e., the hot end of the pulse tube. Eqn. (5.13) represents the rate of pressure change associated with all of the orifice mass flow rates, the dimensions of the components and representative temperatures in the system. In particular, eqn. (5.13) is appropriate for the case that gas flows into the pulse tube at the cold end and flows out of the pulse tube at the hot end. As shown in Fig. 5.4, during one cycle of the 5-valve system, all of four distinct flow patterns can occur, each of which require different boundary temperatures and therefore different forms of the pulse tube energy eqn. (5.12). For example, Fig. 5.4 (a) depicts the constant (high) pressure gas shuttle process that occurs following the compression process, and its boundary temperatures for the pulse tube are the cold heat exchanger temperature for the cold end and the gas temperature of the 1st control volume of the pulse tube for the hot end. It is possible to derive $\frac{dP}{dt}$ equations similar to eqn. (5.13) for all of the flow patterns in Fig. 5.4 (b)~(d) using the same procedure described above, but a slightly different equation for the pulse tube.

For flow pattern (b) in Fig. 5.4, the energy conservation equation for the pulse tube is,

$$\frac{C_v V_{pt}}{R} \frac{dP}{dt} = -\dot{m}_h C_p T_h + \dot{m}_{pt,np} C_p T_{pt,np}$$ (5.14)

Summation of eqn.s (5.7)~(5.9) and (5.14) gives,

$$\frac{dP}{dt} = \frac{\dot{m}_{o_1} - \dot{m}_{o_2} + \dot{m}_{o_3} - \dot{m}_{o_4} - \dot{m}_{o_5} + \dot{m}_h \left(1 - \dfrac{T_h}{T_{pt,np}}\right)}{\dfrac{V_{reg}}{RT_{reg}} + \dfrac{V_{chx}}{RT_c} + \dfrac{V_{hhx}}{RT_h} + \dfrac{V_{pt}}{\gamma RT_{pt,np}}}$$ (5.15)

For flow pattern (c) in Fig. 5.4, the energy conservation equation for the pulse tube is,

$$\frac{C_v V_{pt}}{R} \frac{dP}{dt} = -\dot{m}_h C_p T_{pt,1} + \dot{m}_{pt,np} C_p T_{pt,np}$$ (5.16)

Summation of eqn.s (5.7)~(5.9) and (5.16) gives,

$$\frac{dP}{dt} = \frac{\dot{m}_{o_1} - \dot{m}_{o_2} + \dot{m}_{o_3} - \dot{m}_{o_4} - \dot{m}_{o_5} + \dot{m}_h \left(1 - \dfrac{T_{pt,1}}{T_{pt,np}}\right)}{\dfrac{V_{reg}}{RT_{reg}} + \dfrac{V_{chx}}{RT_c} + \dfrac{V_{hhx}}{RT_h} + \dfrac{V_{pt}}{\gamma RT_{pt,np}}}$$ (5.17)

For flow pattern (d) in Fig. 5.4, the energy conservation equation for the pulse tube is,

$$\frac{C_v V_{pt}}{R} \frac{dP}{dt} = -\dot{m}_h C_p T_h + \dot{m}_{pt,np} C_p T_c \tag{5.18}$$

Summation of eqn.s (5.7)~(5.9) and (5.18) gives,

$$\frac{dP}{dt} = \frac{\dot{m}_{o_1} - \dot{m}_{o_2} + \dot{m}_{o_3} - \dot{m}_{o_4} - \dot{m}_{o_5} + \dot{m}_h \left(1 - \dfrac{T_h}{T_c}\right)}{\dfrac{V_{reg}}{RT_{reg}} + \dfrac{V_{chx}}{RT_c} + \dfrac{V_{hhx}}{RT_h} + \dfrac{V_{pt}}{\gamma RT_c}} \tag{5.19}$$

(a)

(b)

(c)

(d)
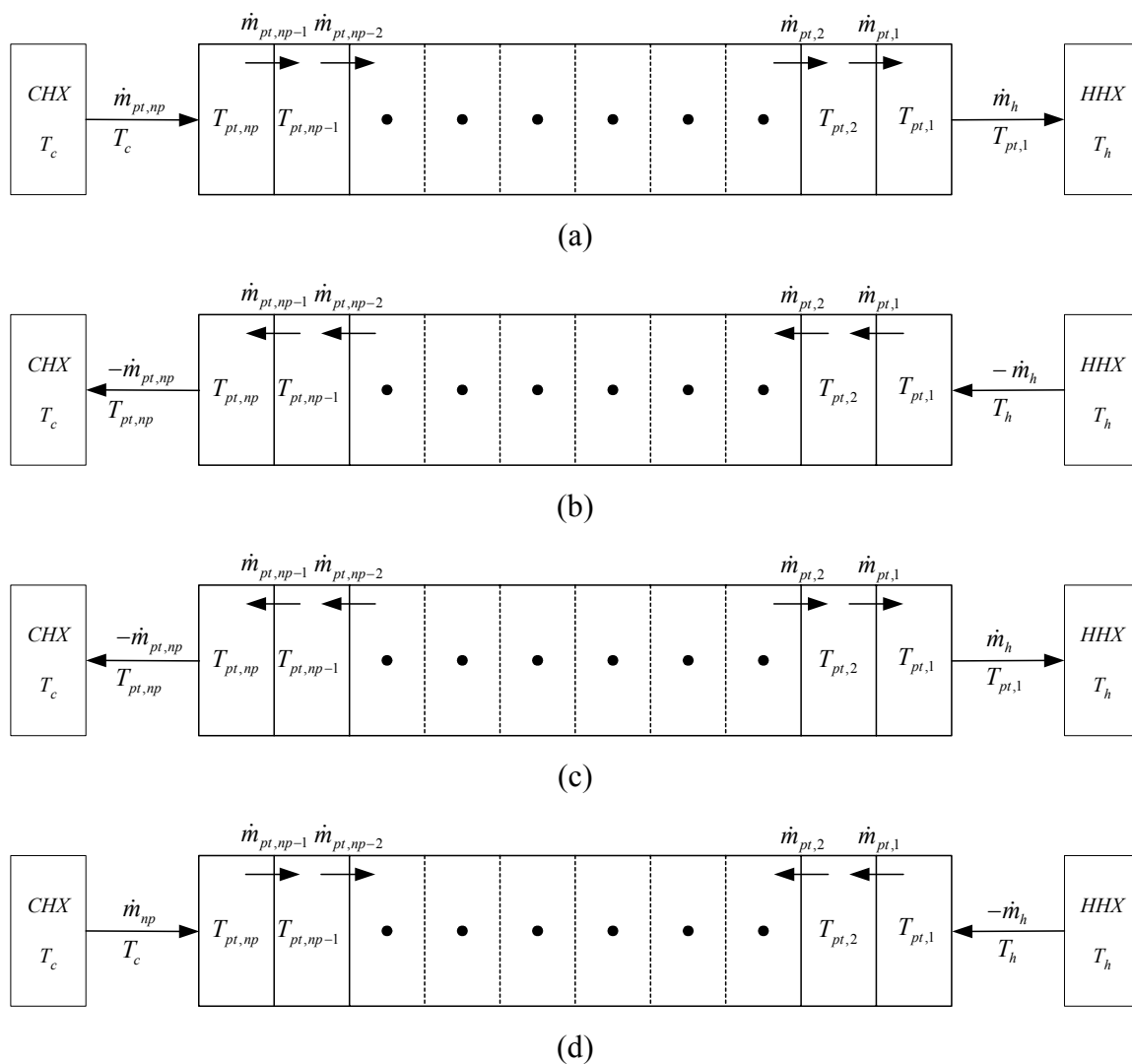
Figure 5.4 Four possible flow patterns in the pulse tube during a cycle.

5.1.5 Other Rate Equations

After the rate of pressure change ($\frac{dP}{dt}$) is calculated, the rate of temperature change at any time in the pulse tube can be calculated using the mass conservation for the ith control volume of the pulse tube as following:

$$\left(\frac{dM}{dt} \right)_{pt,i} = \dot{m}_{pt,i} - \dot{m}_{pt,i-1} = \frac{1}{R} \left(\frac{V_{pt}}{np} \right) \left(\frac{1}{T_{pt,i}} \frac{dP}{dt} - \frac{P}{T_{pt,i}^2} \frac{dT_{pt,i}}{dt} \right)$$

or,

$$\frac{dT_{pt,i}}{dt} = \frac{T_{pt,i}^2}{P} \left[\frac{1}{T_{pt,i}} \frac{dP}{dt} - \frac{\left(\dot{m}_{pt,i} - \dot{m}_{pt,i-1} \right) R}{\left(V_{pt} / np \right)} \right] \tag{5.20}$$

Since the temperature of the reservoir is maintained at ambient temperature, the rate of pressure change in the reservoir can be obtained by applying the mass conservation equation.

$$\left(\frac{dM}{dt} \right)_b = \frac{d}{dt} \left(\frac{P_b V_b}{R T_b} \right) = \frac{V_b}{R T_b} \frac{dP_b}{dt} = \dot{m}_{o_5}$$

or,

$$\frac{dP_b}{dt} = \dot{m}_{o_5} \frac{R T_b}{V_b} \tag{5.21}$$

5.1.6 Computational Algorithm

The solution approach of the numerical simulation is more complicated than that of the Stirling type pulse tube refrigerator since the pressure changes are not sinusoidal. In this numerical scheme, all of the temperatures and mass flow rates are functions of time and position, while pressure is a function of time only. The most valuable results of this numerical simulation are the pressure, temperature profiles and mass flow rates in the pulse tube that will be used in the calculation of the shuttle heat loss and DC flow in the later section. All of these variations should satisfy the requirement of cyclic steady state ; one complete cycle simulation should result in final temperatures and pressures that are the same as those at the beginning of the cycle. In this section, detailed descriptions of the solution approach are explained by using a flow diagram of the numerical code.

5.1.6.1 Constants, Variables and Parameters

Several values related to the operating conditions are given as constants at the beginning of the numerical simulation. Table 5.1 shows the summary of constants, variables and parameters used in the numerical simulation.

Table 5.1 Summary of constants, variables and parameters in the numerical simulation

Component	Constants[1]	Variables[2]	Parameters[3]
Compressor	P_H, P_L, P_{ch}	-	P_H, P_L, P_{ch}
Solenoid valves	Valve opening sequence, steps in a cycle	On/Off, $\dot{m}_{o_1}(t) \sim \dot{m}_{o_5}(t)$	Valve opening sequence
Orifice valves	Discharge coefficients $(C_{d,H}, C_{d,L}, C_{d,R})$	$\dot{m}_{o_1}(t) \sim \dot{m}_{o_5}(t)$	Discharge coefficients $(C_{d,H}, C_{d,L}, C_{d,R})$
Pulse tube	Dimensions, np	$P(t)$ $T_{pt}(i,t), \dot{m}_{pt}(i,t)$	Dimensions
Regenerator	Dimensions, nr, $T_r(i)$	$P(t), \dot{m}_r(i,t)$	Dimensions
Heat exchangers	Dimensions, T_h, T_c	$P(t), \dot{m}_h(t)$	Dimensions
Reservoir	Dimensions, T_b	$P_b(t)$	Dimensions

(1) Not changed during a cycle until the simulation is finished.
(2) Changed during a cycle at any time, or at any position, or at both.
(3) Can be manually changed for different simulations with no change of assumptions to observe the effect on the cooling performance.

5.1.6.2 Initial Assumptions

At the beginning of the analysis, the assumptions of reasonable values for the pressure and the initial temperature in each discrete volume are very important to get reliable numerical results and decrease the calculation time. To obtain an initial pressure variation as a function of time during a cycle, an artificial $\dfrac{dP}{dt}$ equation was derived and successfully employed in a numerical simulation using the adiabatic gas relation (i.e., $Pv^{\gamma} = \text{constant}$). The rate of total mass change in the pulse tube is represented as a summation of the rate of mass change in each control volume in the pulse tube.

$$\left(\frac{dM}{dt}\right)_{pt} = \sum_{i=1}^{np} \frac{dM_i}{dt} = \sum_{i=1}^{np} \frac{d}{dt}\left(\frac{PV_{pt}}{np \cdot RT_{pt,i}}\right) = \frac{1}{R}\left(\frac{V_{pt}}{np}\right)\sum_{i=1}^{np} \frac{d}{dt}\left(\frac{P}{T_{pt,i}}\right) \qquad (5.22)$$

Here, $T_{pt,i}$ represents the temperatures in each discrete control volume in the pulse tube. For adiabatic compression and expansion, the ideal gas law gives

$$Pv_i^{\gamma} \propto P\left(\frac{T_{pt,i}}{P}\right)^{\gamma} = P^{1-\gamma}T_{pt,i}^{\gamma} = \text{constant} \qquad (5.23)$$

By substituting the derivative of eqn. (5.23) with respect to time into eqn. (5.22), we obtain

$$\frac{d}{dt}\left(\frac{P}{T_{pt,i}}\right) = \frac{1}{T_{pt,i}}\frac{dP}{dt} - \frac{P}{T_{pt,i}^2}\frac{dT_{pt,i}}{dt} = \frac{1}{T_{pt,i}}\frac{dP}{dt} - \left(\frac{\gamma-1}{\gamma}\right)\frac{1}{T_{pt,i}}\frac{dP}{dt} = \frac{1}{\gamma T_{pt,i}}\frac{dP}{dt} \qquad (5.24)$$

Therefore, the rate of total mass change in the pulse tube becomes

$$\left(\frac{dM}{dt}\right)_{pt} = \frac{1}{\gamma R}\left(\frac{V_{pt}}{np}\right)\sum_{i=1}^{np}\frac{1}{T_{pt,i}}\frac{dP}{dt} \qquad (5.25)$$

Total mass conservation for the regenerator, pulse tube and hot/cold heat exchangers gives,

$$\frac{1}{R}\left(\frac{V_{reg}}{T_{reg}} + \frac{V_{chx}}{T_c} + \frac{1}{\gamma}\left(\frac{V_{pt}}{np}\right)\sum_{i=1}^{np}\frac{1}{T_{pt,i}} + \frac{V_{hhx}}{T_h}\right)\frac{dP}{dt} = \dot{m}_{o_1} - \dot{m}_{o_2} + \dot{m}_{o_3} - \dot{m}_{o_4} - \dot{m}_{o_5}$$

or,

$$\frac{dP}{dt} = \frac{R\left(\dot{m}_{o_1} - \dot{m}_{o_2} + \dot{m}_{o_3} - \dot{m}_{o_4} - \dot{m}_{o_5}\right)}{\dfrac{V_{reg}}{T_{reg}} + \dfrac{V_{chx}}{T_c} + \dfrac{1}{\gamma}\left(\dfrac{V_{pt}}{np}\right)\displaystyle\sum_{i=1}^{np}\dfrac{1}{T_{pt,i}} + \dfrac{V_{hhx}}{T_h}} \qquad (5.26)$$

Note that in eqn. (5.26), we have one $\dfrac{dP}{dt}$ equation during a cycle regardless of the four flow patterns. Even if the adiabatic gas relation, eqn. (5.23), doesn't represent the real gas behavior in the pulse tube, eqn. (5.26) provides a good guess for the initial pressure variation as a function of time. The use of this initial algorithm makes efficient cycle simulation possible.

Once the physical dimensions and constants in Table 5.1 are fixed for the given system and the operating condition (e.g. valve opening sequences), the rate of mass change in the pulse tube and pressure change in the system are calculated using eqn.s (5.25) and (5.26). At the initial time step, a linear temperature profile is assumed in the pulse tube. The pressure and the mass of the pulse tube for the next time step are simply integrated as

$$P(t + \Delta t) = P(t) + \frac{dP}{dt} \Delta t \tag{5.27}$$

$$M_{pt}(t + \Delta t) = M_{pt}(t) + \left(\frac{dM}{dt}\right)_{pt} \Delta t \tag{5.28}$$

The temperature profiles for the next time step are calculated combining eqn.s (5.23) and (5.27).

$$T_{pt}^{\gamma}(i, t + \Delta t) = \frac{P^{1-\gamma}(t)}{P^{1-\gamma}(t + \Delta t)} T_{pt}^{\gamma}(i, t) \tag{5.29}$$

The mass flow rates at any position in the regenerator and the pulse tube are also calculated from mass conservation for each discrete volume. After the repeated calculations using eqn.s (5.25)~(5.29), each set of pressure, temperature profiles is obtained for a cycle. If each set doesn't fulfill the requirement of a cyclic steady state, the process for the whole cycle is iterated until the pressure, mass, mass flow rate and temperature profiles in the pulse tube satisfy a cyclic steady state. The pressure, mass flow rate and temperature profiles as functions of time and position are used as initial assumptions for the main simulation using the more correct governing equations derived earlier.

5.1.6.3 Consistency among the $\dfrac{dP}{dt}$, T and $\dot{m}$ in the System

The pressure (or rate of pressure change), mass flow rate and temperature profiles in the pulse tube as functions of time and position obtained in 5.1.6.2 are used as initial guess for the main simulation. However, the main simulation uses all of the rate equations derived in Section 5.1.2~5.1.5 to model the behavior of the actual gas in the pulse tube.

At first, according to the valve opening time changes shown in Fig. 5.1, the mass flow rates through the five solenoid / three orifice valve combinations ($\dot{m}_{o_1} \sim \dot{m}_{o_5}$), are

calculated by using eqn. (5.6) based on the initial pressure obtained in section 5.1.6.2. If we set our system as the regenerator, the pulse tube and the cold and hot heat exchangers in Fig. 5.3, we know all of the boundary temperatures and mass flow rates, that is T_{amb} and $\dot{m}_{o_1} \sim \dot{m}_{o_5}$. To calculate the mass flow rates in the regenerator and the pulse tube, the respective equations are used for mass conservation in the regenerator, hot and cold heat exchangers and energy conservation in the pulse tube.

For each discrete volume in the regenerator, the mass conservation gives,

$$\dot{m}_{o_1} - \dot{m}_{o_2} - \dot{m}_{r,1} = \frac{1}{RT_{reg,1}} \frac{V_{reg}}{nr} \left(\frac{dP}{dt} \right)$$

$$\dot{m}_{r,1} - \dot{m}_{r,2} = \frac{1}{RT_{reg,2}} \frac{V_{reg}}{nr} \left(\frac{dP}{dt} \right)$$

$$...$$
$$...$$

$$\dot{m}_{r,nr-2} - \dot{m}_{r,nr-1} = \frac{1}{RT_{reg,nr-1}} \frac{V_{reg}}{nr} \left(\frac{dP}{dt} \right)$$

$$\dot{m}_{r,nr-1} - \dot{m}_{r,nr} = \frac{1}{RT_{reg,nr}} \frac{V_{reg}}{nr} \left(\frac{dP}{dt} \right)$$

or,

$$\dot{m}_{r,1} = \dot{m}_{o_1} - \dot{m}_{o_2} - \frac{1}{RT_{reg,1}} \frac{V_{reg}}{nr} \left(\frac{dP}{dt} \right)$$

$$\dot{m}_{r,2} = \dot{m}_{r,1} - \frac{1}{RT_{reg,2}} \frac{V_{reg}}{nr} \left(\frac{dP}{dt} \right)$$

$$...$$
$$...$$

(5.30)

$$\dot{m}_{r,nr-1} = \dot{m}_{r,nr-2} - \frac{1}{RT_{reg,nr-1}} \frac{V_{reg}}{nr} \left(\frac{dP}{dt} \right)$$

$$\dot{m}_{r,nr} = \dot{m}_{r,nr-1} - \frac{1}{RT_{reg,nr}} \frac{V_{reg}}{nr} \left(\frac{dP}{dt} \right)$$

Note that in eqn. (5.30), if $\frac{dP}{dt}$, $\dot{m}_{o_1}, \dot{m}_{o_2}$ are known values, all of the mass flow rates in the regenerator, $\dot{m}_{r,1} \sim \dot{m}_{r,nr}$ are calculated based on the assumed temperature profile in the regenerator.

For the discrete volume in the cold heat exchanger, mass conservation gives,

$$\dot{m}_{pt,np} = \dot{m}_{r,nr} - \frac{V_{chx}}{RT_c} \left(\frac{dP}{dt} \right)$$

(5.31)

Thus, $\dot{m}_{pt,np}$ can be calculated using eqn. (5.31).

For each discrete volume in the pulse tube, the energy balance equation gives,

$$\dot{m}_{pt,np}T_c - \dot{m}_{pt,np-1}T_{pt,np} = \frac{1}{\gamma R}\frac{V_{pt}}{np}\left(\frac{dP}{dt}\right)$$

$$\dot{m}_{pt,np-1}T_{pt,np} - \dot{m}_{pt,np-2}T_{pt,np-1} = \frac{1}{\gamma R}\frac{V_{pt}}{np}\left(\frac{dP}{dt}\right)$$

$$...$$
$$...$$

$$\dot{m}_{pt,2}T_{pt,3} - \dot{m}_{pt,1}T_{pt,2} = \frac{1}{\gamma R}\frac{V_{pt}}{np}\left(\frac{dP}{dt}\right)$$

$$\dot{m}_{pt,1}T_{pt,2} - \dot{m}_h T_{pt,1} = \frac{1}{\gamma R}\frac{V_{pt}}{np}\left(\frac{dP}{dt}\right)$$

or,

$$\dot{m}_{pt,np-1}T_{pt,np} = \dot{m}_{pt,np}T_c - \frac{1}{\gamma R}\frac{V_{pt}}{np}\left(\frac{dP}{dt}\right)$$

$$\dot{m}_{pt,np-2}T_{pt,np-1} = \dot{m}_{pt,np-1}T_{pt,np} - \frac{1}{\gamma R}\frac{V_{pt}}{np}\left(\frac{dP}{dt}\right)$$

$$...$$
$$...$$

$$\dot{m}_{pt,1}T_{pt,2} = \dot{m}_{pt,2}T_{pt,3} - \frac{1}{\gamma R}\frac{V_{pt}}{np}\left(\frac{dP}{dt}\right)$$

$$\dot{m}_h T_{pt,1} = \dot{m}_{pt,1}T_{pt,2} - \frac{1}{\gamma R}\frac{V_{pt}}{np}\left(\frac{dP}{dt}\right)$$

(5.32)

Note that all the mass flow rates in the pulse tube are calculated by using eqn. (5.32) from the same rate of pressure change used in eqn.s (5.30) and (5.31). It is important to note that eqn. (5.32) is only valid for the flow pattern (a) in Fig. 5.4. For other flow patterns, different values for the boundary temperatures must be used in eqn. (5.32). At the first calculation of mass flow rate in the pulse tube, the initially assumed temperature profile and the resulting rate of pressure change are used. The mass flow rates calculated based

on these profiles should match the flow pattern in Fig. 5.4 (a) and eqn. (5.32). If these are not consistent then, other flow patterns and corresponding energy balance equations similar to eqn. (5.32) are tried. At most, four iteration processes are required for each time step, equal to the number of possible flow patterns. For the discrete volume of the hot heat exchanger, mass conservation gives,

$$\dot{m}_h + \dot{m}_{o_3} - \dot{m}_{o_4} - \dot{m}_{o_5} = \frac{V_{hhx}}{RT_h}\left(\frac{dP}{dt}\right) \tag{5.33}$$

Note that there is no unknown value in eqn. (5.33) since all of the terms have been calculated or were assumed at the beginning. Therefore, eqn. (5.33) is used to check the assumed rate of pressure change. In other words, the assumed rate of pressure change derived from the artificial $\frac{dP}{dt}$ described in section 5.1.6.2 can be corrected through the use of eqn. (5.33). If the two values of $\dot{m}_h$ s calculated in eqn.s (5.32) and (5.33) are out of tolerance, $\frac{dP}{dt}$ is corrected and the process is initiated to calculate the mass flow rates in the system again with $\frac{dP}{dt}$ corrected. Once a self-consistent set of mass flow rates and pressure rate of change are obtained, the rate of temperature change in the pulse tube can

be calculated at each discrete volume using eqn. (5.20). These iterations are performed at each time step during a cycle.

5.1.6.4 Numerical Integration

The pressure in the system and the reservoir pressure are functions of time, and the temperatures and the mass flow rates in the pulse tube are functions of time and position. The number of time steps should be large enough to track the gas movement and the pressure changes of the system. In this analysis, one cycle is divided into 64 steps. A Runge-Kutta 4th order numerical integration method is employed to integrate the rate of change of pressure with respect to time in the system, $\dfrac{dP}{dt}$, the rate of change of pressure with respect to time in the reservoir, $\dfrac{dP_b}{dt}$ and rate of change of temperature with respect to time at each volume in the pulse tube, $\dfrac{dT_{pt,i}}{dt}$. Table 5.2 shows the Runge-Kutta 4th order numerical integration scheme for the system pressure, reservoir pressure and pulse tube temperature in different positions. The integrated pressures and temperatures in the Runge-Kutta 4th order numerical integration scheme at each time step are used as known values for the next time step in the calculations of eqn.s (5.13), (5.15), (5.17), (5.19) and (5.30)~(5.33). The Runge-Kutta 4th order numerical integration steps are repeated until they satisfy the convergence tolerance described in the next section.

Table 5.2 The Runge-Kutta 4th order numerical integration scheme

Derivatives	$$\frac{dP}{dt} = f\left(P, P_b, T_{pt,i}\right)$$ $$\frac{dP_b}{dt} = f\left(P, P_b, T_{pt,i}\right)$$ $$\frac{dT_{pt,i}}{dt} = f_i\left(P, P_b, T_{pt,i}\right)$$
Runge-Kutta 1st order	$$k_1^{\,P} = h \cdot f\left(P, P_b, T_{pt,i}\right)$$ $$k_1^{\,P_b} = h \cdot f\left(P, P_b, T_{pt,i}\right)$$ $$k_1^{\,T_{pt,i}} = h \cdot f_i\left(P, P_b, T_{pt,i}\right)$$
Runge-Kutta 2nd order	$$k_2^{\,P} = h \cdot f\left(P + \frac{k_1^{\,P}}{2}, P_b + \frac{k_1^{\,P_b}}{2}, T_{pt,i} + \frac{k_1^{\,T_{pt,i}}}{2}\right)$$ $$k_2^{\,P_b} = h \cdot f\left(P + \frac{k_1^{\,P}}{2}, P_b + \frac{k_1^{\,P_b}}{2}, T_{pt,i} + \frac{k_1^{\,T_{pt,i}}}{2}\right)$$ $$k_2^{\,T_{pt,i}} = h \cdot f_i\left(P + \frac{k_1^{\,P}}{2}, P_b + \frac{k_1^{\,P_b}}{2}, T_{pt,i} + \frac{k_1^{\,T_{pt,i}}}{2}\right)$$
Runge-Kutta 3rd order	$$k_3^{\,P} = h \cdot f\left(P + \frac{k_2^{\,P}}{2}, P_b + \frac{k_2^{\,P_b}}{2}, T_{pt,i} + \frac{k_2^{\,T_{pt,i}}}{2}\right)$$ $$k_3^{\,P_b} = h \cdot f\left(P + \frac{k_2^{\,P}}{2}, P_b + \frac{k_2^{\,P_b}}{2}, T_{pt,i} + \frac{k_2^{\,T_{pt,i}}}{2}\right)$$ $$k_3^{\,T_{pt,i}} = h \cdot f_i\left(P + \frac{k_2^{\,P}}{2}, P_b + \frac{k_2^{\,P_b}}{2}, T_{pt,i} + \frac{k_2^{\,T_{pt,i}}}{2}\right)$$
Runge-Kutta 4th order	$$k_4^{\,P} = h \cdot f\left(P + k_3^{\,P}, P_b + k_3^{\,P_b}, T_{pt,i} + k_3^{\,T_{pt,i}}\right)$$ $$k_4^{\,P_b} = h \cdot f\left(P + k_3^{\,P}, P_b + k_3^{\,P_b}, T_{pt,i} + k_3^{\,T_{pt,i}}\right)$$ $$k_4^{\,T_{pt,i}} = h \cdot f_i\left(P + k_3^{\,P}, P_b + k_3^{\,P_b}, T_{pt,i} + k_3^{\,T_{pt,i}}\right)$$

Numerical integration	$$k^P = \frac{k_1^P + 2k_2^P + 2k_3^P + k_4^P}{6}$$ $$k^{P_b} = \frac{k_1^{P_b} + 2k_2^{P_b} + 2k_3^{P_b} + k_4^{P_b}}{6}$$ $$k^{T_{pt,i}} = \frac{k_1^{T_{pt,i}} + 2k_2^{T_{pt,i}} + 2k_3^{T_{pt,i}} + k_4^{T_{pt,i}}}{6}$$
Integrated new values	$$t^{n+1} = t^n + h$$ $$P^{n+1} = P^n + k^P$$ $$P_b^{\,n+1} = P_b^{\,n} + k^{P_b}$$ $$T_{pt,i}^{\,n+1} = T_{pt,i}^{\,n} + k^{T_{pt,i}}$$ $$M_{pt,i}^{\,n+1} = \frac{P^{n+1} \cdot \left(V_{pt}/np\right)}{R \cdot T_{pt,i}^{n+1}}$$
Repeat integrations until a cyclic steady state	$$P^o = P^\tau$$ $$P_b^{\,o} = P_b^{\,\tau}$$ $$T_{pt,i}^{\,o} = T_{pt,i}^{\,\tau}$$ where, $\tau = $ period

5.1.6.5 Convergence

For each time step, all of the temperatures and mass flow rates in the system are iterated to satisfy the boundary conditions. Pressure and temperatures at the next time step are calculated using a 4th order Runge-Kutta numerical integration with respect to time. Noting that the cycle operates in a steady state mode requires that the integrations through one complete cycle result in final values that are the same as those at the beginning of the cycle. The iteration procedure is continued until the system achieves a

cyclic steady state at all positions. The allowable relative error (or convergence tolerance) for a cyclic steady state is defined by,

$$\left|\frac{P(t+\tau)-P(t)}{P(t)}\right| \text{ and } \left|\frac{P_b(t+\tau)-P_b(t)}{P_b(t)}\right| < \text{ Convergence tolerance} \qquad (5.34)$$

$$\left|\frac{\dot{m}_{pt,i}(t+\tau)-\dot{m}_{pt,i}(t)}{\dot{m}_{pt,i}(t)}\right|_{for \; i=1\sim np} < \text{ Convergence tolerance} \qquad (5.35)$$

$$\left|\frac{T_{pt,i}(t+\tau)-T_{pt,i}(t)}{T_{pt,i}(t)}\right|_{for \; i=1\sim np} < \text{ Convergence tolerance} \qquad (5.36)$$

Here, the subscript i denotes a different position in the pulse tube, and τ the period of one cycle. The allowable relative errors are set to 10^{-3} for the pressure, the mass flow rates and the temperatures in this report, since there was no significant difference in the results compared to those obtained when the relative error was set to 10^{-4}.

Fig. 5.5 shows the flow diagram of the numerical simulation for the 5-valve pulse tube refrigerator. The 2nd order analysis for the loss mechanisms shown in Fig. 5.5 will be detailed in section 5.4.

START

VALVE
TIMING

SET
$P_H, P_L, T_c, C_{d,H}, C_{d,L}, C_{d,R}, T_{pt,i}, T_{reg,i}$

$t = 0$

CALCULATE
$\dot{m}_{o,1} \sim \dot{m}_{o,5} : (5.6), \dfrac{dP}{dt} : (5.26), \left(\dfrac{dM}{dt}\right)_{pt} : (5.25)$

INTEGRATION
$P(t + \Delta t) : (5.27), \quad M(t + \Delta t) : (5.28)$

CALCULATE
$T(t + \Delta t) : (5.29)$

$t \rightarrow t + \Delta t$

$T_{pt,i}$ corrected

COMPLETE
CYCLE ?

No

Yes

CYCLIC STEADY
STATE ?

No

Yes

INITIALIZATION COMPLETED.
PRINT RESULTS IF REQUIRED.
CONTINUE TO MAIN ROUTINE

From INITIALIZATION
$$P(t), \frac{dP}{dt}(t), T_{pt,i}(t)$$

MAIN ROUTINE
START

$t = 0$

$P, P_b, T_{pt,i}$ *corrected*

CALCULATE
$$\dot{m}_{o,1} \sim \dot{m}_{o,5} : (5.6)$$
$$\dot{m}_{pt,i}, \dot{m}_{r,i}, \dot{m}_h : (5.30) \sim (5.32)$$

$\frac{dP}{dt}$ *corrected*

CHECK
1. Flow Patterns in Fig.5.4
2. $\frac{dP}{dt} : (5.13), (5.15), (5.17), (5.19)$

$\frac{dP}{dt}, T_{pt,i}, \dot{m}_{pt,i}, \dot{m}_{r,i}, \dot{m}_h$
e consistent?

No

$t \rightarrow t + \Delta t$

Yes

The Runge-Kutta 4th order Numerical Integration
$$P(t + \Delta t), P_b(t + \Delta t), T_{pt,i}(t + \Delta t)$$

ETE
CYCLE ?

No

Yes

CYCLIC STEADY
STATE ?

No

Yes

THE 2nd ORDER ANALYSIS
(section 5.4)

PRINT RESULTS
TO FILE

STOP

Figure 5.5 Flow diagram of the numerical analysis for the 5-valve pulse tube refrigerator.

5.2 Verification of Model

Various sample calculations have been performed to verify the feasibility of the numerical model. The selected valve opening sequence for one sample calculation is shown in Fig. 5.6. The cycle starts from the middle of the first compression process through V_5 followed by the second compression through V_1 and V_3. A sudden opening / closing of the solenoid valves at the boundaries of each step in a cycle causes a numerical instability. Thus, the simulations prefer to start in the middle of the 1st compression process during a cycle rather than at the beginning of it. The refrigeration system I was selected to demonstrate the simulation results.

Fig. 5.7 shows the pressure wave during a cycle from both the experiment and the numerical simulation. The maximum and the minimum pressures are in good agreement, as are the time dependent pressure changes. In the real experiments, the pressure waves in the system are not exactly identical during each cycle of operation. This explains the reason for the small discrepancy between the numerical simulation and the experiment at the end of the cycle in Fig. 5.7.

Figures 5.8, 5.9 and 5.10 show the temperature profiles of the gas in the pulse tube determined from the numerical simulation as a function of time and position during a cycle. As expected, the gas temperatures in the pulse tube follow the shape of the pressure wave. As previously reported in the literature [28], the magnitude of the temperature fluctuation is higher in the middle section of the pulse tube than at the ends.

Also as expected, the gas temperature near the hot end is higher than that of the hot heat exchanger. On the other hand, the time-averaged gas temperature near the cold end is slightly higher than that of the cold heat exchanger, even though it happens to have a lower temperature than the cold heat exchanger at some times during the cycle.
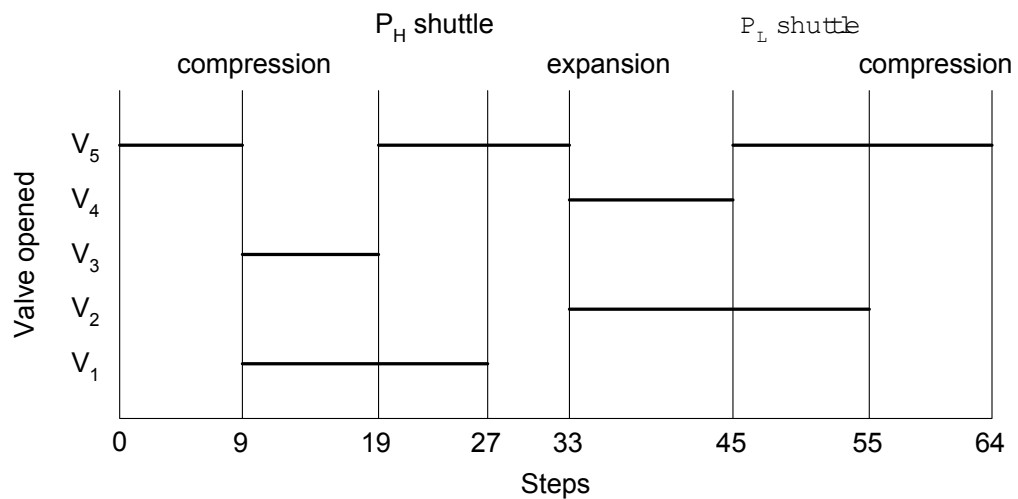
Figure 5.6 The valve opening sequence for the sample calculation.
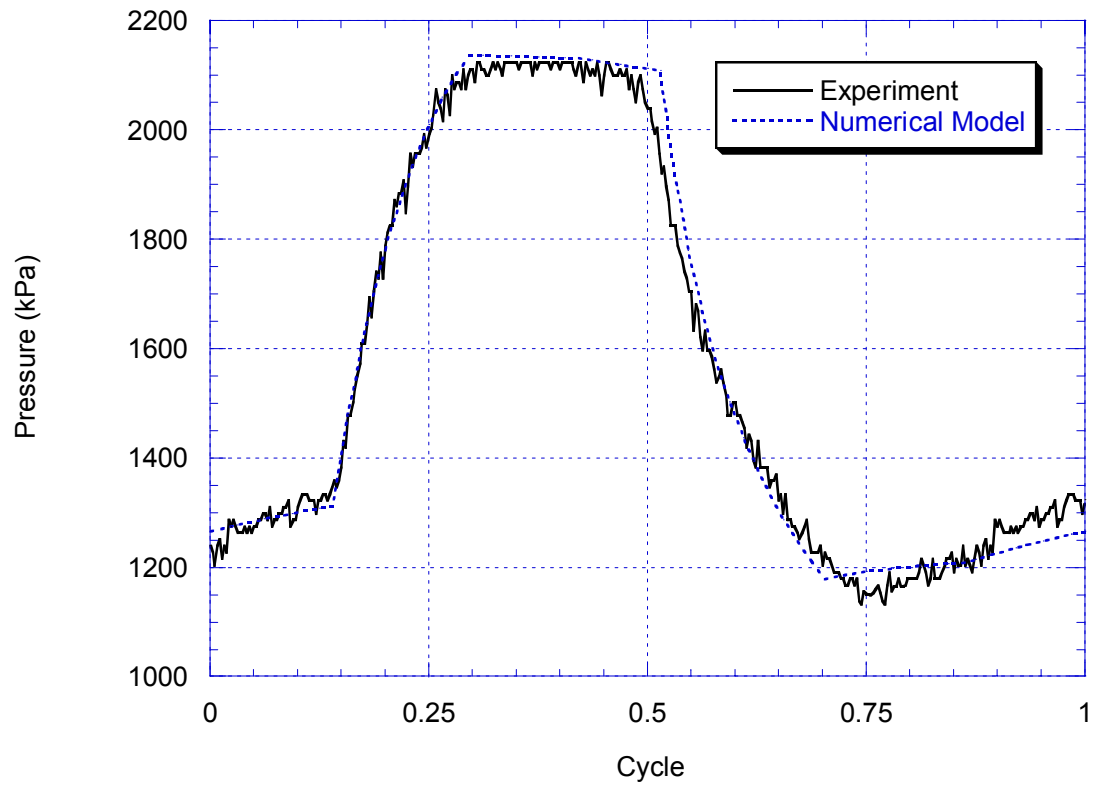
Figure 5.7 Pressure variations during a cycle (pulse tube volume : 360cc, regenerator volume : 123cc, reservoir volume : 3L, compressor pressure : 2205/483kPa, cold heat exchanger temperature : 29K, no-load).
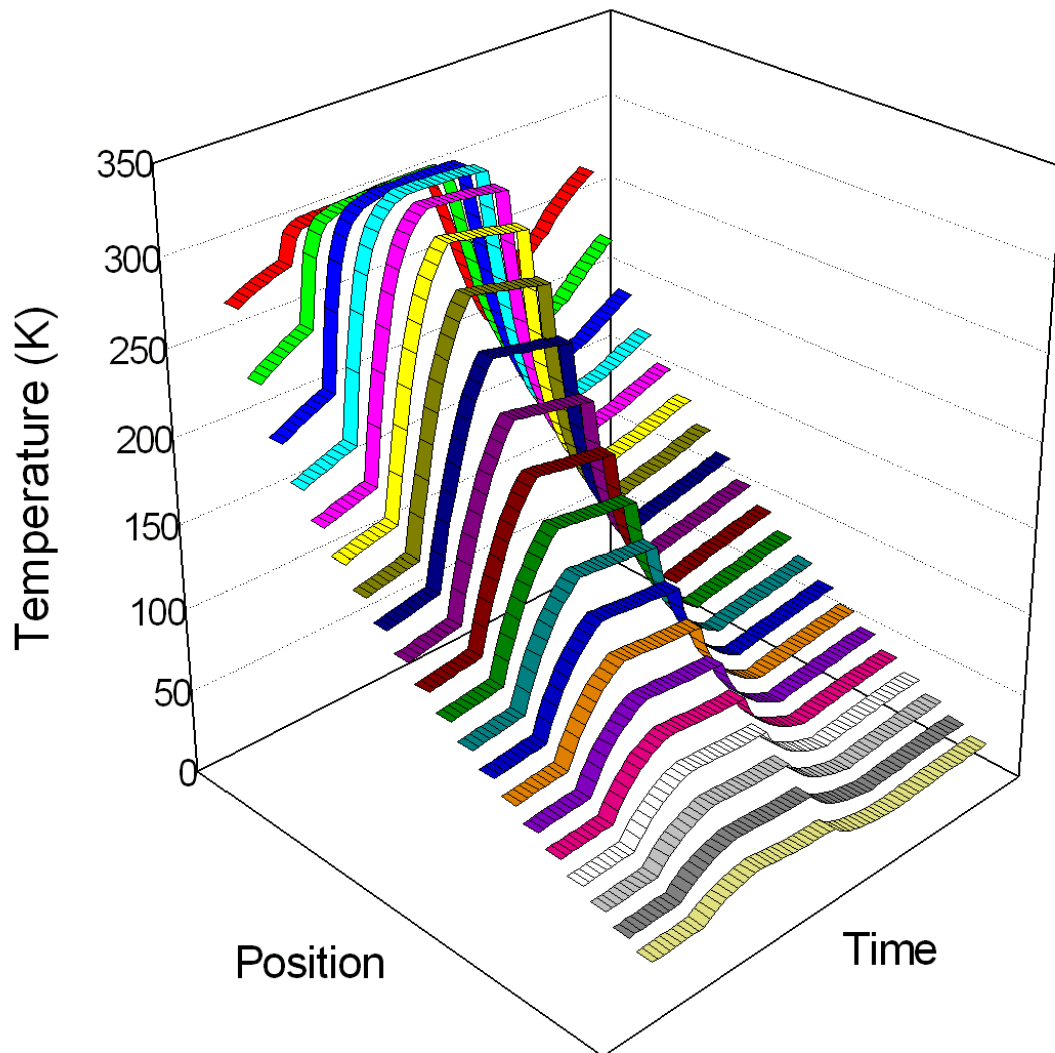
Figure 5.8 Temperature profiles in pulse tube as functions of position and time during a cycle.
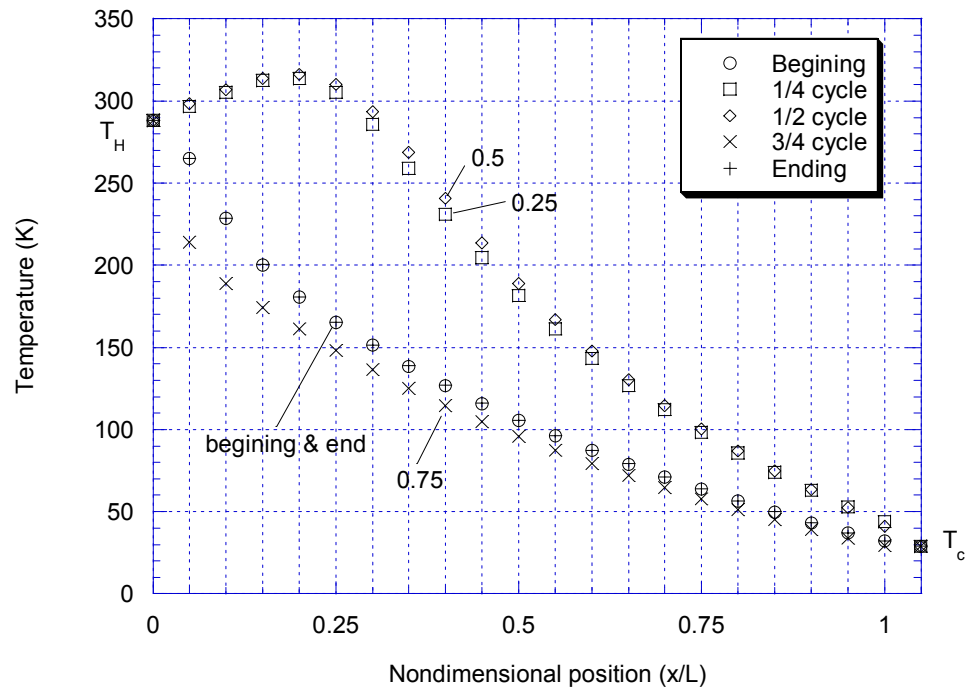
Figure 5.9 Temperature variations as a function of position in the pulse tube at various time during

a cycle.
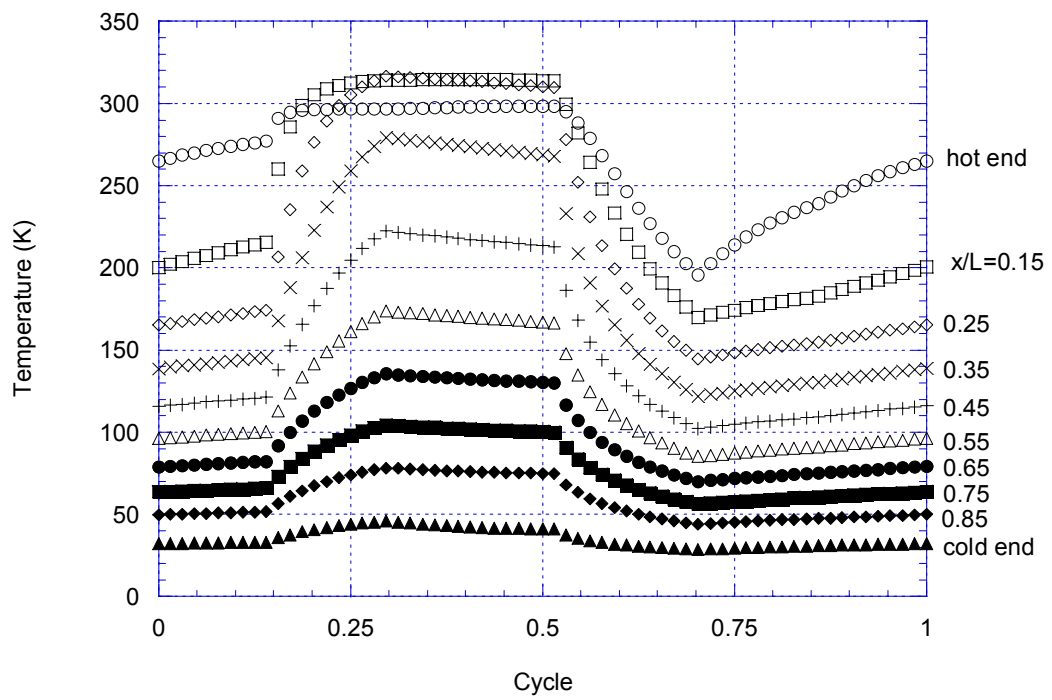
Figure 5.10 Temperature variations as a function of time in the pulse tube at various position.

The pressure and gas temperature distributions as functions of time and position allow us to predict the mass flow rate and velocity at any position and time in the pulse tube and the regenerator. Figures 5.11 and 5.12 show the mass flow rates and the velocities in the pulse tube. The sign conventions for the flow direction follow Fig. 5.3. During the two shuttle processes, the mass flow rates are smaller than during the compression/expansion processes. The gas flows towards the cold end of the pulse tube even if valves V_1 and V_3 are opened at the same time. It seems that the pulse tube has more volume to be compressed in this case. Also, the gas flows towards the hot end of the pulse tube when valves V_2 and V_4 are opened at the same time. The maximum velocity in the pulse tube is ~1.7 m/s during a cycle in this example.

Figures 5.13 and 5.14 show the mass flow rates and the velocities in the regenerator. Since the volume of the regenerator is smaller than that of the pulse tube, the mass flow rates in the regenerator are larger. The gas flows towards the center of the regenerator when valves V_1, V_3 are opened at the same time as expected. On the other hand, the gas moves towards each end of the regenerator when valves V_2, V_4 are opened at the same time. The velocities in the regenerator are also higher than those in the pulse tube, since the free flow area is smaller than in the pulse tube.
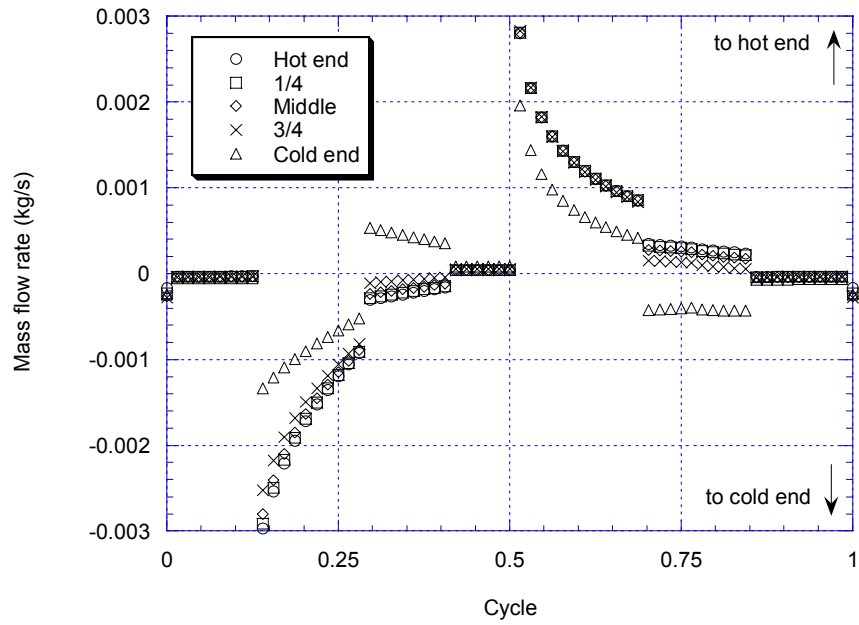
Figure 5.11 Mass flow rates in the pulse tube during a cycle at different positions.
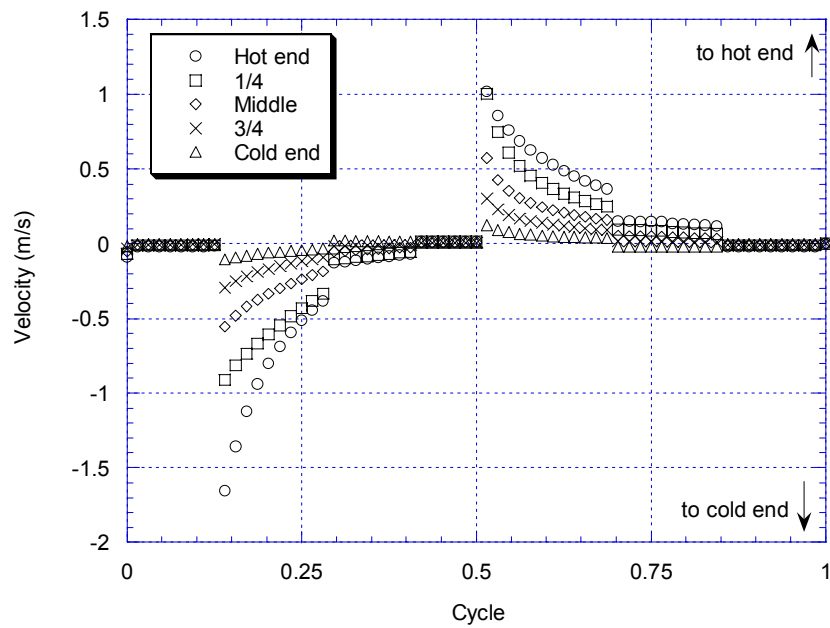
Figure 5.12 Velocities in the pulse tube during a cycle at different positions.
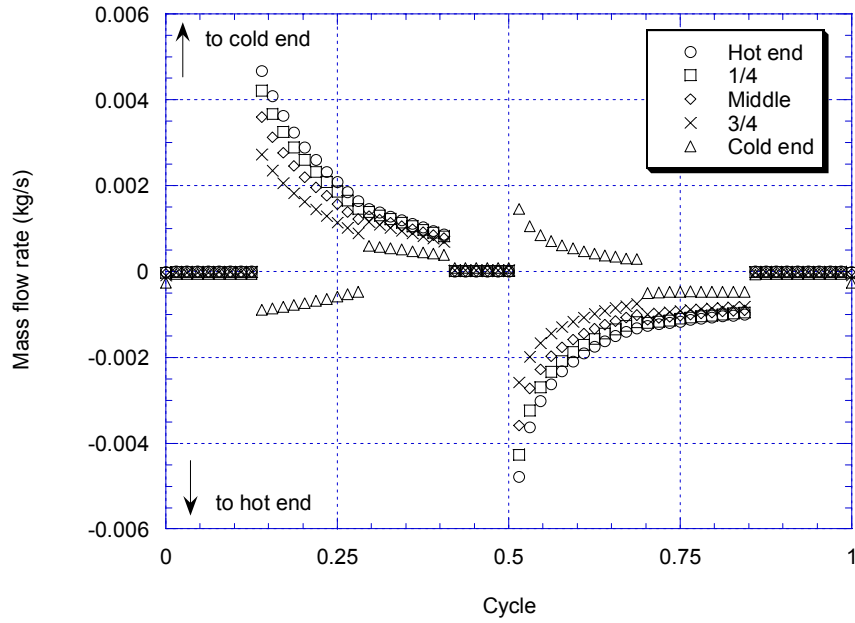
Figure 5.13 Mass flow rates in the regenerator during a cycle at different positions.
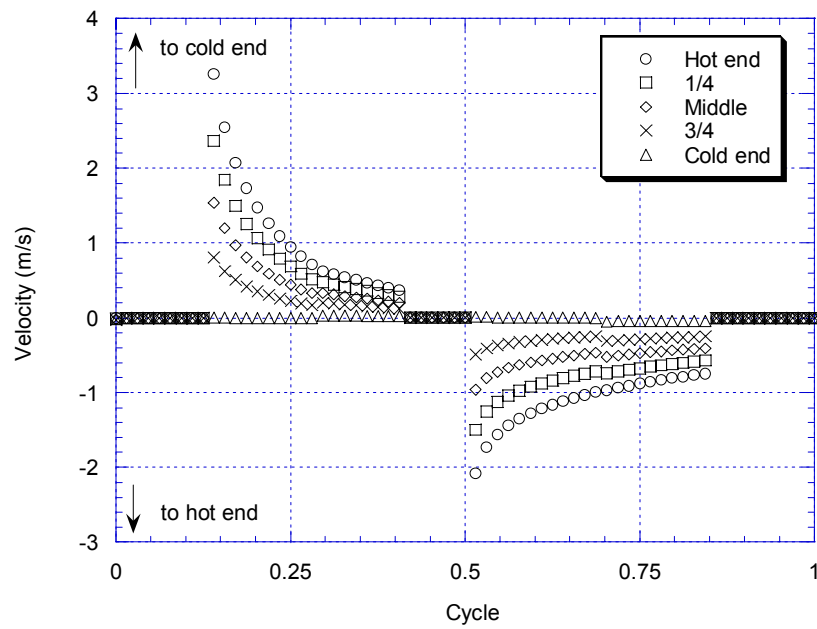
Figure 5.14 Velocities in the regenerator during a cycle at different positions.

5.3 Loss Mechanisms

Since there is a large temperature difference between ambient and the cold head of the pulse tube refrigerator, usually over 200K, a heat loss evaluation is indispensable in the design process of cryogenic refrigerators.

In a pulse tube refrigerator, additional heat loss mechanisms such as shuttle heat loss and DC (direct current) flow are caused by its own specific cooling mechanism. Shuttle heat loss originates from heat transfer between the gas and the pulse tube wall. In a basic pulse tube refrigerator, heat transfer between the gas and wall plays an important role in generating cooling power at the cold end of pulse tube. As the temperature at the cold end of the pulse tube goes down, however, it turns into a non-negligible loss mechanism.

In a double-inlet pulse tube refrigerator, adding an orifice valve between the hot heat exchanger and the compressor makes it possible to reach a lower temperature than a basic and an orifice pulse tube refrigerator. The additional orifice valve allows mass to flow directly to the pulse tube without flowing through the regenerator. This arrangement decreases losses in the regenerator. However, this modification can introduce a mass flow imbalance from the compressor to the hot end of the pulse tube and then to the cold end of the regenerator. In other words, the additional valve introduces the possibility of having a unidirectional secondary flow, such as a direct current in an electrical circuit, that is not found in the basic or orifice pulse tube refrigerators.

In this section, the loss mechanisms in the pulse tube refrigerator including shuttle heat loss and DC flow loss are explained in detail.

5.3.1 Shuttle Heat Loss

As mentioned above, shuttle heat transfer (or, surface heat pumping) is an essential cooling mechanism in a basic pulse tube refrigerator. In a basic pulse tube refrigerator, gas moves towards the hot end of the pulse tube as it is being compressed, and towards the cold end as gas is expanded as shown in Fig. 5.15.

Assuming adiabatic compression/expansion, the temperature and pressure increase/decrease can be related to a change of gas position, x as given by eqn.s (5.37) and (5.38)

$$PT^{\frac{\gamma}{1-\gamma}} = \text{constant} \tag{5.37}$$

$$Tx^{\gamma-1} = \text{constant} \tag{5.38}$$

To demonstrate this concept of motion corresponding to temperature and pressure changes, a high pressure of 1500kPa and a low pressure of 1000kPa of helium gas are selected. Three cold end temperatures, 250K, 150K and 50K are assumed to demonstrate the change of temperature profiles. The average wall temperature distribution is assumed to be linear as is that of the initial gas temperature profile.

compressor regenerator cold HX pulse tube hot HX

(a) compression

compressor regenerator cold HX pulse tube hot HX

(b) expansion
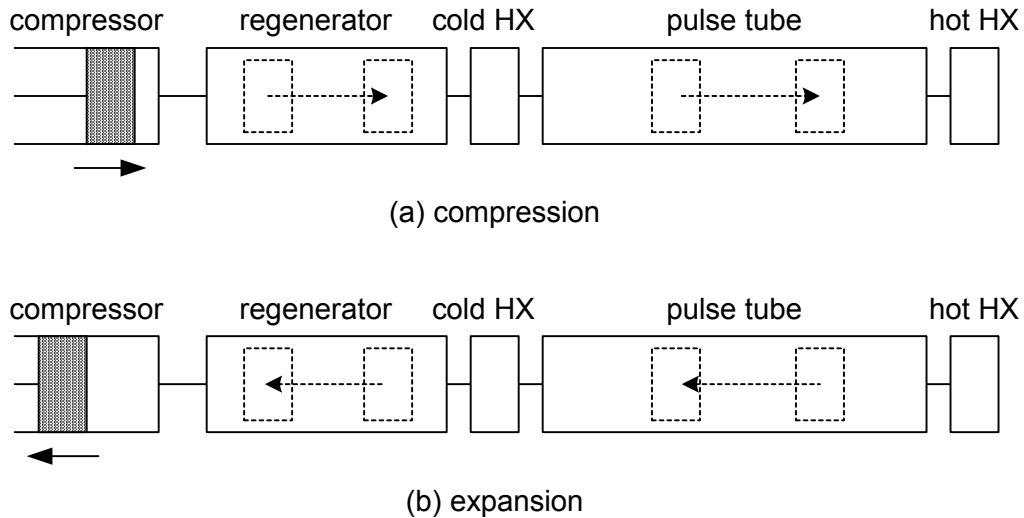
Figure 5.15 Gas movements in a basic pulse tube refrigerator accompanying the movement of compressor piston.

In Fig. 5.16 (a), during the compression process, the gas temperatures increase at every position in the pulse tube and the gas moves towards the hot end of the pulse tube as the pressure increases. In Fig. 5.16 (b), during the expansion process, all of the gas temperatures decrease in the pulse tube and the gas moves towards the cold end of the pulse tube as the pressure decreases. For the case of a 250K cold end temperature, gas temperatures are higher than the adjacent wall temperature everywhere during compression, and are lower than the adjacent wall temperature during expansion. In this case, the gas absorbs heat from the wall as it moves toward the cold end of the pulse tube, and releases it to the wall as it moves toward the hot end. In other words, gas is continuously pumping heat from the cold end to the hot end by heat transfer with the

adjacent wall. This phenomenon is called 'surface heat pumping', and is the basic cooling mechanism for the basic pulse tube refrigerator. However, the shuttle heat transfer mechanism has a limitation that depends on the cold end temperature. When the cold end temperatures are 150K and 50K as shown in Fig. 5.16, the temperature of the gas near the cold end is lower than the adjacent wall even after the compression process is finished. Also, the temperature of the gas near the cold end is higher than the adjacent wall after the expansion process. In this case, the gas absorbs heat from the wall as it is moving toward the hot end and releases heat to the wall as it moves toward the cold end. This will become a significant heat load to the cold end heat exchanger.

The amount of shuttle heat transfer or shuttle heat loss is strongly dependent on the pulse tube dimensions and operating conditions, since it results from heat transfer near the wall and the mass flow rate. The characteristics are time-dependent, as well as position and temperature dependent. For this reason, the gas motion corresponding to pressure and temperature fluctuations is evaluated by numerical simulation and used to calculate the amount of shuttle heat transfer.
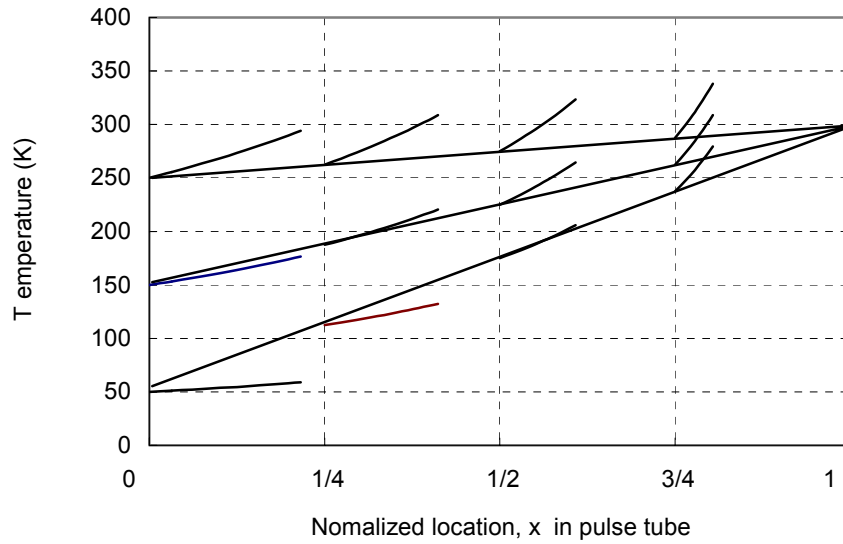
(a) Compression
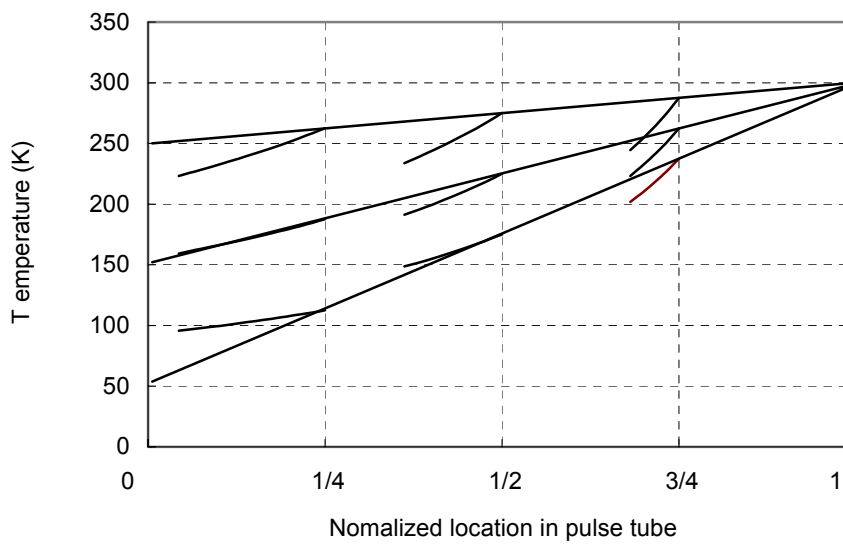
(b) Expansion

Figure 5.16 Adiabatic temperature variations vs. gas movement in the basic pulse tube refrigerator

(P_H=1500kPa, P_L=1000kPa, γ=1.667).

5.3.2 DC Flow Loss

Adding a second orifice valve between the hot end of the pulse tube and the compressor significantly improves the performance by decreasing the mass flow rate through the regenerator that does not contribute to the actual cooling power generation. However, this new configuration also introduces a possibility for unbalanced, unidirectional flow, analogous to direct current in an electrical circuit. Fig. 5.17 shows a schematic diagram of a double-inlet pulse tube refrigerator. During the compression process, high pressure gas flows out of the compressor and is divided into two flow streams; one to the hot end of the regenerator, and the other to the hot heat exchanger through the orifice valve. Flow resistances of the regenerator and the double-inlet orifice valve determine the ratio of the mass flow rates into the system. During the expansion process, mass flows from the regenerator and the hot heat exchanger back to the compressor. However, the flow resistance for gas that returns to the compressor can be different from that for the gas coming out of the compressor. Typically orifice valves have directional characteristics, ie, the mass flow rate at the same pressure ratio may be different when the orifice valve is installed in the reverse direction. Also, in the regenerator, the pressure drop that is represented as flow resistance is a function of the pressure difference between the regenerator ends, as well as the temperature, density and other fluid dynamic values such as velocity. The pressure drop can be different for the compression and expansion process. This potential imbalance in flow resistance can generate a unidirectional net mass flow rate in a pulse tube system. The net mass flow is

zero for an ideal balance of flow resistances. However, in actual conditions, the net mass flow can be 'counterclockwise' (i.e., a positive DC flow through the cold heat exchanger) or 'clockwise' (i.e., a negative DC flow through the cold heat exchanger) in Fig. 5.17. If the system has a positive DC flow, more cold gas flows from the cold end of the regenerator to the cold end of the pulse tube with the result that the gas temperature can be lower during the expansion process. In other words, the system ideally produces more cooling power. However, a positive DC flow also increases the mass flow rate through the regenerator and the pressure drop in the regenerator. The mass flow rate in the regenerator is also unbalanced. On the other hand, a negative DC flow increases the heat load to the cold end of the pulse tube. As the mass flow from the hot end to the cold end of the pulse tube is increased, higher temperature gas may reach the cold end of the pulse tube and this additional mass flow decreases the cooling power of the system. As mentioned above, DC flow causes several different effects and its impact on the system performance is not obvious. In the G-M type 5-valve pulse tube refrigerator, four valves (V_1~V_4) perform the function of the double-inlet orifice valve. Therefore the 5-valve system has the possibility for DC flow. The numerical cycle simulation described above can evaluate the direction and amount of DC flow.
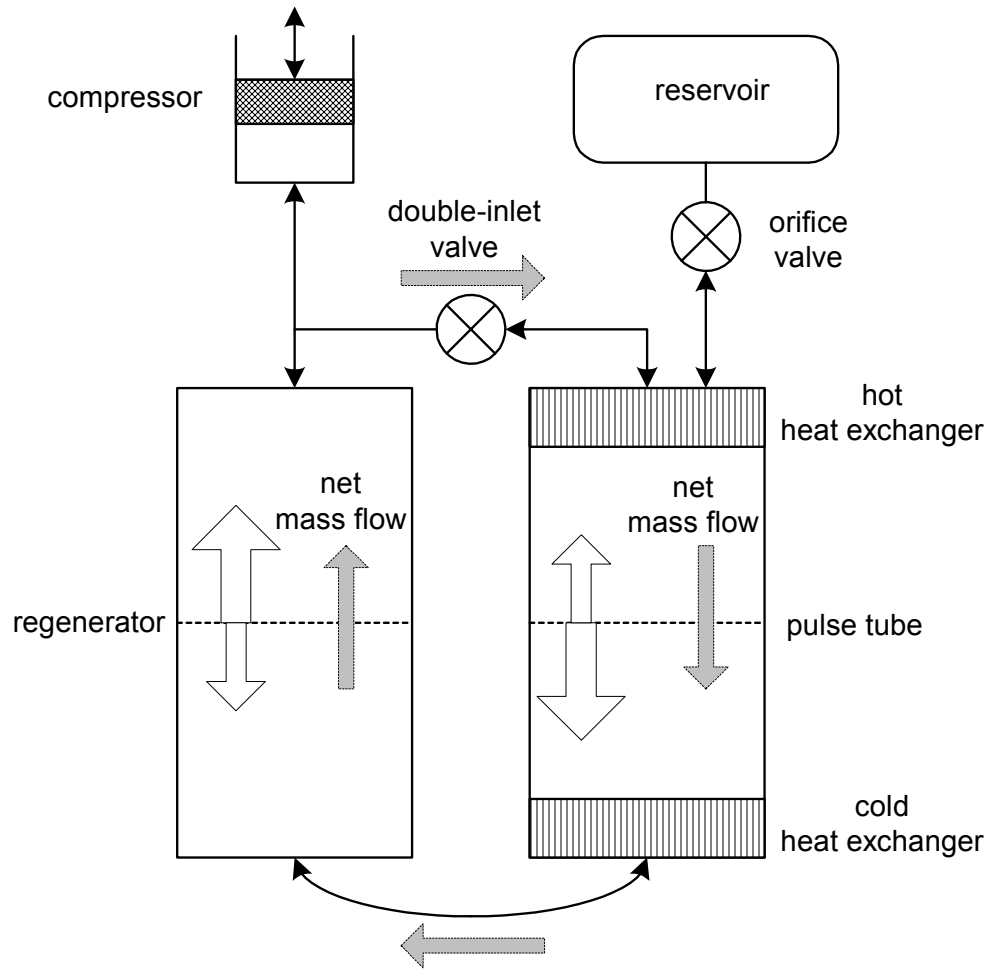
Figure 5.17 Schematic diagram of DC flow in a double-inlet pulse tube refrigerator.

(The net mass flow is a negative DC flow in this figure.)

5.3.3 Heat Transfer Correlations

In a Lagrangian approach, the temperature changes are experienced by each moving gas packet influenced by the heat transfer between the pulse tube wall and the gas. In this report, three heat transfer correlations have been investigated for their applicabilities.

First, the convection heat transfer correlation associated with flow in a combined entry region was investigated. During a cycle, the direction of flow and its temperature fluctuation changes so much that it is hard to imagine the flow being fully developed either thermally and hydrodynamically. The average convection heat transfer coefficient or Nusselt number for the combined entry region is shown in eqn. (5.39) [29].

$$\overline{Nu_D} = 1.86\left(\frac{Re \cdot Pr}{L/D}\right)^{1/3}\left(\frac{\mu}{\mu_w}\right)^{0.14}$$

$$\left(\text{for}\quad T_w = \text{constant},\quad 0.48 < Pr < 16700,\quad 0.0044 < \left(\frac{\mu}{\mu_w}\right) < 9.975\right)$$

(5.39)

Here, *Re* denotes Reynolds number, *Pr* the Prandtl number, *L* the length scale, *D* the tube diameter, μ the viscosity of the gas at the gas temperature, μ_w the viscosity of the gas at the wall temperature and T_w the wall temperature. Since eqn. (5.39) is applicable for constant wall temperature conditions, the pulse tube wall can be assumed to have many segments that each has a constant wall temperature.

Second, the heat transfer correlation for oscillating flow in a reciprocating piston/cylinder apparatus was employed as shown in eqn (5.40) [30]. This correlation was developed only for sinusoidal pressure profiles. While the pressure profile in the G-M type pulse tube is not sinusoidal, it is similar. The effects of pressure change rate, $\dfrac{dP}{dt}$, frequency f and the thermal boundary layer thickness, λ are included in the correlation to calculate the convection heat transfer coefficient in oscillating flow.

$$q_w''(t) = \frac{k}{H}\left(K_s(T_w - T) + K_t \frac{H^2}{k}\frac{dP}{dt}\right) \quad where, \quad K_s, K_t = fn(\lambda, P, T_w, k, f) \tag{5.40}$$

Third, the Chilton-Colburn analogy was employed to calculate the convection heat transfer coefficient based on the analogy between the friction coefficient and heat transfer coefficient as shown in eqn. (5.41) [29]. The disadvantage of this correlation is that the analogy is suitable only for fully developed turbulent flow in a smooth circular tube.

$$\frac{C_f}{2} = St \cdot Pr^{2/3} \tag{5.41}$$

Fig. 5.18 shows an example of gas temperatures as a function of their trajectories and the pulse tube wall temperature as a function of position. In this calculation, the gas temperatures are obtained from the adiabatic numerical simulation in Fig. 5.8. The pulse

tube wall temperature profile as a function of time was calculated using the heat transfer correlation for oscillating flow, eqn. (5.40) and the energy balance between the adiabatic gas temperatures and the wall temperatures as shown in Fig. 5.19. The magnitude of the equilibrium wall temperature fluctuation as a function of time was less than 2K at any position for all three different heat transfer correlations. In Fig. 5.18, the time-averaged wall temperature profile is displayed. Two important features are evident in these results. First, during the cycle each gas packet absorbs heat from the wall as it moves toward a higher temperature position and releases heat to the wall as it moves towards a lower temperature position. This effect clearly displays the shuttle heat loss mechanism. Second, the trajectory of gas packets is not a complete circle, displaying the existence of a DC flow from the hot end toward the cold end of the pulse tube. In other words, the trajectory of gas movement and its temperature change during a cycle can provide complete information for shuttle heat transfer, and the existence of DC flow.

Note that all of the gas temperatures used in Figures 5.18 and 5.19 are resultant from an adiabatic analysis. In a real system, the gas temperatures are also changed by exchanging heat with the pulse tube walls. As one can notice, the amount of shuttle heat loss and DC flow is dependent on the temperatures of the gas and the pulse tube wall. Therefore, more realistic values of losses should be evaluated from the equilibrium gas temperature and the corresponding equilibrium pulse tube wall temperatures. An attempt to determine such results from a 2nd order analysis will be detailed in section 5.4.
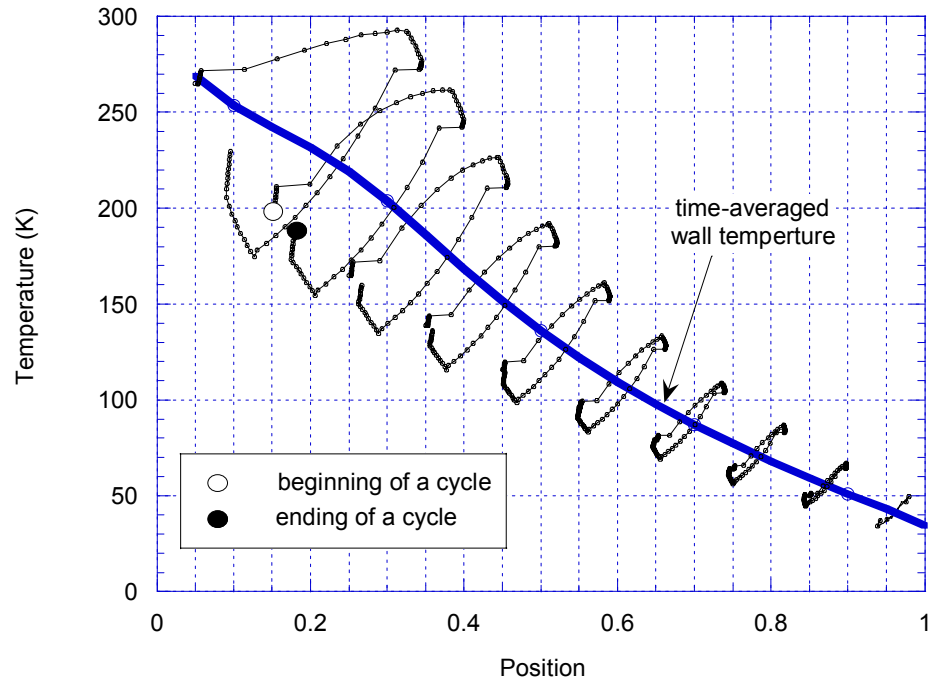
Figure 5.18 **The trajectory of gas movement and temperature as a function of position in the pulse tube during a cycle for several gas packets selected.**

$$h \cdot dA \cdot \left(T_{gas} - T_{wall}\right) = \delta\dot{Q}_{conv}$$
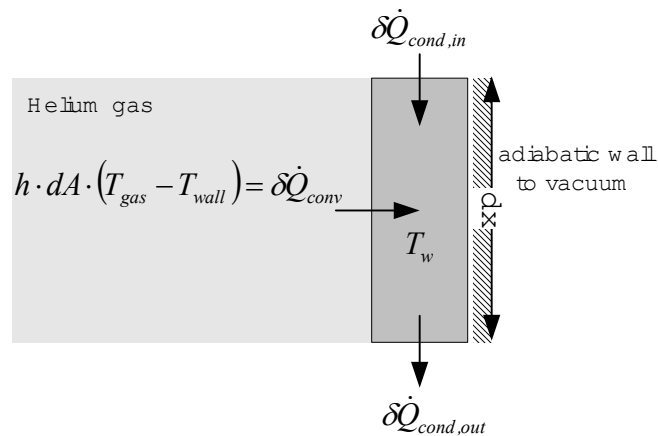
$$\frac{\partial\left(M_w C_{v,w} T_w\right)}{\partial t} = \delta\dot{Q}_{conv} + \delta\dot{Q}_{cond,in} - \delta\dot{Q}_{cond,out}$$

Figure 5.19 **Energy balance for the pulse tube wall including heat transfer.**

5.3.4 Other Losses

Three additional losses associated with the regenerator are the pressure loss, ineffectiveness, and conduction loss. Since a number of screens and lead spheres are tightly packed into the regenerator to increase the heat transfer area, the pressure drop for flow through the regenerator is not negligible. The pressure drop decreases the amplitude of the pressure oscillation in the pulse tube compared to that generated at the compressor. The pressure drop, therefore, decreases the driving potential of the adiabatic compression and expansion and inhibits gas movement. It directly affects the Pressure-Volume characteristics at the cold end of the pulse tube, and consequently results in a cooling power loss.

If we decrease the number of screens and lead spheres in order to reduce the pressure drop in the regenerator then we decrease the heat transfer area. One of the main functions of a regenerator is to provide thermal isolation between ambient temperature and the cold heat exchanger by perfect heat exchange with the gas. Ideally when the gas is flowing from the warm to cold ends, it exits the regenerator at the cold heat exchanger temperature. Less than perfect heat exchange in the regenerator increases the temperature at the cold end of the regenerator, and results an additional load on the cold heat exchanger. This loss is quantified by the regenerator ineffectiveness.

Conduction heat transfer through the regenerator occurs via its walls and through the matrix. In general, the regenerator wall is very thin (~0.5mm) in order to decrease heat conduction. Nevertheless, conduction heat loss may be significant due to short

lengths (typically 3 – 12 inches) and large temperature differences (typically over 200K).

In addition, heat conduction through the gas and matrix must be evaluated. Conductivities associated with stacked screens and packed spheres are typically a factor of ten times less than the bulk conductivities of the same material [26].

5.4   The 2nd Order Analysis for the Loss Mechanisms

As described in section 5.2, the space and time dependent gas temperatures in the pulse tube are obtained from an adiabatic analysis, and therefore do not account for heat transfer between the gas and the wall and the associated shuttle heat loss. However, the DC flow loss that is caused by the imbalance of the mass flow rates in the system may be included in the ideal cooling power, even though the shuttle heat loss is ignored. The concept of the cooling power calculation for the adiabatic analysis is depicted in Fig. 5.20. The amount of the DC flow depends on the balance of mass flow rates in the system. It could be a positive value (flow from the cold end of the regenerator to the cold heat exchanger), a negative value (flow from the cold heat exchanger to the cold end of the regenerator), or zero. Note that a positive DC flow results in an unbalanced flow in the regenerator and decreases its effectiveness. In this analysis, the unbalanced flow effect on the effectiveness of the regenerator is ignored. The influence of heat transfer between the gas and wall is determined from the cycle-averaged energy balance depicted in Fig. 5.20 by comparing the net enthalpy flow into the cold end heat exchanger as calculated with the 'adiabatic' gas temperature profiles, to that realized when the gas temperature profile is modified by heat transfer with the wall. $\left\langle \dot{H}_{out} \right\rangle$ represents the cycle-averaged enthalpy flow across the boundary between the cold heat exchanger and the pulse tube for the 'adiabatic' case – that is, without consideration of heat transfer

between the gas and the pulse tube wall, while $\left\langle \dot{H}_{out} \right\rangle'$ represents the same quantity when the heat transfer is included. The DC flow loss, the ideal cooling power and the heat transfer induced change are calculated by using eqn.s (5.43)~(5.46).
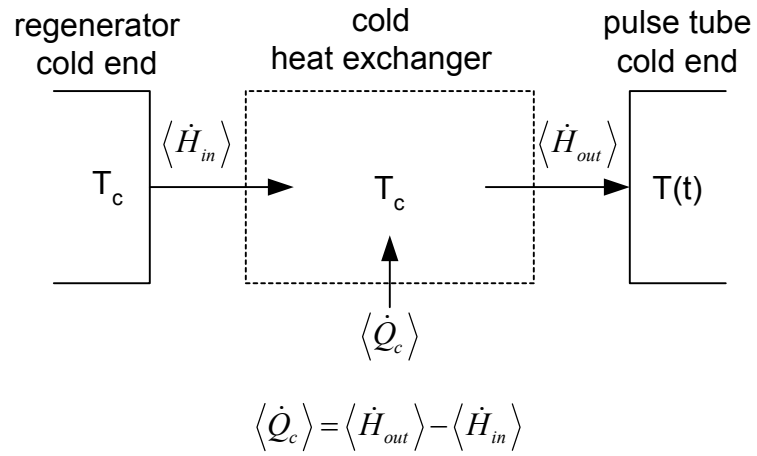
Figure 5.20 Energy balance at the cold heat exchanger.

$$\left\langle \dot{H}_{in} \right\rangle = \left\langle \dot{m}_{r,nr} h\left(T_c\right) \right\rangle = \begin{cases} <0: & \text{negative DC flow} \\ 0: & \text{no DC flow} \\ >0: & \text{positive DC flow} \end{cases} \qquad (5.43)$$

$$\left\langle \dot{Q}_c \right\rangle_{ideal} = \left\langle \dot{H}_{out} \right\rangle - \left\langle \dot{H}_{in} \right\rangle \qquad (5.44)$$

$$\left\langle \dot{Q}_c \right\rangle' = \left\langle \dot{H}_{out} \right\rangle' - \left\langle \dot{H}_{in} \right\rangle \qquad (5.45)$$

$$\text{Change of enthalpy flow} = \left\langle \dot{H}_{out} \right\rangle' - \left\langle \dot{H}_{out} \right\rangle \qquad (5.46)$$

To obtain the space and time dependent gas temperatures when heat transfer with the walls is included, an energy balance is applied to each discrete volume in the pulse tube. The analysis begins with the 'adiabatic' gas temperature profile and calculates a change in temperature just due to the heat transfer with the wall. The pressure, the time-averaged wall temperature and the heat transfer correlation eqn. (5.40) are used to solve the differential equation, eqn. (5.47) for each discrete volume. The same number of time steps (64) was used in this analysis.

$$\dot{m}_{in} C_p T'_{pt,in} - \dot{m}_{out} C_p T'_{pt,out} + \dot{Q}_{wall} = \frac{C_v}{np} \left(\frac{PV_{pt}}{R\overline{T}_{pt,i}} \right) \frac{dT'_{pt,i}}{dt} \tag{5.47}$$

Here, $\overline{T}_{pt,i}$ represents the time-averaged gas temperature from the adiabatic analysis, and $T'_{pt,i}$ is the gas temperature modified by the heat transfer $\dot{Q}_{wall}$ with the pulse tube wall. The $\dot{Q}_{wall}$ in eqn. (5.47) represents the heat transfer between the modified gas temperature, $T'_{pt,i}$ and the wall temperature profiles, T_{wall} obtained from sec. 5.3.3.

$$\dot{Q}_{wall,i}(t) = h_i(t) A_{wall} \left\{ T_{wall,i}(t) - T'_{pt,i}(t) \right\} \tag{5.48}$$

The analysis procedure is as the followings. In the 1st iteration, $T'_{pt,i}$ is calculated at each position and time step based on the adiabatic temperature profiles. Then in the second iteration, a new value of $T'_{pt,i}$, call it $T''_{pt,i}$ is calculated starting with the values of $T'_{pt,i}$ at

each position and time step. This iteration is continued until the temperatures at the end of the cycle match those at the beginning.

Figures 5.21 and 5.22 show the differences between the modified temperature profiles ($T'_{pt,i}$) and the 'adiabatic' temperatures profiles ($T_{pt,i}$) as functions of time and position in the pulse tube. The average gas temperatures are increased near the hot end by absorbing heat from the pulse tube wall. On the other hand, the modified gas temperatures near the cold end become colder than the adiabatic temperatures. Thus, the cycle-averaged enthalpy flow across the boundary between the cold heat exchanger and the pulse tube with the 'modified' temperature profiles, $\left\langle \dot{H}_{out} \right\rangle'$, are increased. Fig. 5.23 shows the trajectory of the gas movement and the temperature differences between the modified temperature and the adiabatic temperature in the pulse tube. Even though the wall temperature remains the same as the adiabatic case, the gas temperatures are increased near the hot end, and are decreased near the cold end of the pulse tube. The existence of the DC flow is also identified. In particular, most of the gases at the cold end of the pulse tube become colder than the adiabatic case. From these results, we expect a net increase of enthalpy flow $\left\langle \dot{H}_{out} \right\rangle'$ at the cold heat exchanger. An example of the computation results showing cooling performance including the losses is summarized in Table 5.3. In this sample calculation, the DC flow loss (or negative DC flow) was 2.67W, and this value remains as a constant until the operation condition is changed. The ideal cooling power is calculated as −5.84W, a value, which if real would mean that the

cold heat exchanger temperature would increase to a higher equilibrium value. The 2nd order analysis, considering heat transfer between the gas and the pulse tube wall, reveals the change of enthalpy flow of 10.21W. Other losses including conduction, pressure drop in the regenerator and so on are total -1.75W. As a result of the gas temperature modification including the heat transfer in the pulse tube and other losses, the actual cooling power modified in the 2nd order analysis becomes –0.05W, a value within the uncertainty of the experimental result. In the experiment, the Minco-brand heater and the DC power supply were used to apply the heat load to the cold heat exchanger. The resolutions of the DC power supply and the heater are $\pm$ 0.3V (= $\pm$ 1% of 30V) and $\pm$ 0.5Ω, respectively. The uncertainty for the heat load measurement is $\pm$ 0.18W.

The observation of the change of enthalpy flow cross the boundary between the cold end of the pulse tube and the cold heat exchanger is somewhat of a surprise. In the sample calculation, the decreased gas temperatures at the cold end of the pulse tube corrected by the consideration of the heat transfer increase the enthalpy flow $\left\langle \dot{H}_{out} \right\rangle'$ at the boundary. It is possible that the adiabatic model did not capture the true temperature profiles of the gas. The corrected gas temperature profile, however, more accurately depicts the real enthalpy flows during a cycle. It also should be noted that the corrected gas temperature profiles more accurately match the qualitative observations of pulse tube wall temperature profiles during the experiments. The change of enthalpy flow is found (from the model) to be quite sensitive to the different valve timings and discharge coefficients of the three orifice valves, and the shuttle heat transfer may reflect real

features that are inherent to the 5-valve operation. The influence of the valve timing and

discharge coefficients on the cooling performance will be discussed in the next section.
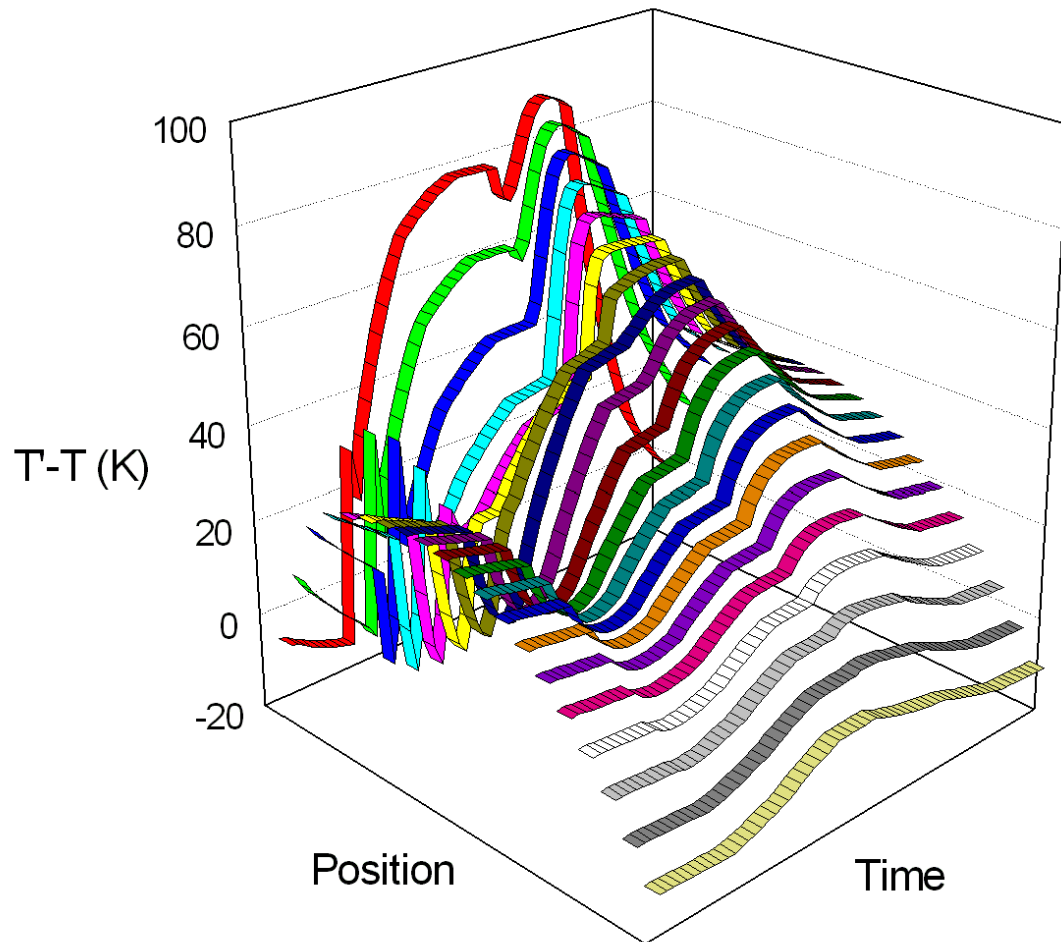
Figure 5.21   Temperature differences between the modified temperature variations and the adiabatic temperature variations in the pulse tube as functions of time and position.
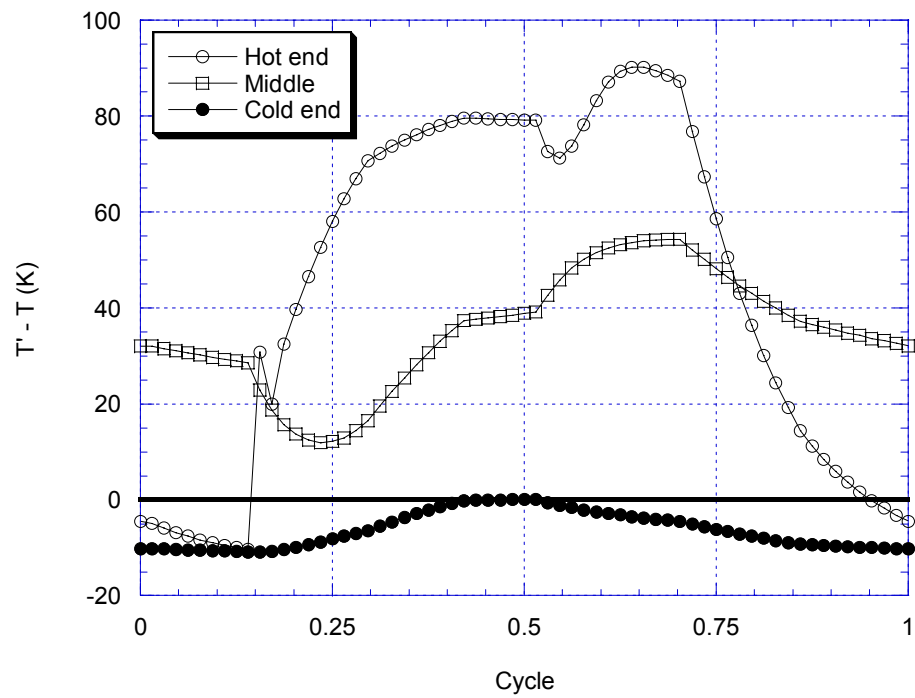
Figure 5.22 Temperature differences between the modified temperature variations and the adiabatic temperature variations at selected positions in the pulse tube as a function of time.
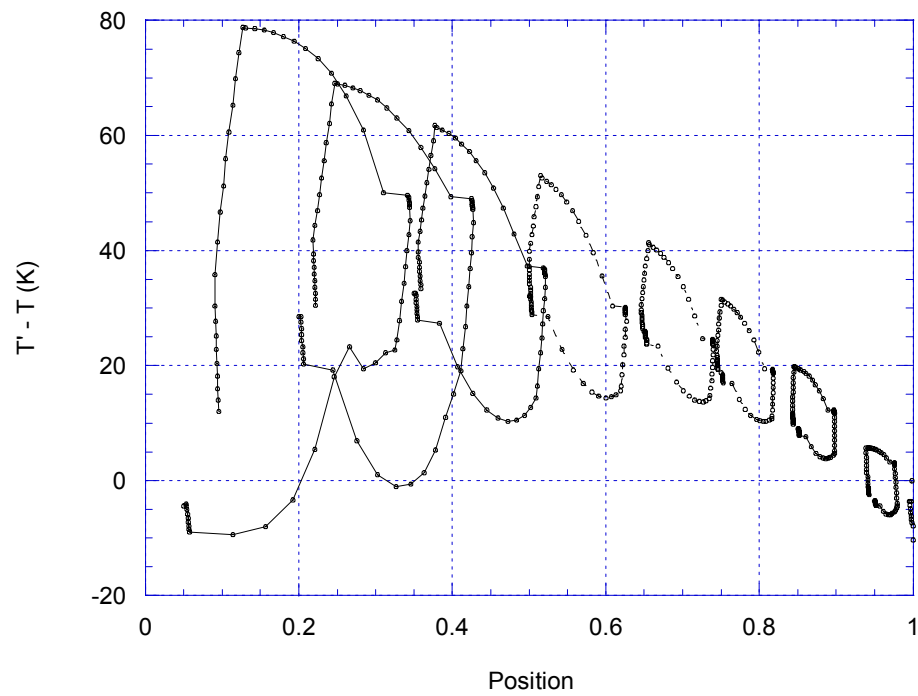
Figure 5.23 The trajectory of gas movement and the temperature difference between the modified temperature and the adiabatic temperature in the pulse tube as a function of position during a cycle for several gas packets selected.

Table 5.3 Summary of the losses and the cooling performance

1st order analysis (adiabatic)	DC flow, $\left\langle \dot{H}_{in} \right\rangle$	-2.67 W
	Net enthalpy flow $\left\langle \dot{H}_{out} \right\rangle$	-8.51 W
Ideal cooling power	$\left\langle \dot{Q}_c \right\rangle_{ideal} = \left\langle \dot{H}_{out} \right\rangle - \left\langle \dot{H}_{in} \right\rangle$	-5.84 W
2nd order analysis (heat transfer)	Change of enthalpy flow, $\left\langle \dot{H}_{out} \right\rangle' - \left\langle \dot{H}_{out} \right\rangle$	10.21 W
	Net enthalpy flow, $\left\langle \dot{H}_{out} \right\rangle'$	1.70 W
Other losses	Conduction, Pressure drop etc.	-1.75 W
Actual cooling power	$\left\langle \dot{Q}_c \right\rangle_{actual} = \left\langle \dot{H} \right\rangle_{out}$ + other losses	*-0.05W*
Experiment at 29K	$\left\langle \dot{Q}_c \right\rangle_{exp}$	*0 W*

5.5 Discussion

In the previous section, the direction and the amount of DC flow were determined in the 1st order analysis. The 2nd order analysis considering the heat transfer between the gas and the pulse tube walls allowed the gas temperature to be decreased near the cold end of the pulse tube and in turn, the cooling power to be increased. This modification of the gas temperature in the 2nd order analysis improves the predictability of the numerical analysis. In the numerical analysis for the 5-valve pulse tube refrigerator, it is found that the mass flow rate profiles are very sensitive to the flow resistances through the orifice valves. Since the DC flow and the shuttle heat transfer are also determined by these mass flow rate profiles in the system, the cooling power is also very sensitive to the flow resistances of the orifice valves. Three discharge coefficients for the orifice valves were varied to investigate their effects on the cooling performance. As explained in Chapter 3, the solenoid valves V_1 and V_3 are connected to the high pressure orifice valve, V_{o-H}, valves V_2 and V_4 to the low pressure orifice valve, V_{o-L}, and valve V_5 to the reservoir orifice valve V_{o-R}.

Figures 5.24 and 5.25 show the effects of the high pressure discharge coefficient, $C_{d,H}$ on the various enthalpy flows and the cooling powers. In Fig. 5.24, the maximum positive DC flow, $\langle \dot{H}_{in} \rangle$ can be obtained with $C_{d,H} \sim 1.3$, and the ideal cooling power, $\langle \dot{Q}_c \rangle_{ideal}$ is maximum for the smallest value of $C_{d,H}$. However, if the heat transfer between the gas and the pulse tube wall is included as shown in Fig. 5.25, the maximum

actual cooling power can be obtained with $C_{d,H} \sim 1.9$, and its value becomes higher than the maximum ideal cooling power by virtue of the gas temperature changes, and in turn the change of enthalpy flow.

Fig. 5.26 and Fig. 5.27 show the effects of the low pressure discharge coefficient, $C_{d,L}$ on the various enthalpy flows and the cooling powers. The influence of the low pressure discharge coefficient is stronger than the high pressure discharge coefficient since the magnitude of $C_{d,L}$ is smaller than that of $C_{d,H}$. In Fig. 5.27, the actual cooling power increases continually with $C_{d,L}$. However, larger values of $C_{d,L}$ will decrease the lowest pressure of the system, and thus decrease the average system pressure followed by the reduced pressure oscillation potential and the reduced cooling performance.

Fig. 5.28 and 5.29 show the effects of the reservoir discharge coefficient, $C_{d,R}$ on the various enthalpy flows and the cooling powers. The cooling powers and various losses are extremely sensitive to $C_{d,R}$. The same sensitivity is also observed in the experiments. A small change of $C_{d,R}$ can easily change the phase difference between the pressure and the mass flow rate at the hot end of the pulse tube. Therefore, $C_{d,R}$ plays a very important role in determining overall system performance.

All of the discharge coefficients influence the pressure, temperature and mass flow rate profiles and thus the system performance. Each of them can be optimized for various pulse tube and regenerator dimensions. The combined effects of the valve coefficients and the compressor performance must be considered in an optimal design process. One of the remarkable advantages of this numerical analysis is that it can

simulate any type of valved G-M type pulse tube system including the two-valve or the four-valve system, by controlling their discharge coefficients. Also, any G-M type compressor can be simulated if the appropriate mass flow rate correlation is available as a function of operating pressures. Such a correlation can be easily obtained from a simple test of the compressor.
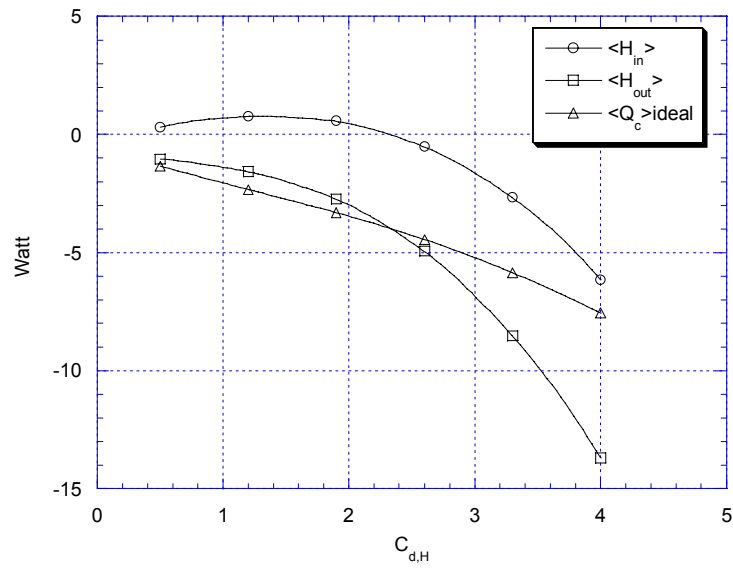
Figure 5.24 The enthalpy flows and the ideal cooling power based on the 1st order, adiabatic analysis for various high pressure discharge coefficients ($C_{d,L}$ =0.85 and $C_{d,R}$ =0.09 are fixed).
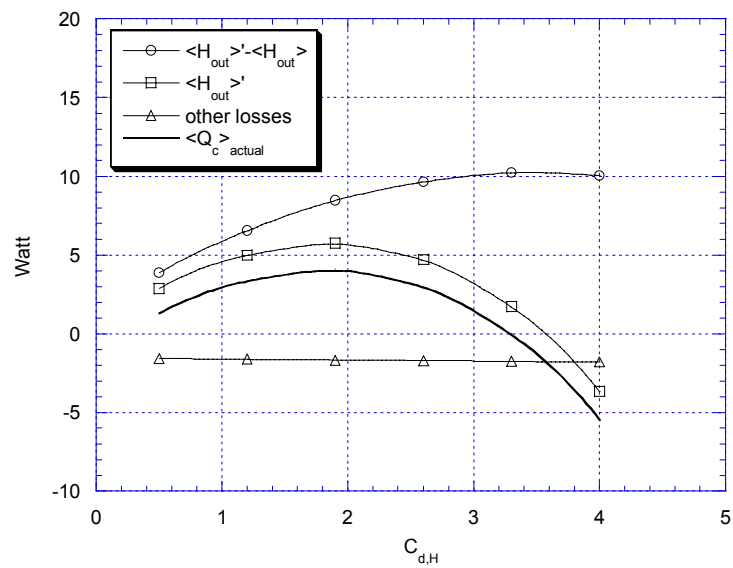
Figure 5.25 The actual cooling power including the losses based on the 2nd order analysis for various high pressure discharge coefficients ($C_{d,L}$ =0.85 and $C_{d,R}$ =0.09 are fixed).
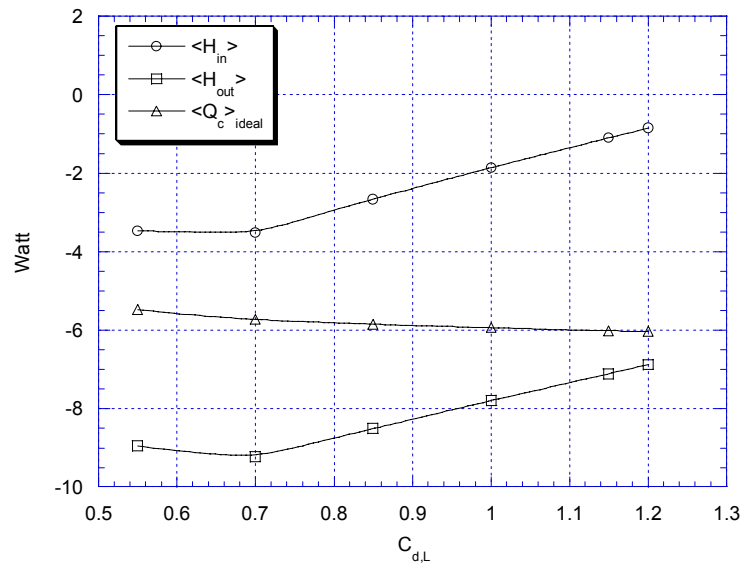
Figure 5.26 The enthalpy flows and the ideal cooling power based on the 1st order, adiabatic analysis for various low pressure discharge coefficients ($C_{d,H}$=3.3 and $C_{d,R}$ =0.09 are fixed).
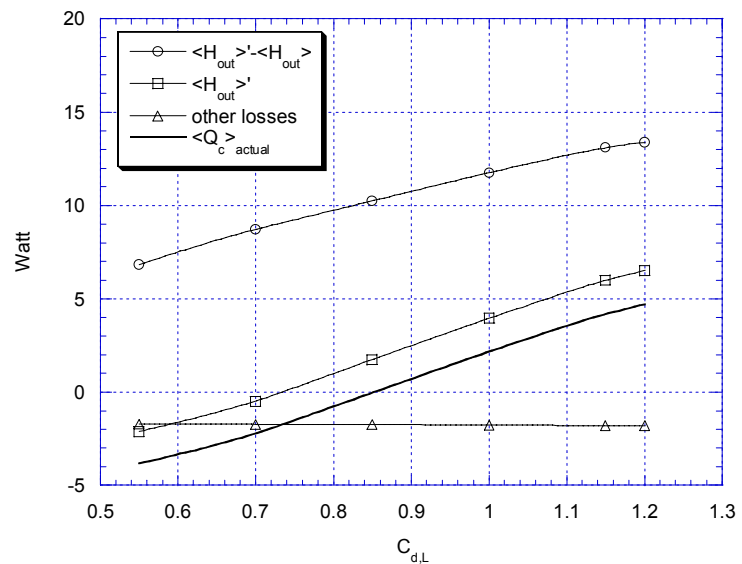
Figure 5.27 The actual cooling power including the losses based on the 2nd order analysis for various low pressure discharge coefficients ($C_{d,H}$=3.3 and $C_{d,R}$ =0.09 are fixed).
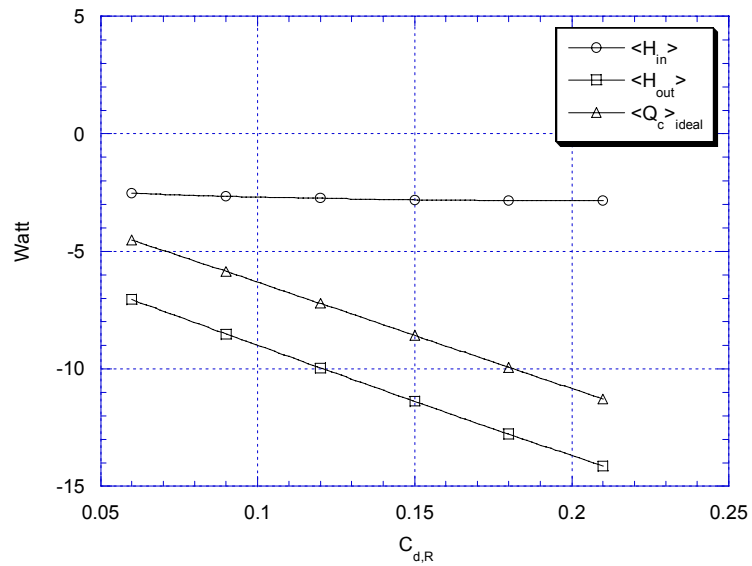
Figure 5.28 The enthalpy flows and the ideal cooling power based on the 1st order, adiabatic analysis for various reservoir discharge coefficients ($C_{d,H}$=3.3 and $C_{d,L}$=0.85 are fixed).
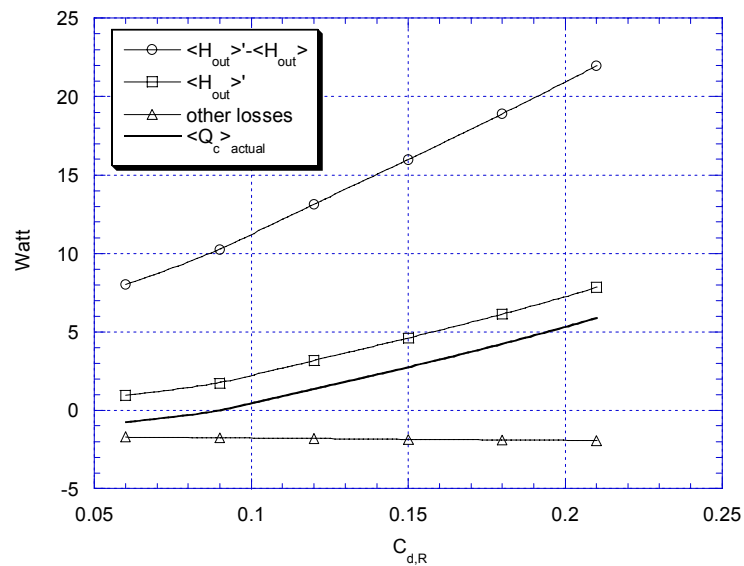
Figure 5.29 The actual cooling power including the losses based on the 2nd order analysis for various reservoir discharge coefficients ($C_{d,H}$=3.3 and $C_{d,L}$=0.85 are fixed).

Figures 5.30~5.32 show the comparisons of the cooling power obtained experimentally and with the numerical models. Three different valve opening timings for each refrigeration systems are used to verify the feasibility of the model. The pressure waves acquired from each experiment are used to determine the appropriate valve coefficients in each simulation. A match of the experimental and numerical pressure waves determines the correct values of the flow coefficients. Even if the same refrigeration system is under operation with the same valve opening timing, the pressure profiles are different for various operating temperatures. The numerical models for three different refrigeration systems with three different valve opening timings display a good agreement with the experimental results of the temperature dependent cooling power.
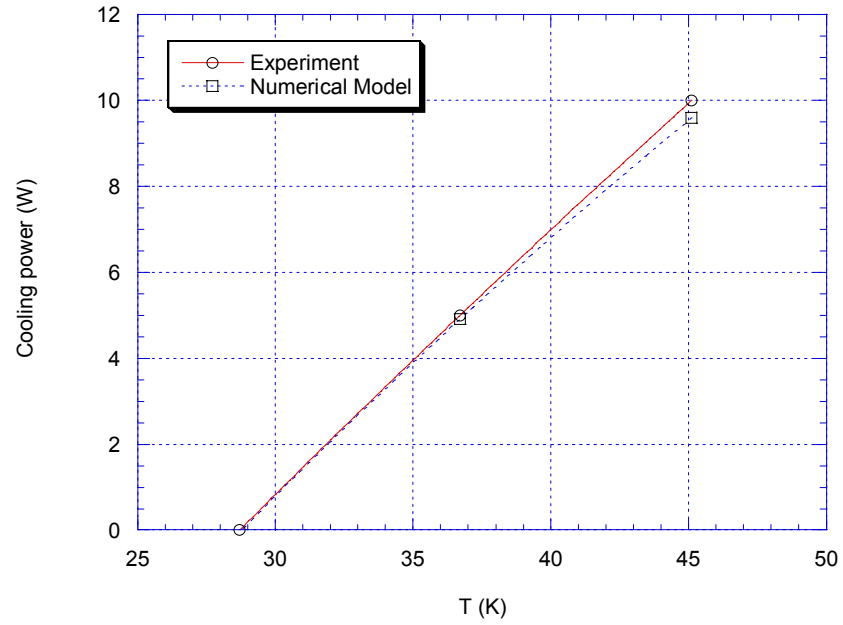
Figure 5.30 Comparison between the experiment and the numerical model for system I.
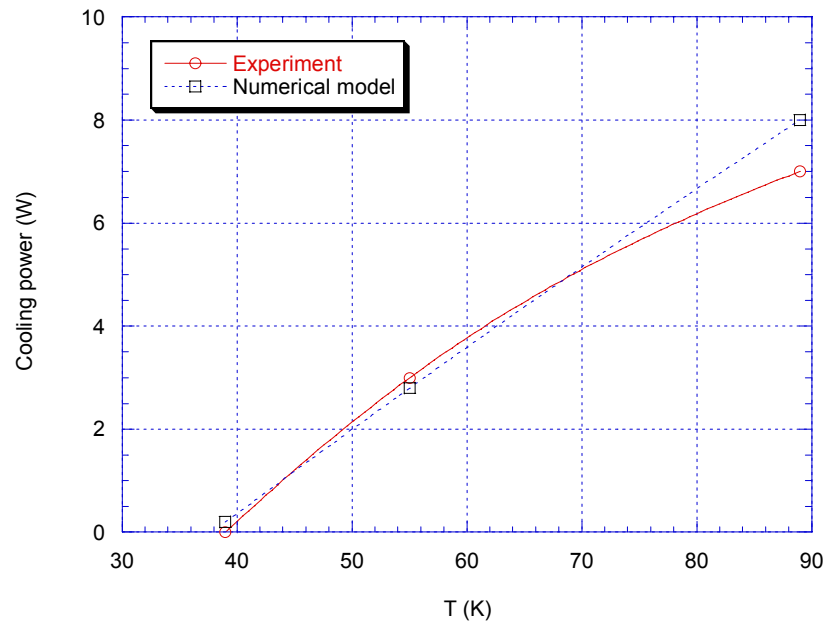
Figure 5.31 Comparison between the experiment and the numerical model for system II.
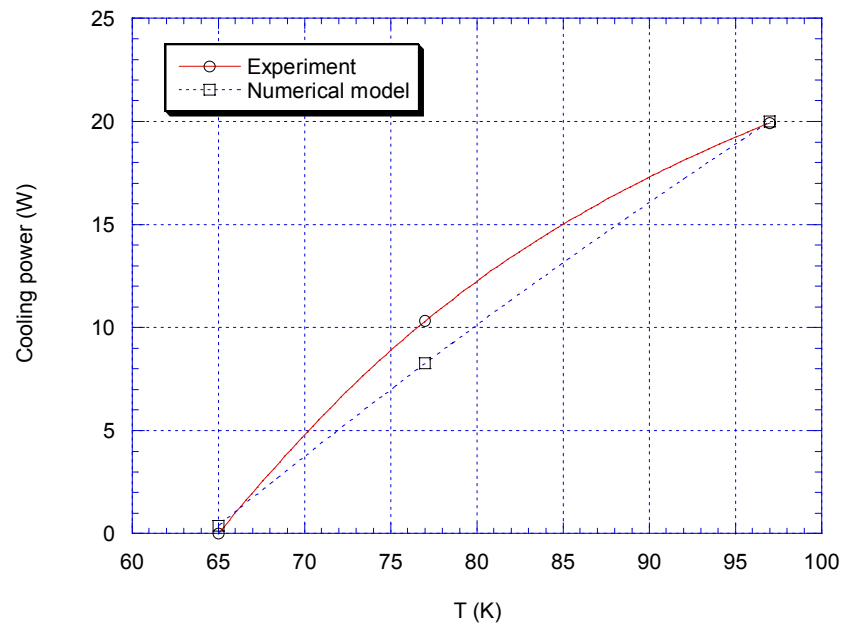
Figure 5.32 Comparison between the experiment and the numerical model for system III.

Chapter 6   Conclusion

Three 5-valve G-M type pulse tube refrigeration systems have been built and tested. Each refrigeration system has different geometries of pulse tube and regenerator, but use the same commercial compressor. A simple thermodynamic model developed in a previous study was used to compare their performances. The comparison showed a temperature-dependent discrepancy between the experiment and the thermodynamic model and inspired the development of improved design methods and better understanding of the loss mechanisms in the 5-valve pulse tube system.

A compressor-specific design method has been developed to optimize the cooling power of a G-M type pulse tube refrigerator. One, commercial G-M type compressor has been selected in the development of the design method. Measuring the mass flow rates as a function of the operating pressures produced a simple mass flow rate correlation to be used in the design. The results were converted to a compressor performance map that includes mass flow rates, pressures, and compressor electrical power. An iterative design method to optimize the geometry of the pulse tube refrigerator for a given compressor performance has been suggested. For the ideal pulse tube system without any loss, it is observed that the volume should be made as large a possible to produce larger cooling performance. However, considering the well-known loss mechanisms such as a pressure

drop through the regenerator and conduction losses significantly modifies the optimum volume of the pulse tube and other geometries of the refrigeration system. The substantial influence of the losses on the optimum design motivated an in-depth investigation of shuttle heat loss and DC flow loss. Using the selected compressor, the efficiency of a G-M type pulse tube operating at 30K is limited to less than 15% of the Carnot efficiency.

A one-dimensional numerical simulation of a 5-valve pulse tube refrigerator has been developed to investigate the shuttle heat loss and the DC flow loss. The numerical simulation uses both thermodynamic and fluid dynamic considerations to predict the gas flow characteristics in the system. A sophisticated numerical scheme has been developed and tested to solve the highly non-linear governing equations. Pressure, temperature and mass flow rates have been obtained as a function of time at all positions in the system. The numerical simulation has been tested against experimental results to verify its feasibility with very favorable results. The good agreement can be seen in both the time dependent pressure profiles during a single cycle, and the temperature dependent cooling power. Three reasonable heat transfer correlations are employed and tested to calculate the heat transfer near the pulse tube wall. The trajectory of gas movement and its temperature through a cycle display both shuttle heat loss and DC flow loss mechanisms. A 2nd order model has been employed to provide a better understanding of the cooling mechanism at the cold heat exchanger, and to identify the combined shuttle heat transfer and the DC flow. The 2nd order model revealed that the discharge coefficients of the orifice valves have a strong influence on the loss mechanisms and the cooling

performance. In addition, the 2nd order model shows that the shuttle heat transfer and DC flow can increase or decrease the cooling performance, and it depends on the system configurations, the operating conditions and the orifice valves. The comparison with experiments verifies an improved understanding of both the cooling and loss mechanisms in the pulse tube system.

Chapter 7 Proposed Works

This study has numerically verified that the effects of the discharge coefficients of the orifice valves on the performance of the pulse tube refrigerator are very significant. Even for a given compressor and fixed system geometry, the system can produce a wide range of performances by changing the discharge coefficients. To predict the system performance more accurately, an improved description of the relationship between the actual mass flow rate and the compressor pressures is recommended. The same can be said regarding the correlations between the mass flow rates, discharge coefficients, and the valve openings. In particular, the discharge coefficient of the reservoir valve has been found to be the most influential to the system performance. Using an orifice valve that has smaller pressure drop is recommended.

Regarding the solution scheme for the numerical analysis, non-dimensionalizing the governing equations and variables could increase the computation accuracy, especially since the order of magnitude among the variables such as mass flow rates, pressures and temperatures are not similar to each other. Detailed investigations into the flow regimes and heat transfer in the regenerator materials are also suggested. In this report, the effectiveness of the regenerator was calculated at the end of the simulation using the time-averaged mass flow rate and given regenerator temperature profile. It does

not simulate the actual heat transfer mechanism between the gas and the regenerator materials in real time steps. Relaxing the constant gas temperature assumption in the regenerator will provide a better description of the gas behavior in both thermal and fluid dynamic aspects. The development of an appropriate heat transfer correlation between the gas and the pulse tube wall is suggested. A heat transfer correlation that can be used in G-M type pulse tubes is preferable. In this report, three correlations are tested to verify their feasibilities. A favorable comparison between the experiment and the model was demonstrated by one of the three correlations. However, explicit correlations that include oscillating and compressing or expanding flows are not available in the literature. An iteration design process combining the compressor-specific design method and the numerical simulation including all losses can be used to define the optimum performance of a 5-valve pulse tube system. The 5-valve pulse tube system was developed to produce larger cooling powers than other single stage G-M configurations. This goal can yet be achieved and verified by the iteration process combining the geometry optimizing process and the numerical simulations.

References

1. W. E. Gifford and R. C. Longsworth, "Pulse Tube Refrigeration," ASME paper No. 63-WA-290, presented at Winter Annual Meeting of the ASME, Philadelphia, Pennsylvania (1963).

2. J. Yaun and J.M. Pfotenhauer, "Thermodynamic Analysis of Active Valve Pulse Tube Refrigerators," *Cryogenics, vol. 39,* (1999), pp. 283-292.

3. J. Yaun, *A Study of Pulse Tube Refrigerators*, Ph. D. thesis, University of Wisconsin-Madison (1998).

4. H. Pan, A. Hoffmann, L. Oellrich, "Single stage 4-valve and active buffer pulse tube refrigerators," *Cryogenics*, vol. 41, (2001), pp. 281-284.

5. W. E. Gifford and R. C. Longsworth, "Surface Heat Pumping," *Advances in Cryogenic Engineering,* vol. 11, Plenum Press, New York (1966), pp. 171-179.

6. E. I. Mikulin, A. A. Tarasov, and M.P. Shkrebyonock, "Low Temperature Expansion Pulse Tubes," *Advances in Cryogenic Engineering,* vol. 29, Plenum Press, New York (1984), pp. 629.

7. A. Ravex, P. Rolland and J. Liang, "Experimental study and modelization of the pulse tube refrigerator," Proceedings of ICEC 14 Cryogenics Supplements, Vol.32 (1992).

8. Y. Matsubara and J. L. Gao, "Multi-stage Pulse Tube Refrigerator for Temperature below 4K," Proceeding of 8th Cryocooler Conference (1994), pp. 345.

9. S. Zhu, Y. Kakimi, K. Fujioka, and Y. Matsubara, "Active-buffer Pulse Tube Refrigerator," *Proceedings of 16th International Cryogenic Engineering Conference / International Cryogenics Materials Conference* (1996), pp. 291.

10. C. Wang, S. Q. Wang, J. H. Cai and Z. Yuan, "Experimental Study of Multi-bypass Pulse Tube Refrigerator," *Cryogenics,* Vol. 35 (1995), pp. 555-558.

11. R. Radebaugh, "The development of Pulse Tube Refrigerator as an efficient and reliable cryocooler," *Journal of Australian Refrigeration, Heating and Air conditioning*, February–March (2001).

12. S. Fujimoto, Y.M. Kang, and Y. Matsubara, "Development of a 5 to 20 W at 80 K G-M Pulse Tube Cooler," *Cryocoolers 10*, Plenum Press, New York (1999), pp. 213-220.

13. C. Wang, G. Thummes, C. Heiden, "Performance Study on a Two-Stage 4 K Pulse Tube Cooler," *Advances in Cryogenic Engineering* vol. 43, Plenum Press, New York (1998), pp. 2055-2062.

14. A. Ravex, J.M. Poncet, I. Charles, and P. Bleuze, "Development of Low Frequency Pulse Tube Refrigerators," *Advances in Cryogenic Engineering,* vol. 43, Plenum Press, New York (1990), pp. 1957-1964.

15. J. Yuan, J. Maquire, A. Sidi-Yekhlef, and P. Winn, "30-50K Single Stage Pulse Tube Refrigerator for HTS Applications," *International Cryocooler Conference 11th proceedings*, Keystone, Colorado (2000).

16. L. W. Yang, "Shuttle Loss in Pulse Tube," *International Cryocooler Conference 11th proceedings*, Keystone, Colorado (2000).

17. I. Charles, L. Duband, and A. Ravex, "Permanent flow in low and high frequency pulse tube coolers- experimental results," *Cryogenics*, Vol 39, (1999), pp. 777-782.

18. Swagelok, *Metering Valve – L series Catalog* (2002).

19. Springer CO-AX Inc., *Technical specification of Co-ax valves* (2002).

20. Endevco, *Technical specifications : Piezoresistive Pressure Transducer - Model 8510B* (2002).

21. Lakeshore, *Web Catalog : Temperature Sensors* (2002).

22. P. Popovic and H.N. Shapiro, "A Semi-empirical Method for Modeling a Reciprocating Compressor in Refrigeration Systems*," ASHRAE Transactions,* vol. 101 (2), (1995), pp. 367-382.

23. D. Jaehnig, S.A. Klein, and D.T. Reindl, "A Semi-Empirical Method for Representing Domestic Refrigerator/Freezer Compressor Calorimeter Test Data.", *ASHRAE Transactions*, Minneapolis, MN (2000).

24. D. Jaehnig, "A Semi-Empirical Method for Modeling Reciprocating Compressors in Residential Refrigerators and Freezers," MS Thesis, University of Wisconsin – Madison (1999).

25. R. Akhavan, R.D. Kamm, and A.H. Shapiro, "An Investigation of Transition to Turbulence in Bounded Oscillatory Stokes Flows - Part 1. Experiments," *J. Fluid Mech.,* vol. 225, (1991), pp. 395-422.

26. V. Arp and R. Radebaugh, "Interactive Program for Microcomputers to Calculate the Optimum Regenerator Geometry for Cryocoolers (REGEN and REGEN2)," *AFWAL-TR-87-3040* Wright-Patterson Air Force Base (1987).

27. T. M. Flynn, *Cryogenic Engineering*, Marcel Dekker, Inc., New York (1997), pp. 471.

28. T. Schmauder, A. Waldauf, M. Thürk, , R. Wagner and P. Seidel, "Investigation on a Single Stage Four-Valve Pulse Tuber Refrigerator for High Cooling Power," *International Cryocooler Conference 11th proceedings*, Keystone, Colorado (2000).

29. F. P. Incropera and, D. P. De Witt, "*Introduction to Heat Transfer*", 2nd ed., John Willey & Sons, New York (1990).

30. E. S. Jeong, "Heat Transfer with Oscillating Pressure in Reciprocating Machinery", Ph. D. Thesis, M.I.T. (1991).